A NUMERICAL INVESTIGATION OF THE INFLUENCE OF MONSOONAL WIND REVERSALS OVER THE EAST AFRICAN COASTAL OCEAN

JOHN GATURU MUNGAI

Department of Oceanography, University of Cape Town,

Rondebosch, South Africa

Dissertation submitted to the faculty of Science, University of Cape Town, in partial fulfilment of the requirements for the Applied Marine Science, Master of Science Degree.

February 2008

Abstract

In this dissertation, the variability in the East African coastal ocean (Somali basin) due to the monsoon transition is investigated. The monsoon is characterized by wind reversals and seasonality in the precipitation of a region. The surface circulation of the western Indian Ocean during the summer (JAS) and winter (JFM) monsoon winds is investigated using the Regional Ocean Modelling System (ROMS). ROMS is forced with the Comprehensive Ocean Atmosphere Data Sets (COADS) while the initial and lateral boundary conditions are derived from the World Ocean Atlas. The domain area of the model study is constrained by 10°S to 15°N and 35°E to 65°E. An overview of the surface circulation of the Somali basin is given, discussing the Somali Current, East African Coastal Current, South Equatorial Counter Current, Southern Gyre, and the Great Whirl. The motivation of this dissertation is to improve the understanding of the circulation patterns within the Somali Basin from intra-seasonal to seasonal timescales, using the ROMS model.

The model results suggest a seasonally reversing Somali current with a sub-surface counter current, consistent with observations. Other prominent features such as the Great Whirl, which occurs during the Southwest monsoon and the Southern Gyre, are also apparent in the simulation. The East African Coastal Current (EACC) and the South Equatorial Counter Current (SECC) are also major features of the Somali basin circulation that are equally apparent from the model simulation. The model equally reproduces the equatorial jets as expected during the transition period of April/May and October/November with the net result of mass transport from the western end of the basin towards the east.

Acknowledgements

To the two women in my life; my dear wife, Anne and my beloved Mother for their continued support and prayers. Then to my big brother who looks after my affairs back home.

Then, I would like to thank my two supervisors Prof. Frank Shillington and Prof. Chris Reason for their guidance and excellent supervision during the execution of this work. Special thanks to Dr Pierrick Penven (IRD, France), for his initial support with the ROMS model and for the development of the ROMS Tools Graphical Interface that has made running the ROMS model much easier. I appreciate the assistance that I received from the international ROMS users' community through their website: (www.myroms.org, and http://marine.rutgers.edu). I wish to thank all the global atmospheric and oceanic data centres who have availed their useful scientific data to the public domain. These include NOAA/AOML, NCEP and NODC. Satellite altimeter data was provided by SSALTO/DUACS and distributed by AVISO (http://www.aviso.oceanobs.com/) with CNES support. Thanks to all the Oceanography department students and staff for their moral support.

I am indebted to the Director of Meteorological Services, Dr. J.R. Mukabana, for his support in the procurement of my scholarship by the Government of the Republic of Kenya.

"The chief end of man is to glorify God and to enjoy Him forever."
- Westminster Catechism

TABLE OF CONTENTS

List of Figures

Chapter 1

1.1 Introduction

The Indian Ocean is surrounded by the East African highlands to the west and the Himalayan Mountains to the north, and is bounded by Asia to the north, and hence the ocean circulation and wind flow in this region is greatly influenced by these orographic features (Figure1.1). The monsoon is basically characterized by wind reversals and seasonality in the precipitation of a region. In this study, the wind reversals during the monsoon and its effect on the East African coastal ocean circulation will be considered.

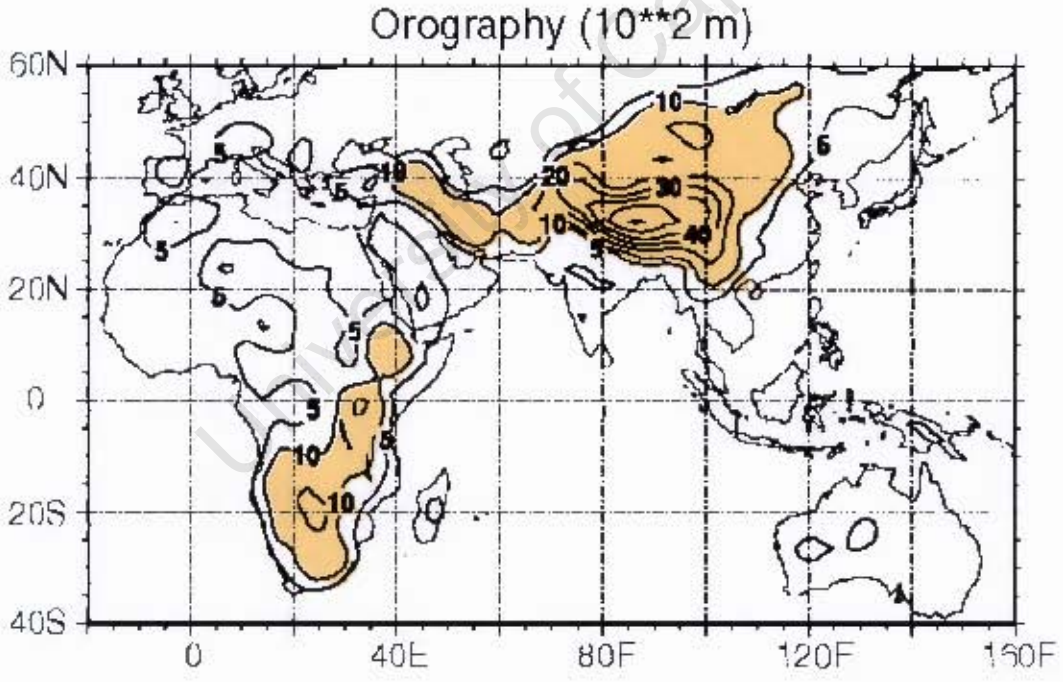

Figure 1.1: Orographic structure of the eastern hemisphere (units are 10**2 m). Orographic elevations greater than 1 km are shaded.

The Indian Ocean response during the annual cycle of the monsoon winds is as shown in figure 1.2. During April to May, weak alongshore winds occur off the Somalia coast. The subsequent onset of the monsoon over the Arabian Sea has been found to occur in several different ways (Fieux and Stommel, 1977). The onset can be an abrupt change from the weak pre-monsoonal winds into the fully developed Southwest Monsoon in early to mid-June (Schott and McCreary, 2001). The Southwest Monsoon becomes most strongly developed in late July but then may undergo phases of breaks. The geographic location of the East African Coastal Current (EACC) and by extension the Somali Current at or near the equator implies that the wind fields and transition of the associated surface wind stress is governed by the large scale atmospheric systems in the subtropics namely the Arabian High (ridge) in the Northern Hemisphere and the Mascarene High located offshore of Madagascar in the Southern Hemisphere. These semi-permanent anticyclonic high pressure cells have a great influence on the seasonal reversal of the winds during the seasons.

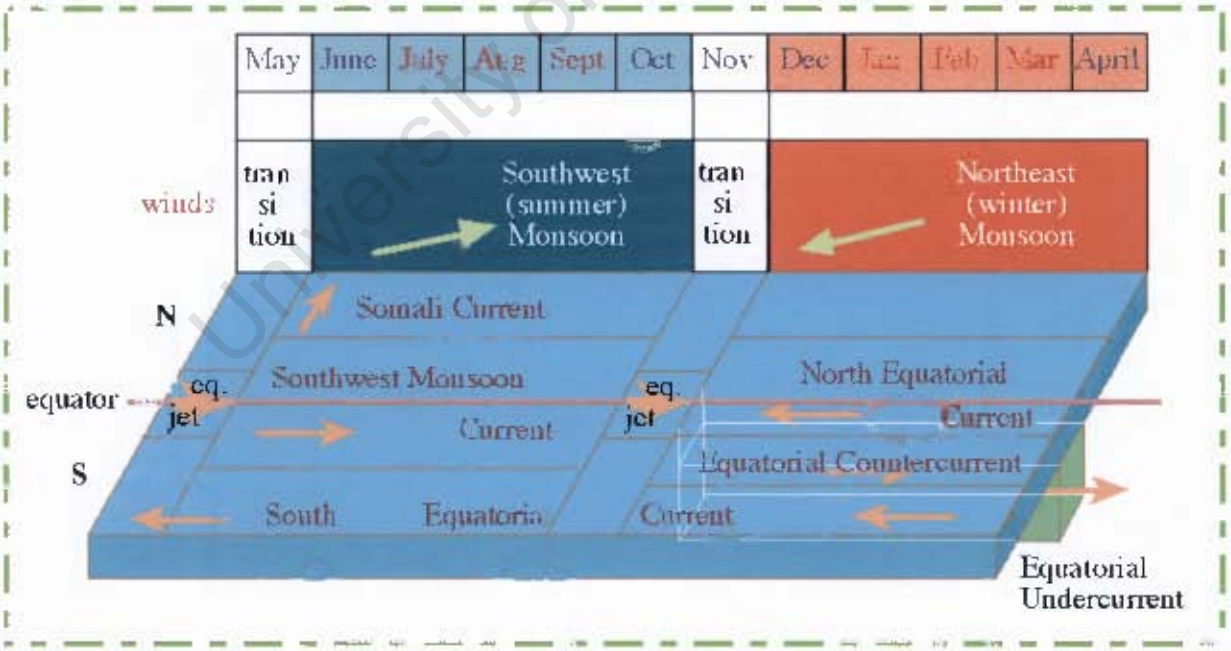

Figure 1.2: A Schematic of the Monsoon system in the Indian Ocean. The top part indicates the wind cycle; the lower part shows the major currents that develop in response to the wind (Tomczak et al., 1994).

The domain area of the study is bounded by 10°S to 15°N and 35°E to 65°E. In the northern hemisphere summer, the ocean circulation adjacent to the East African (Kenyan) coast is characterized by the EACC to the south and the Southwest Monsoon Somali current to the north of the equator as shown in Figure 1.3(b). The offshore South Equatorial Current (SEC) and the EACC feed the northward flowing Somali current. Based on the monsoon season and hence the wind field involved, the Somali current can develop into different cells and gyres as shown in Figures 1.3 (a and b). In northern summer, after crossing the equator, one part of the Somali Current turns offshore at about 4°N, forming a cold upwelling wedge on its left shoulder; the other part re-circulates across the equator as the 'Southern Gyre' (SG). In the north, a second gyre is formed, the 'Great Whirl' (GW). Both of these gyres have been reproduced in model simulations (Schott and McCreary, 2001).

On the other hand, certain aspects of the Indian Ocean western boundary circulation (detailed in succeeding sections) still remain unresolved. The disappearance of the Somali Undercurrent in the boreal spring (Jensen, 1991), for instance, has not been fully explained. Furthermore, the southward interior Ekman transport during boreal summer is complicated at the equator by northward cross-equatorial winds forcing a shallow equatorial roll (Miyama et al., 2003) with northward flow in the upper 20 metres and southward flow underneath. It is not clear if diapycnal transfers are involved in this mechanism. Indeed, the top-to-bottom meridional overturning of the Indian Ocean is a matter of ongoing debate, with large discrepancies between estimates of deep inflow and corresponding upwelling (Schott and McCreary, 2001).

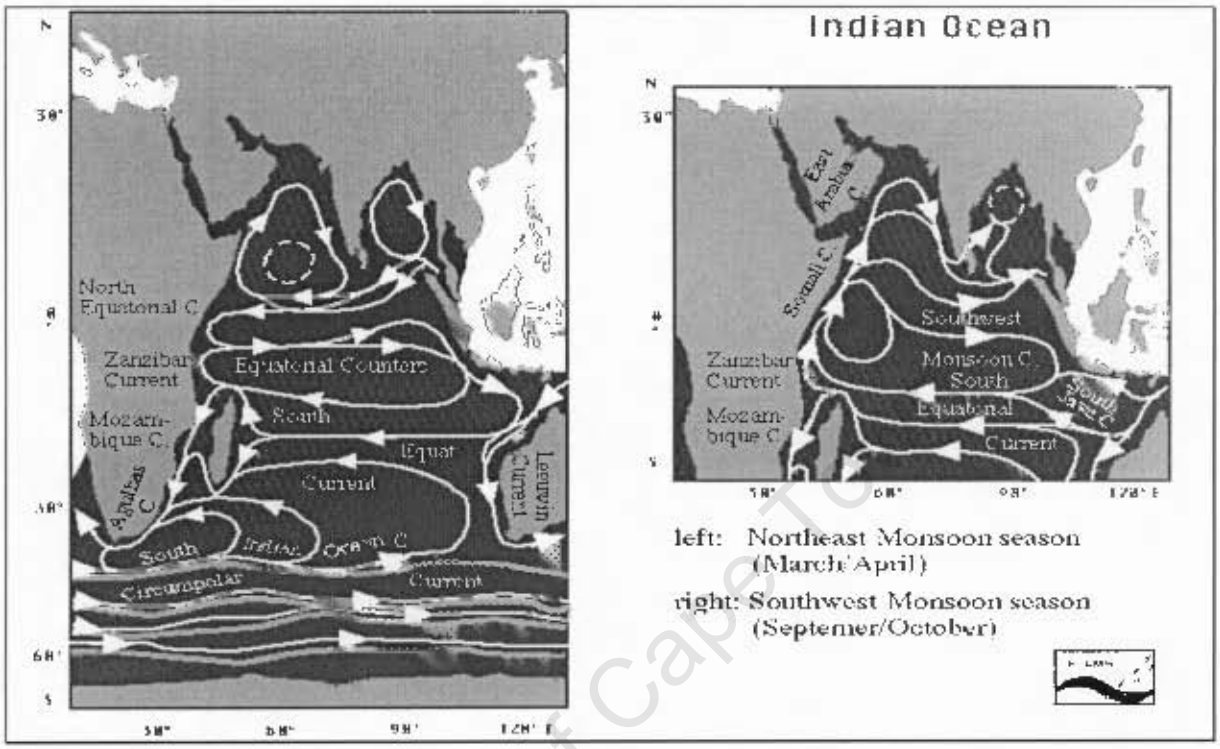

Figure 1.3 (a) and (b): Indian Ocean Currents (M. Tomczak and S. J. Godfrey, 1994).

Levitus (1988) found that during the Southwest summer monsoon, the Ekman flow is directed southward on both sides of the equator, suggesting that there is a southward flow of surface water across the equator in the interior of the ocean. Observational evidence for the concept of southward Ekman transport was given by Chereskin, Wilson, Bryden, Ffield, and Morrison (1997), who evaluated surface-layer Acoustic Doppler Current Profiler (ADCP) currents across the 8°N line in the Indian Ocean and contrasted these with geostrophy; they obtained good agreement between measured Ekman transports and those derived from wind stress. Undercurrents have been observed under the Somali Current during different times of the year. Similar work has been done by Shillington (1998) and Boyd and Shillington (1994) in the Benguela upwelling system off southwestern Africa.

During the northern hemisphere winter, the coastal ocean circulation is characterized by the EACC which connects with the then southward flowing Somali current in a confluence zone at 2- 4°S, and the two currents then supply the eastward flowing South Equatorial Counter Current (SECC) as in figure1.4.

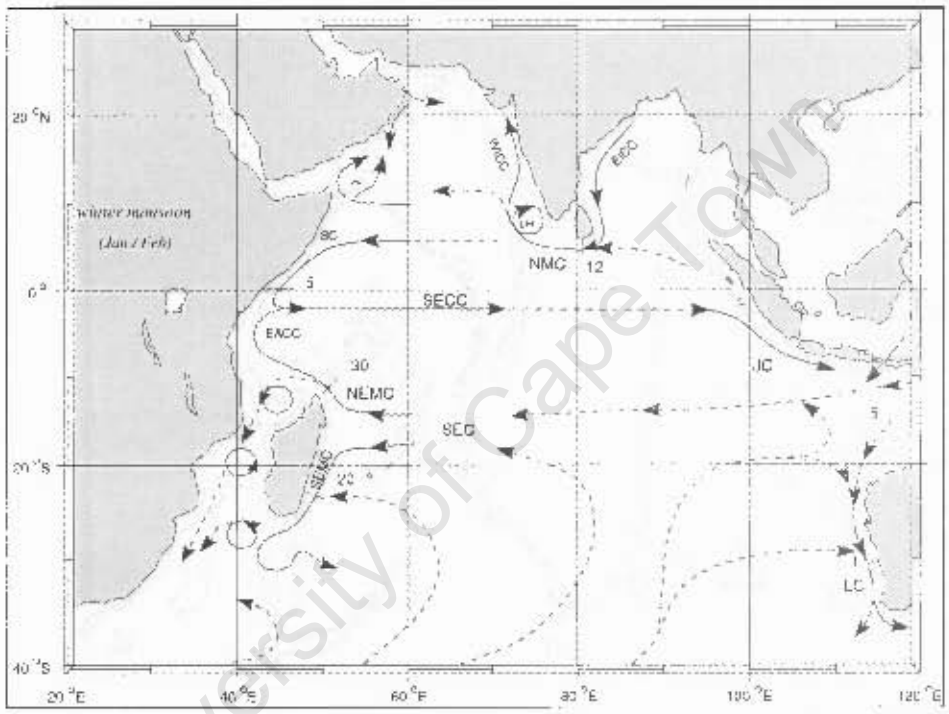

Figure1.4: Northeast Monsoon Circulation in the Indian Ocean (after Schott and McCreary, 2001).

1.2 Objective and Motivation for Study:

This work seeks to improve the understanding of the circulation patterns (surface currents) from intra-seasonal to seasonal timescales, within the western boundary of the Indian Ocean (Somali Basin), using COADS mean monthly wind stress data and

heat fluxes as forcing for a regional scale model to address the subsequent objective and research questions.

The main objective of the study will be to investigate the response of the East African Coastal ocean processes to the summer and winter monsoon wind transitions.
In this study, the following research questions will be investigated:

- How do the seasonal transitions of the East African monsoon influence the flow of the East African coastal ocean circulation including the western part of the equatorial jet?
- How do the monsoon wind reversals influence the coastal ocean transport?
- How do the monsoon wind reversals affect the upper ocean heat content?

With these objectives in focus, this dissertation will be structured as follows:
Chapter 2 reviews the appropriate literature that relates to the atmospheric circulation patterns and ocean circulations occurring at the northwestern boundary of the Indian Ocean (East African Coastal Ocean); this includes the East African monsoon, the Asian monsoon, the Inter Tropical Convergence Zone (ITCZ), the East African Low Level Jet, Equatorial jets and the Cross-equatorial Cell. Chapter 3 deals with the various satellite-derived data used in the study and the various methods used to investigate the posed research questions (preceding section). It includes a brief synopsis of the ROMS model physics and parameterization schemes that is deemed relevant to this study. Chapter 4 relates to the findings from the methods used. It includes a description of the results and discussions of the same. Chapter 5 is a summary of the findings from the study.

Chapter 2:

Literature Review

2.1 Monsoon over East Africa

The term "monsoon" stems from seasonal variations in winds but it is now more generally applied to tropical and subtropical seasonal reversals in both the atmospheric circulation and associated precipitation. These changes arise from reversals in temperature gradients between continental regions and the adjacent oceans with the progression of the seasons, and the extremes are often best characterized as "wet" and "dry" seasons rather than summer and winter (Trenberth et al, 2000). A monsoon region is characterized by large changes in the direction of surface wind between summer and winter seasons. By this criterion, the tropical and adjoining sub-tropical regions of Africa, South Asia, East Asia and North Australia constitute the monsoon region.

In the last two decades, there have been a number of reviews of the monsoon system (e.g., Ramage, 1971; Fein and Stephens, 1987; Hastenrath et al., 1991). Ramage (1971) provided a rather strict definition of a monsoon and identified the African, Asian, and Australian regions as satisfying both a wind reversal and seasonal precipitation criterion. He defined the monsoon area as encompassing regions with winter (DJF) and Summer (JJA) surface circulations in which:

(1) The prevailing wind direction shift by at least 120° between January and July;
(2) The average frequency of prevailing wind directions in both January and July exceeds 40%;
(3) The mean resultant winds in at least one of the two months exceed three metres per second ($3ms^{-1}$);

(4) Less than one cyclone-anticyclone cell alternation occurs every two years in either January or July in a 5° latitude-longitude rectangle.

These criteria indicated that for a region to be considered monsoonal there must be highly persistent winds from different directions in summer and winter.

The monsoon over East Africa is associated with a north-south movement of the ITCZ. The ITCZ moves southward along the east coast of Africa from 2°S in October to 12°S by the end of December. It remains in the extreme southern position up to the end of January and then moves northward. By the end of April, it is back to about 2°S. During May, it is transformed into the Southern Hemisphere near-equatorial trough (NET) while the Northern Hemisphere NET takes up the role of the ITCZ. As a result, over eastern Africa, monsoon rains in the near-equatorial region occur twice in a year, once when the ITCZ moves northward and once when it moves southwards.

East Africa, and Kenya in particular, experience two rainy seasons associated with the summer (Southwest) and winter (Northeast) monsoon and the corresponding north-south march of the ITCZ. In its southward journey, the ITCZ brings rain to Kenya and parts of East Africa from October to December. This period is locally called the season of the "Short Rains". These regions again receive rains from about middle of March to beginning of June with the northward journey of the ITCZ, locally known as the season of "Long Rains". A comprehensive study of the seasonal rainfall variability of eastern Africa has been carried out by Nyenzi, (1988); Ogallo et al., (1988); Mukabana and Pielke, (1996); Ininda, (1998); Indeje et al., (2000); Mutai and Ward, (2000); Kijazi and Reason, (2005).

During the period of "Short Rains", northeasterlies and northerlies replace the south-easterlies in the lower troposphere along the coast of East Africa, in association with the build-up of the anti-cyclonic ridge over Arabia. During the season of the "Long Rains", south easterlies push forward from the south in the lower troposphere along

the East African coast until the East African Low Level jet (or Somali jet) is established by the end of June (Asnani, 1993).

Fluctuations in the monsoon activity over East Africa are influenced greatly by the pressure patterns and consequently by the wind stress fields as seen on a synoptic chart. When stationary or very slow-moving high pressure cells face each other on either side of the equator, confluence and horizontal velocity convergence results between the high pressure cells. There are fluctuations in the intensity and orientation of the seasonal quasi-stationary high pressure cells on either side of the equator. On the other hand if, instead, two low pressure cells face each other across the equator, the result is inflow into each cell, leading to diffluence and horizontal velocity divergence in the region between the two pressure cells. When wind observations are lacking, as is often the case, these simple rules are helpful in predicting the weather and wind pattern variations over the tropics.

On a synoptic scale, the wind flow pattern is controlled by the relative strengths of the seasonal quasi-stationary Arabian ridge of high pressure north of the equator and the sub-tropical high pressure cell near Madagascar (Mascarene High) south of the equator. During northern hemisphere winter, the northeasterly wind around the eastern side of the Arabian ridge crosses the equator with a slight deflection and meets the southeasterly winds from the eastern side of the sub-tropical cell off Madagascar. Even when the ITCZ is not clearly discernible, as is often the case; the strength, orientation and the moisture content of these two airflows greatly influence the intensity of the monsoon activity over East Africa. A longer travel over the ocean before the winds reach land increases the moisture content and hence possibility of rainfall over the landmass. A stronger component of wind along the upslope of the Highlands favours precipitation in this region.

2.2 Monsoon Seasonal Cycle:

The monsoon cycle of the wind stress fields is as shown in Figure 2.0, for January, April, July and October from the NCEP seasonal-mean climatology. South of 10°S, the Southeast Trades persist throughout the year. They have their seasonal maximum and most northerly extent during southern winter.

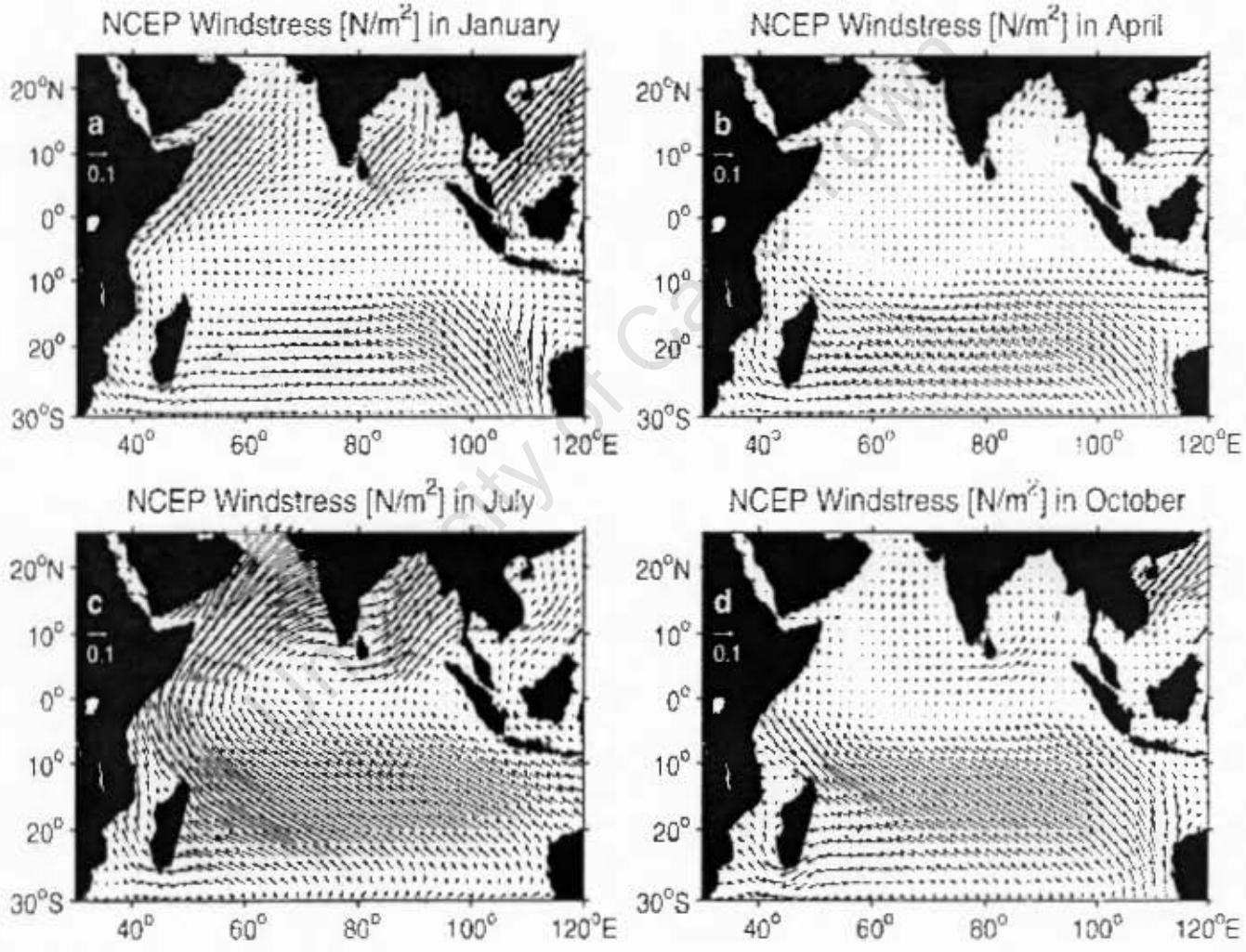

Figure 2.0: Monsoon wind stress fields (Nm^{-2}) from the NCEP climatology for: a) January, b) April, c) July and d) October.

Monsoons are caused by the larger amplitude of the seasonal cycle of land temperature compared to that of nearby oceans. This differential warming happens because heat in the ocean is mixed vertically through a "mixed layer" that may be fifty to a hundred metres deep, through the action of wind and buoyancy-generated turbulence, whereas the land surface conducts heat slowly, with the seasonal signal penetrating perhaps a metre or so.

The upper tropospheric flow pattern during summer identifies clearly the thermal contrast between continents and oceans (e.g., Krishnamurti, 1971a and b). Additionally, the specific heat of liquid water is significantly higher than that of most materials that make up land. Together, these factors mean that the heat capacity of the layer participating in the seasonal cycle is much larger over the oceans than over land, with the consequence that the land warms faster and reaches a higher temperature than the ocean. The hot air over the land tends to rise, creating an area of low pressure. This creates a steady wind blowing toward the land, bringing the moist near-surface air over the oceans with it. Similar rainfall is caused by the moist ocean air being lifted upwards by mountains, surface heating, convergence at the surface, divergence aloft, or from storm-produced outflows at the surface. However the lifting occurs, the air cools due to expansion in lower pressure, which in turn produces condensation.

In winter, the land cools off quickly, but the ocean keeps the heat longer. The hot air over the ocean rises, creating a low pressure area and a breeze from land to ocean while a large area of drying high pressure is formed over the land, increased by wintertime cooling. Monsoons are similar to sea breezes, a term usually referring to the localized, diurnal (daily) cycle of circulation near coastlines everywhere, but they are much larger in scale, stronger and seasonal. However, the picture of a monsoon overturning circulation, as something like a thermally driven sea breeze on a larger scale, and therefore modified somewhat by the Coriolis Effect is, highly idealized. Moreover, often only the cross-equatorial overturning comprising the local Hadley

circulation has been emphasized: it is referred to as the "lateral monsoon" in Webster et al. (1998).

2.3 East African Low Level Jet (EALLJ)

The EALLJ, also commonly known as the Findlater or Somali Jet, is an integral feature of the coupled ocean-atmosphere monsoon system. This jet has assumed great importance since its discovery in the early 1960s. It is an important component of northern summer monsoon circulation in the lower troposphere from the South Indian Ocean to the Arabian Sea across the equator. Besides being a critical element in driving the Somali Current (Knox, 1987) and thus being a key element in cross-equatorial ocean transports, the Jet is responsible for a large part of the atmospheric transport of water vapour across the equator. The Jet also exhibits variability on many timescales and is a keen reflector of the variability of the inter-hemispheric monsoon vortex and the active and break periods of the monsoon (Krishnamurti and Bhalme, 1976). The strength of the Jet should have strong impacts on the ocean, the tropical western Indian Ocean especially. A weak jet, for example, would be expected to alter the SST distribution of the north Indian Ocean by reducing upwelling, Ekman transport, and evaporation. The early Findlater studies (Findlater, 1969a and b) were supplemented during the WCRP Summer Monsoon Experiment (MONEX, 1979). The jet is centred around 1. 5 km altitude and maximum core speeds of 10 -15 metres per second extend from the northern tip of Madagascar to the central Arabian Sea.

There have been many studies attempting to understand the physical processes that determine the location and structure of the Findlater Jet (Anderson, 1976; Hart, 1977; Bannon, 1979; Krishnamurti and Wong, 1979). The first four papers are theoretical studies that liken the jet stream to oceanic western boundary currents with the East African Highlands as the western boundary. Krishnamurti and Wong (1979) and Krishnamurti et al., (1990) modelled the baroclinic boundary layer of the western Indian Ocean driving a cross-equatorial flow against the model western boundary by

an imposed vertically varying pressure gradient force. In each of the studies the structure of the jet stream is modelled fairly well. Perhaps the most important result of these studies is the setting of model vertical and horizontal resolution requirements for the adequate representation of cross-equatorial flow. If the scales are not fine enough, the cross-equatorial flow will not be concentrated in the western Indian Ocean but may spread across Africa and effectively disperse. Such was the case in early low-resolution general circulation experiments (e.g., Washington and Dagupatty, 1975). In coupled ocean-atmosphere experiments, a diminished Findlater Jet would be a critical omission as it would drive an inadequate Somalia Current and would probably lead to major changes in the heat balance of the North Indian Ocean.

2.4 Tropical Indian Ocean Climatology

The prevailing wind system is the major driving force, together with buoyancy fluxes, for ocean currents. In the open ocean, the winds tend to be mainly zonal. The present configuration of the distribution between land and water determines the ocean's response to the winds. The combined action of the Southeast trades and the seasonally reversing monsoon winds creates a unique ocean circulation in the Indian Ocean, namely the EACC, Somali Current and the equatorial jets (Wyrtki jets).

The regular variation in surface currents between summer and winter in this part of the Indian Ocean, observed by mariners for over 1000 years (Warren, 1966), is depicted in all good atlases: Schott (1935), for example, portrays it excellently. Soon after the onset (normally in June) of the Southwest Monsoon, when winds north of the Equator go into reverse and an extensive region of strong south-west wind comes into being, there is an approximate reversal of most current directions in this area, which oceanographers have normally viewed as related to the changes in prevailing winds. Important knowledge of the corresponding distributions of current in depth was added during the International Indian Ocean Expedition (IIOE) in 1964-66. It consisted of a basin wide survey that subsequently resulted in a comprehensive hydrographical atlas

(Wyrtki, 1971) and a number of regional studies, including the first survey of the monsoon circulation of the Somali Current by Swallow and Bruce (1966). The next intensive study was the Indian Ocean Experiment (INDEX), which investigated the summer monsoon response of the Somali Current (Swallow, Molinari, Bruce, Brown, and Evans, 1983). Of special interest among currents present only during the northern hemisphere summer is the Somali Current, which flows northward from the neighbourhood of the Equator to about 9°N, where it separates from the coast (Warren, Stommel and Swallow, 1966; Swallow and Bruce, 1966).

The Somali Current has been found to be markedly baroclinic; that is, there is a strong variation of velocity with depth, associated with a horizontal density gradient which comes into being in a matter of a few weeks, a month at most, after the winds over the northern Indian Ocean change to the Southwest Monsoon pattern (Lighthill, 1969). Except near its inception, the Somali Current is a strong current with a velocity maximum normally around 2 m/s and, indeed, Swallow (1967) observed a local surface speed of over 3 m/s near the separation point; a current which like other western boundary currents such as the Gulf Stream and the Kuroshio is regarded as too strong to be a merely local response of the ocean to the local winds. By analogy with other currents, it tends to be interpreted rather as part of the ocean's dynamic response to the pattern of wind stress over a large part of it (Lighthill, 1969).

2.5 The Western Indian Ocean Circulation

The seasonal development of the Somali Current system was very well described by Schott et al. (1990). During the *March–May* period, before the onset of the southwest monsoon, the southern Somali Current is an extension of the East African Coastal Current (EACC) that flows northward across the equator to about 3–4°N. There, it turns offshore, and a cold wedge develops along its shoreward shoulder. Farther north, alongshore winds cause an upwelling regime to develop with a shallow northward coastal flow overlying a southward undercurrent. Its width scale is of the order of 50–100 km.

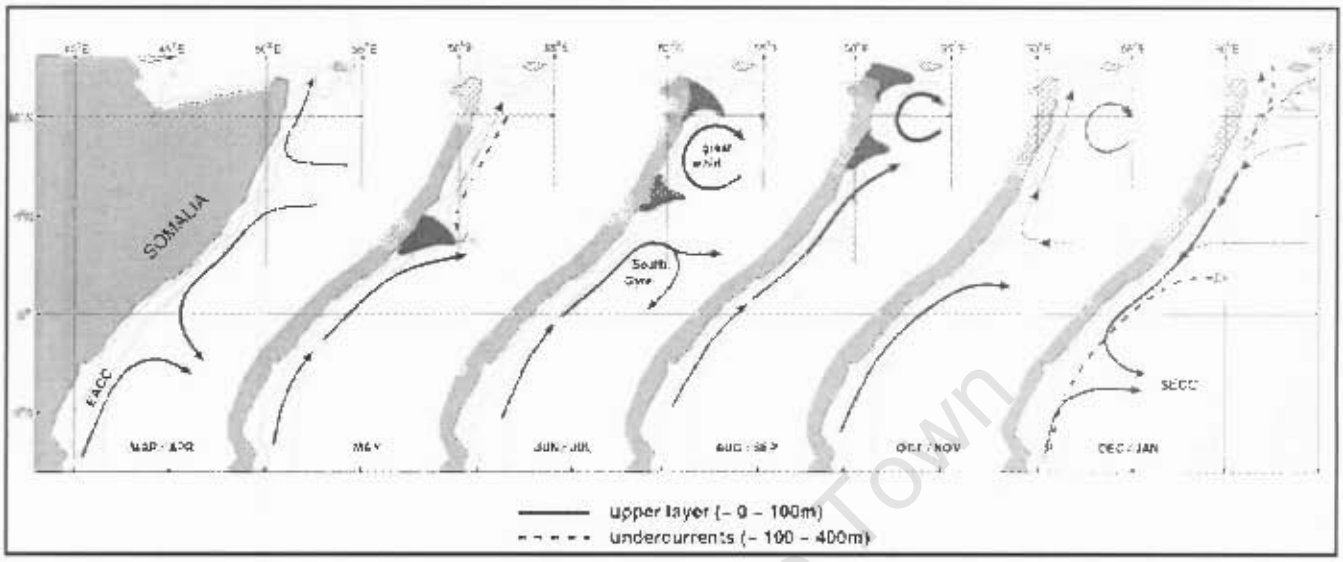

Figure 2.1: Schematic diagram of the Somali Current upper-layer flow patterns over the course of the year (Schott et al., 1990).

With the southwest monsoon onset in June (JJA), the 'Great Whirl' develops from 4–10°N (Figure 2.1), and a second cold wedge appears between the 10–12°N latitude where it turns offshore. Schott and Quadfasel (1982) conducted observations from moorings in the northern Somali-Current regime. During their observational year, there was a sudden onset of the monsoon, and they reported distinct westward-propagating signals after the onset. They interpreted them as first-mode Rossby waves, and concluded that the onset of the Great Whirl was a response to the very strong anticyclonic wind stress curl offshore from the East African - Somali coast by these long Rossby waves which reflected into short Rossby waves at the boundary, accumulating energy there. The importance of this forcing mechanism is supported in several of the modelling studies carried out by Schott et al (2001).

The cross-equatorial flow continues during this time (JJA), now transporting about 20 Sv in the upper 500 m (Figure 2.3). It leaves the coast south of 4°N, where part turns eastward and part flows back across the equator in a circulation pattern referred to as the 'Southern Gyre' (Figure 2.1). The fraction of the direct cross-equatorial offshore return flow in the Southern Gyre appears to vary from year to year (Schott et al., 1990), and the mechanisms responsible for this split, as well as the fate of the eastward outflow north of the equator, need further study. Water-mass signatures of both gyres indicate that there is very little exchange between the Great Whirl and the Southern Gyre at this time. Thus, water that crosses the equator with the shoreward part of the Southern Gyre does not continue to flow up the Somali coast, but instead bends eastward with part recirculating southward across the equator and part flowing across the Arabian Sea near the equator.

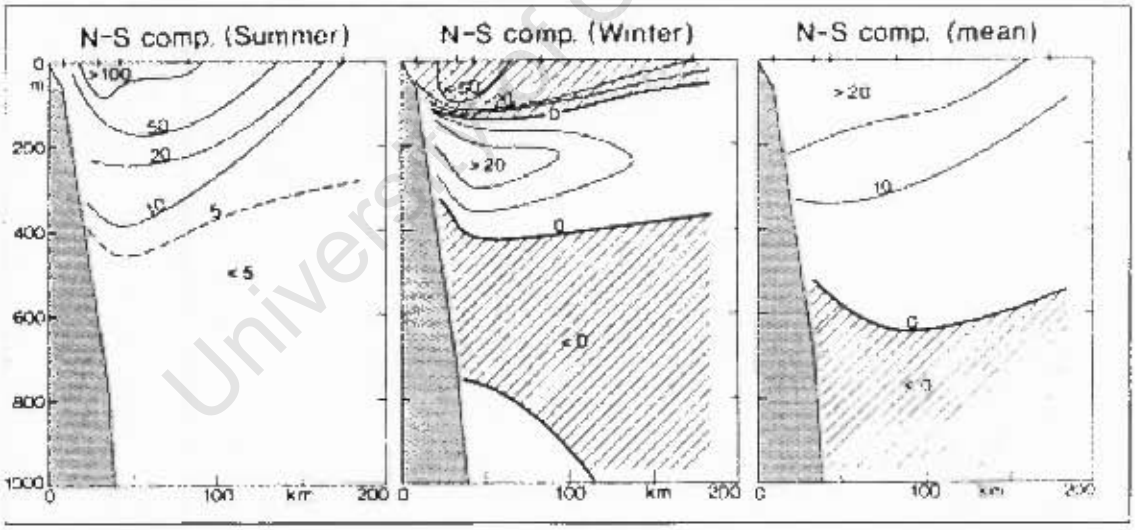

Figure 2.2: Somali Current (cm/s) on the equator during the summer monsoon (left), during the winter monsoon (middle) and annual mean. Shaded area is southward flow and unshaded is northward flow across equator (right: from Schott et al., 1990).

Meridional currents cannot cross the equator freely because the flow has to reverse the sign of its potential vorticity when changing hemispheres. As a result, subsurface cross-equatorial exchange must take place largely via the western boundary current, (Figure 2.2) where frictional effects can compensate the vorticity change. On the other hand, near-surface exchange can occur in the interior ocean as a result of forcing by the wind stress curl (Schott et al, 2001). After crossing the equator, western boundary currents typically turn offshore to join near-equatorial eastward flows in the interior ocean, as do the North Brazil Current in the Atlantic and the New Guinea Coastal Current in the Pacific. The eastward deflections generally occur after the boundary current first overshoots the latitude band of the eastward flow and then retroflects equatorward. The Southern Gyre appears to develop from a retroflection of this sort (Schott and Quadfasel, 1982, Schott et al., 2001). A cut through the Great Whirl for the mean currents of the summer monsoon, determined from a line of moored stations south of Socotra, shows that the Great Whirl reaches down to almost 1000 m with speeds of 10 cm/s, and that the gyre structure remains visible even at greater depths. At this time, there is a net upper-layer outflow from the Somali Current system into the Gulf of Aden through the passage between Socotra and the Horn of Africa. From moored current-meter observations in the passage, the mean northward outflow throughout the summer monsoon was estimated to be about 5 Sverdrup (Schott et al., 1997) as captured by the annual mean NCEP Sverdrup transport in figure 2.3, and the upper-layer water masses have characteristics of upwelled subsurface water (Fischer, Schott, and Stramma, 1996).

In the late phase of the summer monsoon (Aug - Sep), the Great Whirl has become an almost closed circulation cell (Figure 2.4) with very little exchange between its offshore recirculation branch and the interior Arabian Sea, as is apparent from the differences in surface salinities between the GW and the region to the east of it (Fischer et al., 1996).

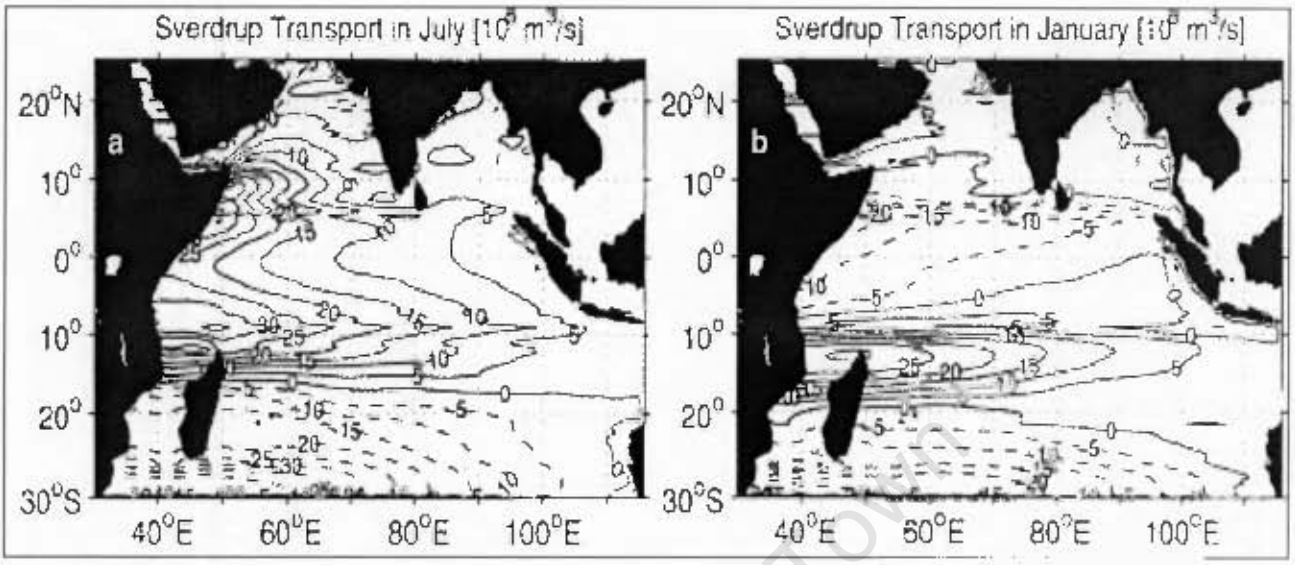

Figure 2.3: The mean field of Sverdrup transport function (in Sv=$10^6 m^3$ s^{-1}), from NCEP climatology for a) Boreal Summer, b) Boreal Winter

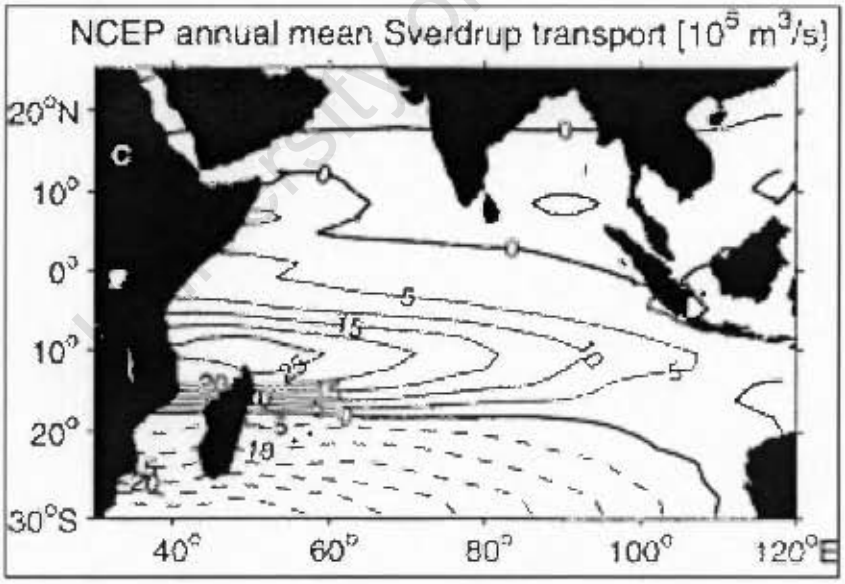

Figure 2.3: (c) The Annual mean field of Sverdrup transport function (Sverdrup=10^6 m^3 s^{-1}), from NCEP climatology.

When the Southwest Monsoon dies down in October-November, the cross-equatorial Somali Current turns offshore again at 3°N, while the Great Whirl continues to spin in its original position. The Great Whirl is even discernible underneath the developing Northeast Monsoon circulation well toward the end of the year (Bruce, Fieux, and Gonella, 1981).

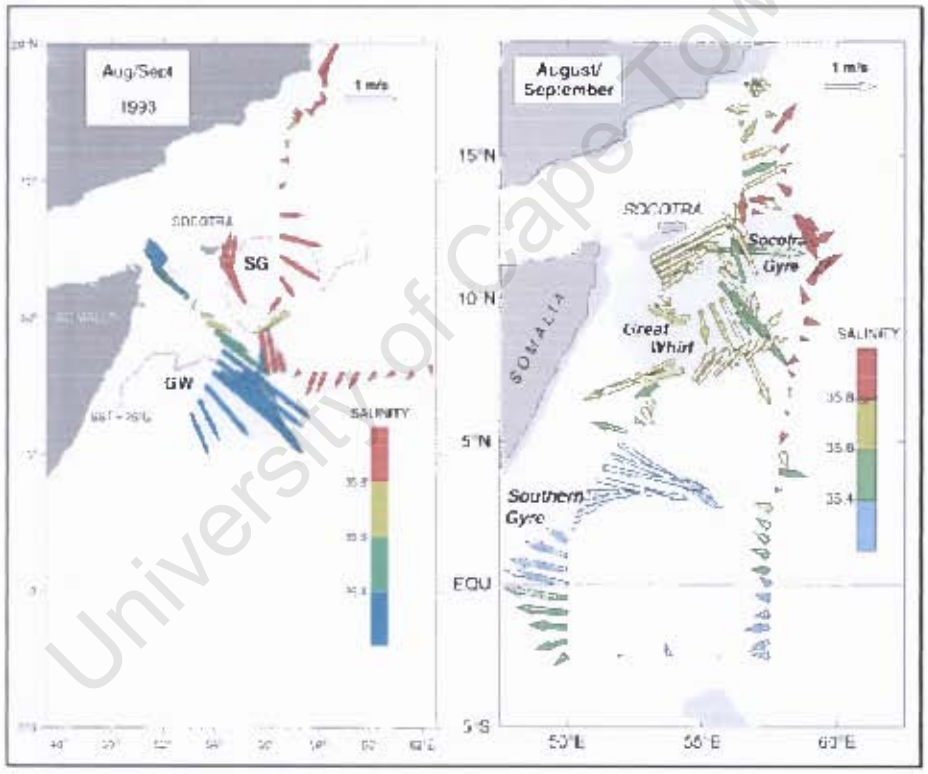

Figure 2.4: Somali Current flow patterns during the late summer monsoon phases of (a) 1993 (after Fischer et al., 1996) and (b) 1995, (after Schott et al., 1997). Marked are the Southern Gyre, Great Whirl (GW) and Socotra Gyre (SG).

2.6 Equatorial (Wyrtki) Jets:

At the surface of the Indian Ocean, a narrow jet-like current flows eastward along the equator at high speed during both transition periods between the two monsoons. This is the equatorial jet also known as the Wyrtki jet (1973) after the man who discovered its existence several decades ago. This phenomenon is singular to the Indian Ocean owing to the semiannual eastward winds along the equator associated with the transition seasons between the monsoons. The jets net effect is to carry warm upper-layer waters eastwards, lowering sea level and hence decreasing the mixed-layer depth in the west but increasing the sea level in the east as shown by Monterey and Levitus (1997) in figure 2.5.

The subsequent formation of the jet is accompanied by thermocline uplifting/shoaling at the western origin of the jet and by sinking at its eastern terminus. This demonstrates that a time-variable current can have profound effects in changing the mass structure in the ocean (Luyten et al, 1976). The jets have roughly the same strength of about $100cms^{-1}$, being somewhat stronger in November (boreal autumn) than in May (boreal spring) in the smoothed data of figure 2.6 (Han et al., 1999).

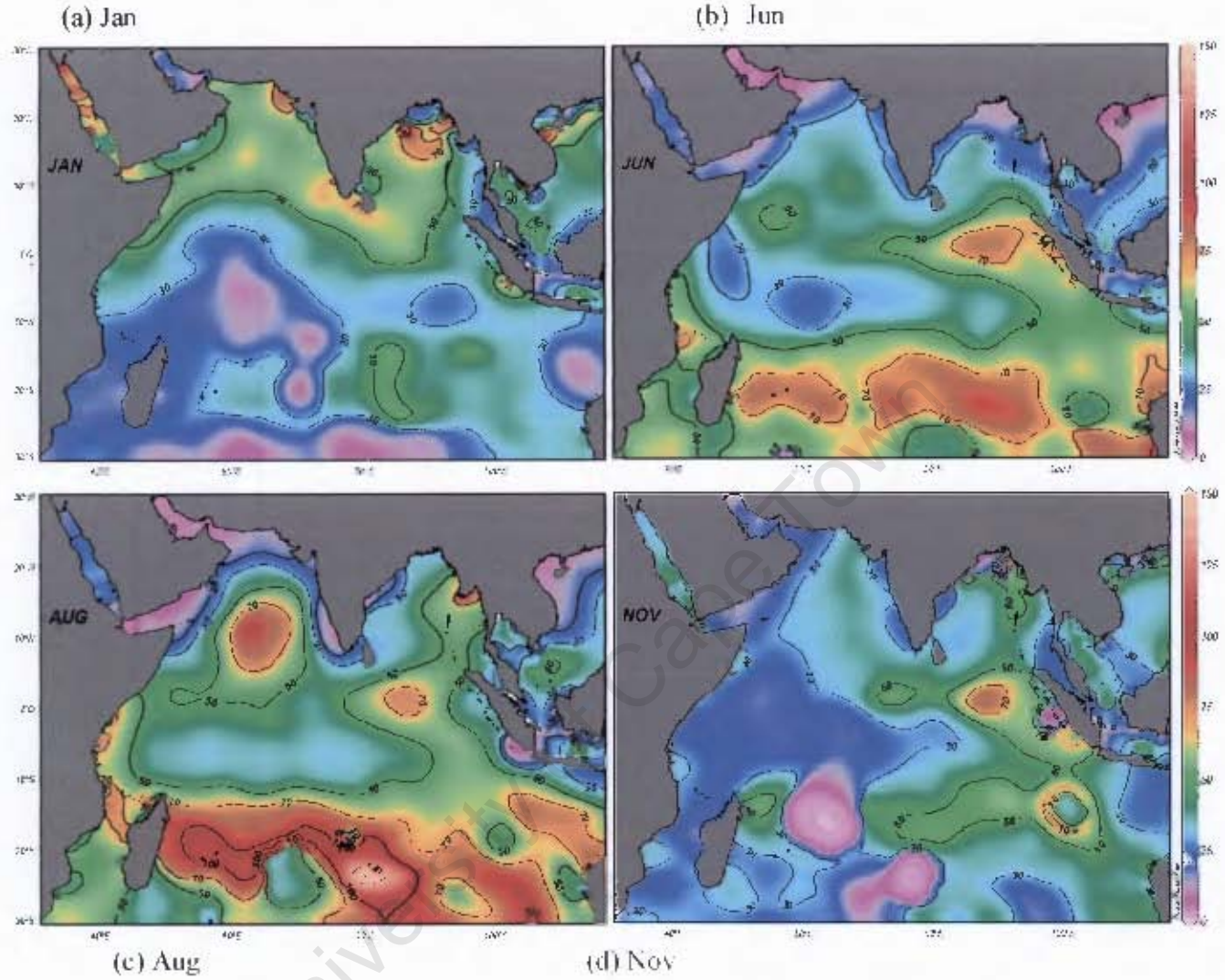

Figure 2.5: Mixed-layer depths for a) January, b) June, c) August and d) November (From Monterey and Levitus, 1997).

Measurements were made in the equatorial Indian Ocean during spring and summer 1979 from the East African coast to 62°E in the interior of the western basin. The detailed vertical profiles of horizontal current show that the energetic dominance throughout the region of variability was on vertical scales of several hundreds of metres, confined to within a few degrees of the equator, as observed in 1976. The near-surface equatorial circulation responded directly to variations in the

wind field, and satellite-tracked drifter buoys showed the equatorial surface jet extending across the width of the ocean. The zonal velocity fluctuations extended in a consistent pattern over the observation region. The time and meridional scales of the variability were similar to those observed in 1976, suggesting that the velocity field is dominated by long term, equatorially trapped motions with long zonal scales.

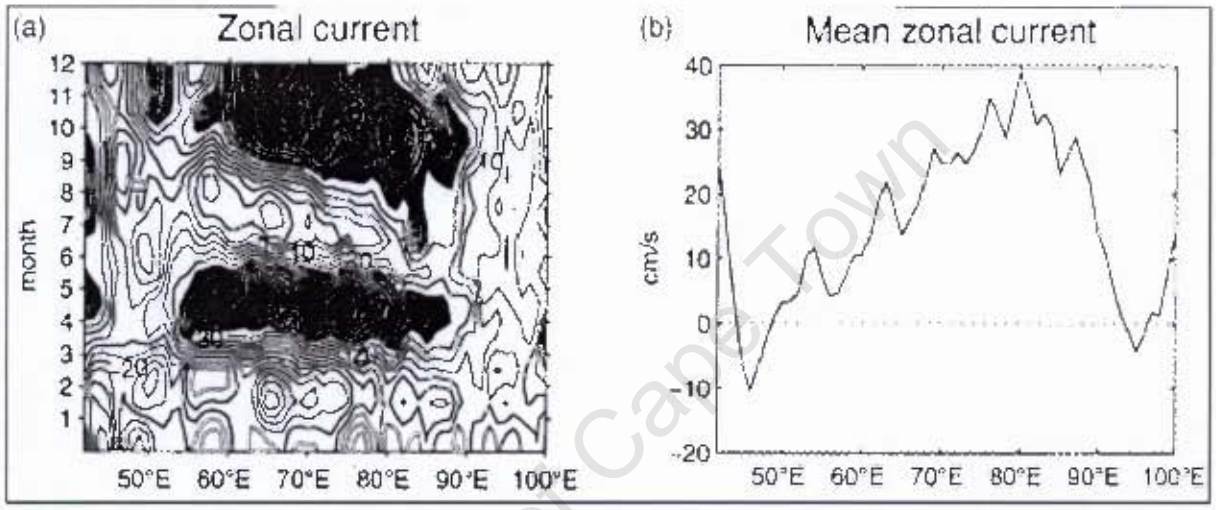

Figure 2.6: Longitude-time Hovmöller plots of zonal currents in the 1°S-1°N latitude band, showing the (a) total current; and (b) annual mean (After, Han et al., 1999).

A number of modelling studies have sought to identify the forcing mechanisms of the Wyrtki Jets, and to assess their relative importance. In his original work, Wyrtki (1973) suggested that the eastward jets are forced directly by the equatorial westerlies between the two monsoons. Shortly after, O'Brien and Hurlburt (1974) used a 2-layer model to demonstrate that a strong eastward jet does develop as a direct response to switched-on westerlies. They also noted that Rossby waves reflected from the eastern boundary of their model basin were an important part of the equatorial response that tended to cancel the directly forced eastward jet two months after the wind onset. They also observed the width of the transient current to be 500 kilometres, consistent with a value explained from theory to be twice the baroclinic equatorial radius of deformation.

Based on a current record obtained near Gan Island (0°41'S, 73°10'E), part of the Maldives, Knox (1976) and McPhaden (1982) confirmed the importance of direct wind forcing. Knox (1976) determined further that the pressure gradient term was a significant part of the zonal momentum balance at Gan, indicating the importance of remote forcing by propagating equatorially trapped waves. McPhaden (1982) later noted the presence of signals with vertical phase propagation there, an almost certain indicator of wave propagation.

2.7 CROSS EQUATORIAL CELL (CEC)

In the Indian Ocean, there are two types of meridional overturning cells, the deep overturning cell involving deep water transport into the basin from the south and the shallow overturning cell that involves shallower circulations that carry thermocline water from subduction zones in the southern Hemisphere to upwelling regions north of the equator. In this study, we will be concentrating mainly on the shallow overturning cells since the northward flowing thermocline Somali current forms part of the shallow overturning cell. Shallow overturning cells also exist in the tropical-subtropical Atlantic and Pacific Oceans. They consist of subduction in the subtropics, upwelling in the tropics and the circulations that connect the two regions. In contrast to the Atlantic and Pacific Oceans, significant upwelling does not occur along the equator in the Indian Ocean, but predominantly occurs in the Northern Hemisphere off Somalia, Oman and India and in the thermocline ridge northeast of Madagascar; the subduction regions are largely confined to the Southern Hemisphere. Thus, this Indian Ocean cell necessarily involves currents that cross the equator, and for this reason we refer to it as the 'Cross-Equatorial Cell'.

The surface branch of the Cross-Equatorial Cell is largely Ekman transport. As indicated by the wind stress distribution (Figure 2.0), the meridional Ekman transports on both sides of the equator are southward during southwest monsoon and northward during the winter monsoon, and hence one expects a seasonally reversing meridional

cell. In the mean, the shallow cell connects the subduction areas in the southern subtropics and parts of the Indonesian Through flow waters with the upwelling areas of the northern hemisphere via the cross-equatorial Somali Current. Its near-surface branch includes a shallow equatorial roll (Miyama et al., 2003) that is seasonally reversing. The northward cross-equatorial flow at thermocline depth occurs as part of the Somali Current, and the southward upper-layer return flow is carried by Ekman transport in the ocean interior directed southward in both hemispheres. The meridional transports in the CEC demonstrate marked monsoon variability.

2.8 Summary and motivation

This review has highlighted previous research that has already been carried out in the study area by several authors relating to the ocean circulation patterns and the monsoon wind variability on an intra-seasonal to seasonal time scale. The preceding sections (introduction and literature review) have exposed the various knowledge gaps that still linger in the study area. It is hoped from this work that a better understanding of the western boundary currents of the Indian Ocean and in particular the EACC and the Somali Current will be achieved. Much work has been done in the Somali basin, however, due to sparse observational data; a lot of study still needs to be done to better understand the interacting processes that take place.

The recently available decade of satellite altimetry and scatterometer data such as the *merged dynamic altimetry topography data*, has made it possible to carry out model studies that were hitherto difficult or near impossible to validate due to sparse data. It is now possible to validate or verify almost any area of the Indian Ocean upper surface processes using the plethora of recently available data. Furthermore, a better understanding of the Regional Ocean Modelling System (ROMS) hind-cast techniques, and how well it replicates the ocean processes within the study area (10°N - 15°S; 38°E - 65°E) would enhance East African capacity in ocean modelling of the region.

CHAPTER 3

Data and Methodology

A regional ocean model (ROMS) is used in this study to investigate the Somali basin variability. Details of the model physics and configuration are given in the first part of the chapter. The COADS, NCEP and AVISO datasets used in this study are discussed in the second part of this chapter. The third part of the Chapter gives an overview of the methods used. The fourth part highlights some useful variables and formulations that are considered important in this study.

3.1 Ocean Model

3.1.1 Regional Ocean Modelling System (ROMS)

ROMS is a free-surface, terrain-following, primitive equations ocean model widely used by the scientific community for a diverse range of applications (e.g., Haidvogel et al., 2000; Marchesiello et al., 2004; Peliz et al., 2003; Penven et al., 2001, 2005, 2006; Di Lorenzo, 2003; Warner et al., 2005, b; Wilkin et al., 2005; Colberg and Reason, 2006), however, not much work has been done in the current study area of Somali basin using this model. ROMS solves the primitive equations in an Earth-centered rotating environment, based on the Boussinesq approximation and hydrostatic vertical momentum balance

The algorithms that comprise ROMS computational nonlinear kernel are described in detail in Shchepetkin and McWilliams (2003, 2005). ROMS includes accurate and efficient physical and numerical algorithms and several coupled models for biogeochemical, bio-optical and sediment applications. It also includes several vertical mixing schemes (Warner et al., 2005).

For computational economy, the hydrostatic primitive equations for momentum are solved using a split-explicit time-stepping scheme which requires special treatment and coupling between barotropic (fast) and baroclinic (slow) modes. A finite number of barotropic time steps, within each baroclinic step, are carried out to evolve the free-surface and vertically integrated momentum equations. In order to avoid the errors associated with the aliasing of frequencies resolved by the barotropic steps but unresolved by the baroclinic step, the barotropic fields are time averaged before they replace those values obtained with a longer baroclinic step. A cosine-shape time filter, centred at the new time level, is used for the averaging of the barotropic fields (Shchepetkin and McWilliams, 2005). In addition, the separated time-stepping is constrained to maintain exactly both volume conservation and consistency preservation properties which are needed for the tracer equations (Shchepetkin and McWilliams, 2005). Currently, all 2D and 3D equations are time-discretized using a third-order accurate predictor (Leap-Frog) and corrector (Adams-Molton) time-stepping algorithm which is very robust and stable. The enhanced stability of the scheme allows larger time steps, by a factor of about four, which more than offsets the increased cost of the predictor-corrector algorithm.

In the vertical, the primitive equations are discretized over variable topography using stretched terrain-following coordinates (Song and Haidvogel, 1994). The stretched coordinates allow increased resolution in areas of interest, such as thermocline and bottom boundary layers. In the horizontal, the primitive equations are evaluated using boundary-fitted, orthogonal curvilinear coordinates on a staggered Arakawa C-grid. The general formulation of curvilinear coordinates includes both Cartesian (constant metrics) and spherical (variable metrics) coordinates. Coastal boundaries can also be specified as a finite-discretized grid via land/sea masking.

ROMS has various options for advection schemes: second- and forth-order centred differences; and third-order, upstream biased. The latter scheme is the model default and it has velocity-dependent hyper-diffusion dissipation as the dominant truncation error (Shchepetkin and McWilliams, 1998). There are several sub-grid scale parameterizations in ROMS. The horizontal mixing of momentum and tracers can be

along vertical levels, geopotential (constant depth) surfaces, or isopycnic (constant density) surfaces. The mixing operator can be harmonic or bi-harmonic. Haidvogel and Beckmann (1999) have an elaborate overview of all these operators.

The vertical mixing parameterization in ROMS can be either by local or non local closure schemes. The local closure schemes are based on the level 2.5 turbulent kinetic energy equations by Mellor and Yamada (1982) and the Generic Length Scale (GLS) parameterization (Umlauf and Burchard, 2003). The non local closure scheme that has been used for this study is based on the K-profile, boundary layer formulation by Large et al. (1994). The K-profile scheme has been expanded to include both surface and bottom oceanic boundary layers. The GLS is a two-equation turbulence model that allows a wide range of vertical mixing closures, including the popular k-kl (Mellor-Yamada level 2.5) scheme. Several stability functions (Galperin et al., 1988; Kantha and Clayson, 1994; Canuto et al., 2001) have been also added to provide further flexibility. A recent study (Warner et al., 2005) evaluated the performance of these turbulence closures in ROMS in terms of idealized sediment transport applications. In addition, there is a wave/current bed boundary layer scheme that provides the bottom stress (Styles and Glenn, 2000) and sediment transport which become important in coastal applications.

Currently, the air-sea interaction boundary layer in ROMS is based on the bulk parameterization of Fairall et al. (1996). It was adapted from the Coupled Ocean-Atmosphere Response Experiment (COARE) algorithm for the computation of surface fluxes of momentum, sensible heat, and latent heat. This boundary layer is used for one or two-way coupling with atmospheric models.

ROMS has extensive pre- and post-processing software for data preparation, analysis, plotting, and visualization. The entire input and output data structure of the model is via Network Common Data Forms (Netcdf) which facilitates the interchange of data between computers, user community, and other independent analysis software.

3.1.2 ROMS Model Configuration

The main run of the ROMS model analysed in this dissertation is a climatological simulation of ten years with a parent grid defined by 10°N to 15°S and 38°E to 65°E at a resolution of 1/3 of a degree and 32 vertical levels of which more than 15 levels are concentrated in the upper ocean. This run will be for establishing the climatology of the domain area under study. The ten-year climatological simulation is used to investigate the intra-seasonal to seasonal variations and coastal ocean processes that occur in the East African coastal ocean (hereafter, Somali basin).

This run is forced with the Comprehensive Ocean-Atmosphere Datasets (COADS) monthly climatological marine surface data of Da Silva et al., (1994). The initial and lateral boundary conditions are derived from the World Ocean Atlas (Conkright et al., 2002) and COADS marine monthly climatology datasets.

The run will be primarily to establish the semi-annual to annual variability that prevails in the Somali basin by use of altimetry data for validation. COADS climatological wind stresses and SSTs will be used to compare the model simulation with observations and how well they replicate the monsoon induced coastal ocean processes.

3.2 Datasets

In recent years, winds, wind stresses and air-sea fluxes have become available from atmospheric forecast models at diurnal or even higher resolution, such as from the European Centre for Medium-range Weather Forecast (ECMWF), the UK Meteorological Office (UKMO), the US National Centres for Environmental Prediction (NCEP), and the Fleet Numerical Meteorology and Oceanography Centre (FNMOC). In the following, we use the COADS wind stresses and surface heat fluxes to discuss overall patterns of variability and as model forcing for the ROMS, comparing them with other products in particular areas of interest. A new method of measuring winds that has become available during the past decade is satellite scatterometry from the

Quickscat satellites (e.g., Halpern et al., 1998), and we will show inter-comparisons between intra-seasonal to seasonal variability of these winds and NCEP.

The data to be used in this research includes NCEP Re-analysis datasets of SST and wind stress. COADS surface marine seasonal climatology wind stress data and heat fluxes (Da Silva et al., 1994) will be used to force the ROMS model. SSH AVISO data will be used to reproduce some sea level features of the East African coastal ocean. The World Ocean Circulation Experiment data, if available, may be used in this study to validate the model output. AVISO data will also be used to reproduce the surface geostrophic currents in the Somali basin and to consequently validate the model output.

3.2.1 NCEP/NCAR Project

The NCEP/NCAR Reanalysis Project is a joint project between the National Center for Environmental Prediction (NCEP) and NCAR, the National Center for Atmospheric Research, (Kalnay et al., 1996). This effort involves the recovery of land surface, ship, rawinsonde, pibal, aircraft, satellite, and other data; quality controlling and assimilating these data with a model data assimilation system that is kept unchanged over the reanalysis period. This eliminates perceived climate jumps (anomalies) associated with changes in the model data assimilation system.

These data are gridded with a resolution of 2.5 by 2.5 degrees. Four different levels of data are available. Level A is strongly influenced by observed data and is the most reliable level of data. Level B has observational data that is greatly influenced by the Reanalysis process. Level C data is not reliable since the variables are solely derived purely from the model fields. Level D represents a field that is obtained from climatological values and thus does not depend on the model. NCEP/NCAR reanalyzed data are used in various sections of this study.

3.2.2 COADS Surface Marine Data

The surface marine atlas series presents objectively analyzed fields of surface marine climatology and anomalies of fluxes of heat, momentum, and fresh water along with several other parameters of interest. These fields are derived from individual observations in the Comprehensive Ocean-Atmosphere Data Set (COADS) from January 1945 to December 1989 and are analyzed on a 1-degree-by-1-degree global grid. Corrections have been made to reduce wind speed bias associated with an erroneous Beaufort equivalent scale, to quality control night-time fractional cloud cover observations according to the brightness of the sky, and to assign clear weather to certain present weather observations recorded as missing.

3.2.3 AVISO ALTIMETRY DATA (SSALTO/DUACS)

The geostrophic surface current velocity and Sea Surface Height data used to verify the ROMS model output were produced from satellite altimeter data provided by SSALTO/DUACS and distributed by AVISO (http://www.aviso.oceanobs.com/) with CNES support. The model validation data to be used for this study will be mainly from the DUACS (Data Unification and Altimeter Combination System) which is part of the CNES multi-mission ground segment (SSALTO). This database is a result of merged observations from all altimeter missions: Jason-1, TOPEX/Poseidon, ENVISAT, GFO, ERS1/2 and even EOSAT. This achieves a spatial and temporal resolution of 1/3 degree and seven (7) days in global coverage. Poleward of 5°N and 5°S, the zonal and meridional geostrophic velocity components (u,v) are calculated, respectively, from the meridional and zonal slopes of the dynamic height derived from the Sea Level Anomalies (SLA).

In the 2°N-S equatorial band, where geostrophy is subject to singularity, velocities are calculated using second derivatives of ζ (sea surface setup) according to Picaut (1989) and Lagerloef, et al. (1999). The Absolute Dynamic Topography used in the calculations of u and v are obtained by adding sea level anomalies (SLA) to the Mean Dynamic Topography (MDT), which is obtained from the Mean Surface Height (MSH) subtracted from the standard geoid.

DUACS provides a consistent and homogeneous catalogue of products for varied applications, both for near real time applications and offline studies such as this current study. Developed and operated by CLS, it started as an European Commission Project (Developing Use Of Altimetry for Climate Studies), funded under the European Commission and the Midi-Pyrénées regional council. It has been integrated to the CNES multi-mission ground segment SSALTO in 2001, and it is maintained, upgraded and operated from CNES. At the beginning of 2004, DUACS was redefined as the Data Unification Altimeter Combination System (SSALTO/DUACS: User Handbook, 2004).

3.3 Methods

3.3.1 Statistical Software (MATLAB™)

This is the main tool of analysis used to perform all the model output analysis. This is a powerful tool for manipulating model output data in any given format such as Netcdf, ASCII or binary data, but in this case the ROMS output is in Netcdf format. It can be used to perform model output statistics (MOS) and also plot the data graphically in temporal and spatial scales. All the necessary spatial plots are done through programming scripts written for this purpose.

3.3.2 Wavelet analysis

Many time series in geophysics (e.g. Meteorology and Oceanography) exhibit non-stationarity in their statistics. While the series may contain dominant periodic signals, these signals can vary in both amplitude and frequency over long periods of time. The simplest method for analyzing non-stationarity of a timeseries would be to compute statistics such as the mean and variance for different time periods and see if they are significantly different.

Wavelet analysis attempts to solve the statistical limitations of time and frequency localization by decomposing a time series into time/frequency space simultaneously. One gets information on both the amplitude of any "periodic" signals within the series, and how this amplitude varies with time.

In this study, the Morlet wavelet transform is preferred. This "wavelet" has the advantage of incorporating a wave of a certain period, as well as being finite in extent. The Morlet wavelet is nothing more than a Sine wave (green curve in Figure 3.1b) multiplied by a Gaussian envelope (red curve).

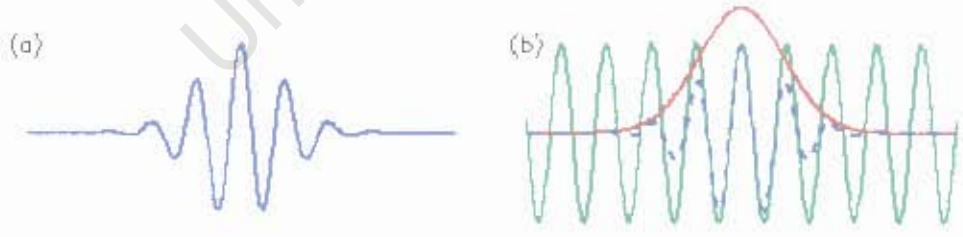

Figure 3.1: (a) Morlet wavelet of arbitrary width and amplitude, with time along the x-axis. (b) The construction of a Morlet wavelet (blue dashed, After Torrence and Compo, 1998).

One can then vary the "scale" of the wavelet by changing its width. This is the real advantage of wavelet analysis over the other methods such as Fast Fourier Transform (FFT). The wavelet analysis always uses a wavelet of the exact same shape, only the size scales up or down with the size of the window

In practice, the Morlet wavelet shown in Figure 3.1a is defined as the product of a complex exponential wave and a Gaussian envelope:

(Equation 3.1) . . . . . $\Psi(t) = \pi^{-1/4} e^{i\omega_o t} e^{-t^2/2}$,

Where *Psi* (Ψ) is the wavelet value at non-dimensional time *(t)*, $i = (-1)^{1/2}$ and w_o is the wave number, which is chosen large enough to ensure that Ψ(*t*) satisfies the admissibility condition.

The scaled Morlet wavelet is defined as:

(Equation 3.2) . . . . . $\Psi_{\tau,a} = \frac{1}{a}\Psi_o\left\{\frac{t-\tau}{a}\right\}$

where a>0 is the dilation parameter used to change the scale (Frequency localization), and τ is the translation parameter used to slide in time (time localization). The factor of $1/a$ *in equation 3.2* is a normalization to keep the total energy of the scaled wavelet constant.

With a given geophysical data time series X, with values of x_t, at time index t, the wavelet transform $\Psi_{\tau,a}$ is just the inner product (or convolution) of the wavelet function with our original time series.

In this study, the Morlet wavelet transform is applied to investigate the temporal variability of signals prominent in the upper ocean of the Somali basin. In addition de-trended time series plots are also used to demonstrate the semiannual to annual variations of strong and weak signals in the basin.

3.4 ANALYSED VARIABLES and OCEANIC PROCESSES

In this section, a brief outline is given of some of the fundamental variables that are of importance to this work. In particular, geostrophic currents, wind stress, and Sverdrup balance are discussed herein.

3.4.1 Wind Stress

Wind stress (kg m^{-1} s^{-2} or Newton m^{-2}) is an important driving force for coastal and upper ocean currents. To estimate surface wind stress, τ at each grid point, the bulk formulation is used:

Equation 3.3 ..... $\tau = (\tau_x, \tau_y) = \rho C_D W(u, v)$;

Where W, is the surface wind speed, u is the zonal component (eastward) of wind velocity and v is the meridional component (northward) of wind velocity. The surface wind is assumed to be parallel to the stress vector. ρ is the density of surface air often assumed constant at 1.225 kg/m^3 and C_D is the drag coefficient.

The magnitude of the wind stress is:

Equation 3.4 ..... $|\tau| = \rho C_D W^2$

There have been many estimates of C_D as apparent in Figure3.1. The drag coefficient chosen by the WOCE community and largely used in calculation of $|\tau|$ is the one recommended by Smith (1988) and is a function of observed wind speed. The 10m neutral coefficient formulation over the ocean is

Equation 3.5 ..... $C_D = a + b \times W$

The values of *a*, and *b* are determined for each wind speed range. The behavior of C_D as a function of wind speed is shown by Figure 3.1. The main known drag coefficients are also presented. Typical values for drag coefficient are between: $C_d = 1.5 \times 10^{-3}$ and $C_d = 0.5 \times 10^{-3}$ (Figure 3.1).

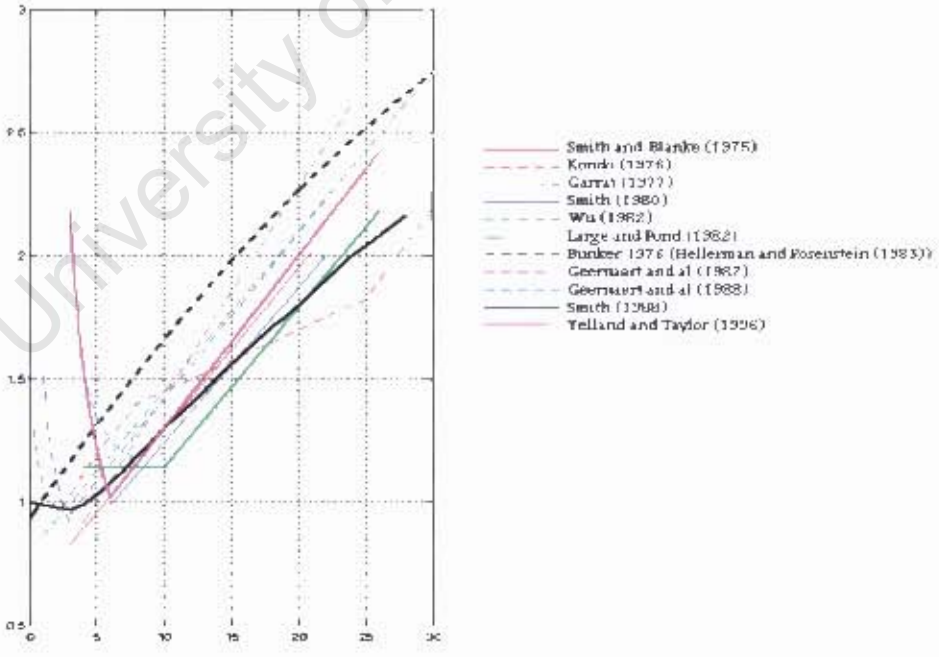

Figure 3.2: Comparison between various drag coefficients (dimensionless) versus wind speed (m/s)

3.4.2 Geostrophic currents

Geostrophic approximation is used to obtain the horizontal currents for the AVISO SSH datasets. This method needs to be applied with care close to the equator where the Coriolis parameter disappears and the geostrophic formulation does not hold. For the model, this is resolved by the extrapolation of the currents outside an equatorial band (2°S - 2°N) to get an approximation of the equatorial currents. For the AVISO datasets, this is achieved by using a formulation developed by Lagerloef et al., (1999). He found that the geostrophic velocity near the Equator can be computed with a β-plane approximation (f= βy) and is given as:

Equation 3.6..... $\beta U_b + \beta y \frac{\partial U_b}{\partial y} = ig \frac{\partial Z}{\partial y}$

Where $i = \sqrt{-1}$ is a complex number; $\beta = \partial f / \partial y$ and U_b denotes the geostrophic velocity near the Equator.

On the Left Hand Side (LHS), the second term is generally neglected near the equator ($y \approx 0$). At some distance away from the equator, the conventional f-plane geostrophic calculation is used, denoted as fu_g.

Equation 3.7 ..... . $fu_g = -\frac{1}{\rho}\frac{\partial p'}{\partial y}$; where u_g is the geostrophic current and p' is the perturbation pressure.

3.4.3 Sverdrup solution for the wind-driven circulation

The Sverdrup's relation assumes that there is zero velocity in the deep water or that the ocean bottom is level and that the friction there is small compared with that at the surface.

The Sverdrup relation is defined as follows:

Equation 3.8 ..... $M_y = \frac{1}{\rho\beta} curl_z \tau_\eta$

Where, M_y is the meridional mass transport, $\beta = \frac{\partial f}{\partial y}$ is variation of Coriolis parameter with latitude and $curl_z \tau_\eta = \frac{\partial \tau_y}{\partial x} - \frac{\partial \tau_x}{\partial y}$ is the z-component of wind stress curl.

CHAPTER 4

RESULTS

4.0 ROMS Climatological Diagnosis of the Western Indian Ocean

ROMS is an adaptable model which is used to study mesoscale high-resolution ocean processes occurring at high frequency such as the diurnal tides or as a regional ocean model covering an entire basin. In this section of this chapter, we investigate the Indian Ocean variability that occurs within the Somali basin. As discussed earlier in the Introduction and later in the Methods section, the various circulations in the East African coastal upper ocean are modelled from monthly (intra-seasonal) to seasonal timescales using ROMS.

In this section, sea surface height (SSH), sea surface temperature (SST) and geostrophic horizontal velocities are diagnosed from the ROMS simulation. The seasonal development of currents in the Somali basin was described in the preceding chapters; in this section, the ability of the ROMS model to reproduce the major surface and sub-surface features of the Somali basin is discussed.

4.1 Somali Basin Surface Circulation

During January to March (JFM), the northeast monsoon is fully developed and the northeasterly winds off the East Africa coast cause the near-surface Somali current to flow southwards across the equator where it merges with the EACC that flows equatorward to about 2-4°S. This confluence between the southward flowing Somali current and the EACC results in the eastward moving South Equatorial Counter Current (SECC) in the 2 - 6°S latitudinal band. The model output of figures 4.1 (a), (b), (c), and (d) demonstrate this circulation quite well. Figure 4.1(a) shows some prominent eddies that could be the result of the Northern Equatorial Current near 3°N that feeds into the eddy. The eddies seem to be trapped in the SECC; they are quasi-stationary with a length scale of about 300 - 400km.

The eddy flow pattern is anti-cyclonic and as a result has elevated sea surface heights (Figure 4.2). The SECC will be discussed in detail in subsequent sections. At this time of the year, the model shows a diminished surface Somali current flowing southwards with a net speed of approximately $0.5ms^{-1}$ with an undercurrent flowing northwards between the 150-200m depth with speeds comparable to the surface current (Figure 4.3 and Figure 4.4). The flow pattern of the Somali basin during this time is also reproduced in the kinetic energy, SST and SSH maps (Figure 4.2).

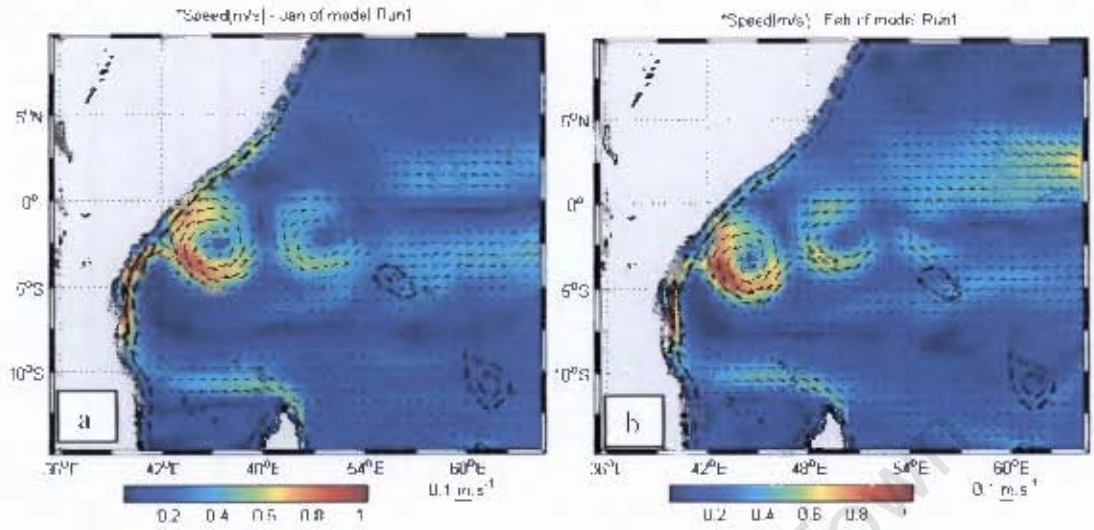

Figure 4.1: (a) Somali basin Mean Current speeds $\sqrt{u^2 + v^2}$, in ms^{-1} for the month of January with the surface current vectors overlaid; and (b) as (a) but for the month of February.

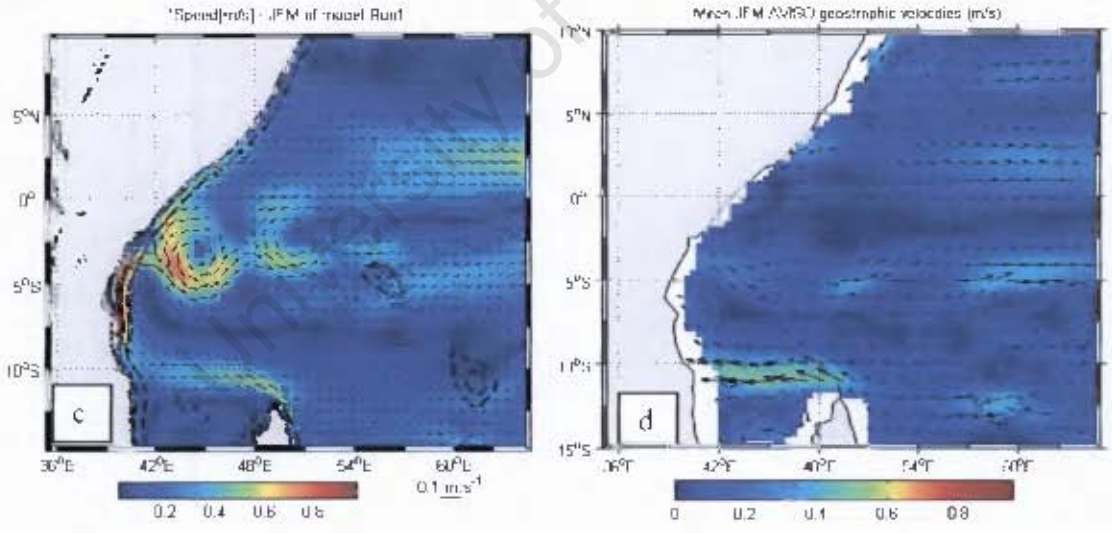

Figure 4.1: (c) Somali basin current speeds (ms^{-1}) for March (The dashed contours in ROMS figures represent the 500 and 1000m isobaths); (d) the AVISO mean state geostrophic velocities (ms^{-1}) for the Jan-March period.

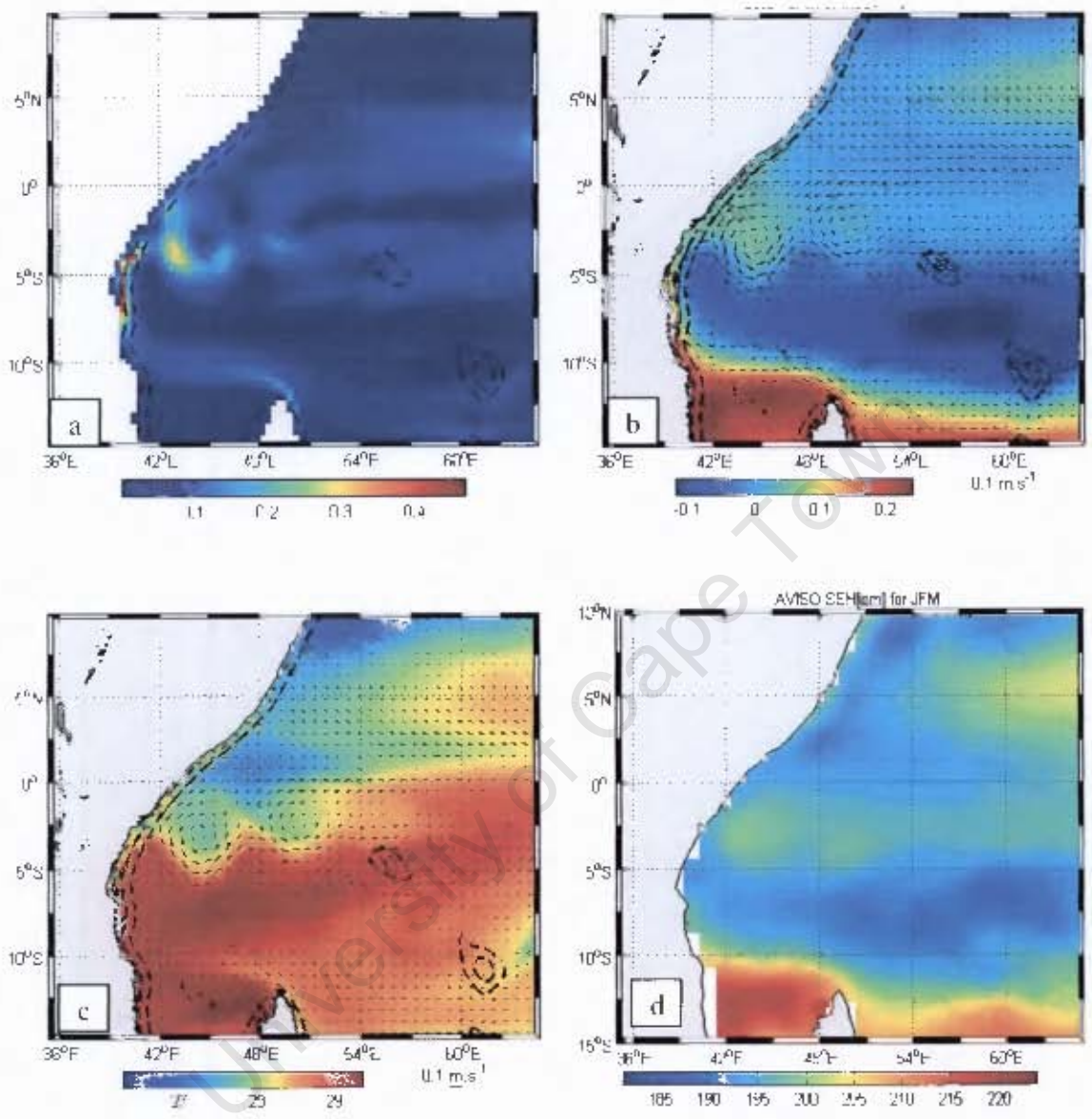

Figure 4.2: (a) Kinetic energy,(m^2s^{-2}) of Somali basin for the JFM season; (b) Model simulated Sea Surface elevation in metres (shading) with model surface currents overlaid; (c) Model simulation SST (°C) and (d) AVISO Sea surface Height (cm) mean climatology for JFM. The anti-cyclonic eddies north of 5°S are visible in the altimetry map above. Isobaths of 500m and 1000m are shown in the ROMS panels.

During JFM, kinetic energy of $0.35m^2s^{-2}$ associated with the anti-cyclonic eddies is apparent in the ROMS simulation (Figure 4.2a) and is marked by raised SST and SSH apparent in the datasets (Figure 4.2b - d). The EACC is also marked by high kinetic energy values ($0.4m^2s^{-2}$). It is noteworthy that the southern domain is marked by raised SSH (220cm) and the northern domain with lower values of SSH (185cm).

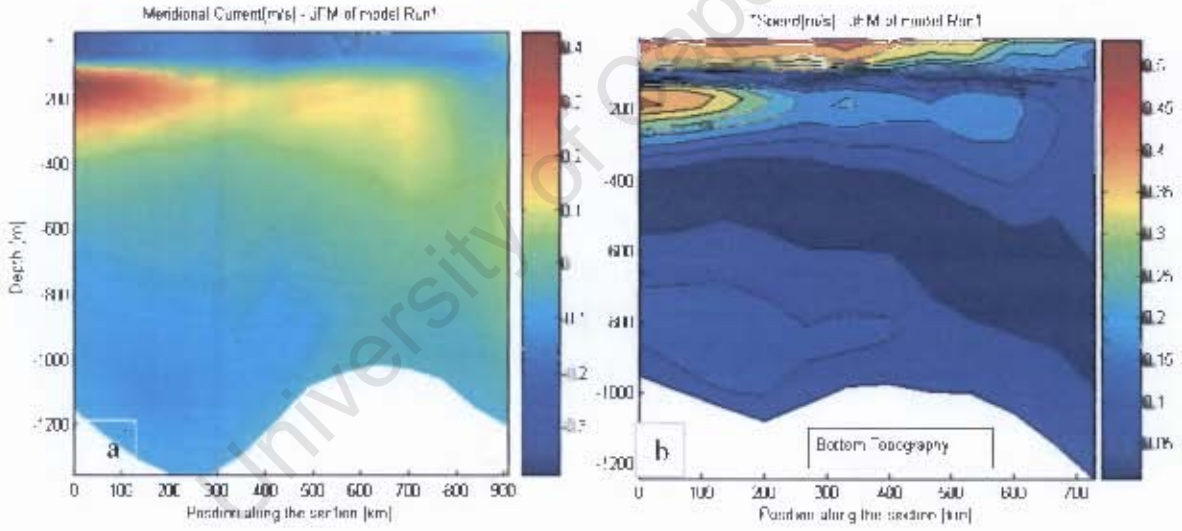

Figure 4.3: (a) Vertical section from 0° to 5°N along the meridional component of the Somali current showing the southward (negative) surface current and the northward (positive) flowing under-current (ms^{-1}) for the JFM season; (b) same as (a) but for the current speed ($\sqrt{u^2 + v^2}$).

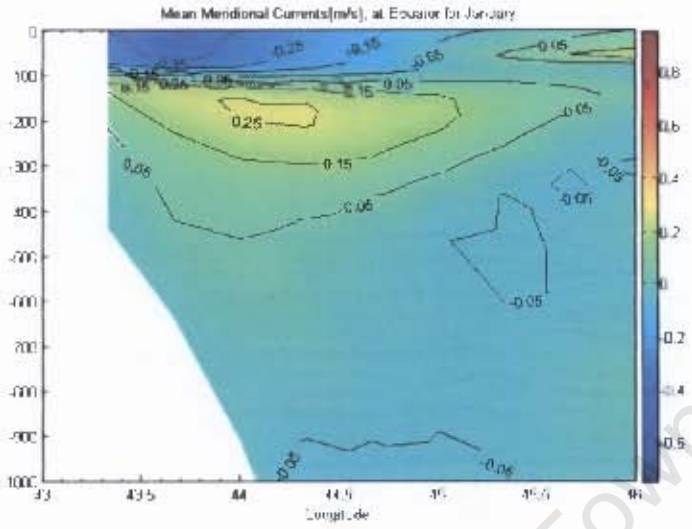

Figure 4.4: Vertical section at 0°N, 43°E- 46°E of the cross-equatorial Somali Current (ms^{-1}) for January. The contour interval is 0.10 ms^{-1}.

In boreal spring (April-May), the model shows (Figure 4.5) that the Somali current speeds are reduced to about 0.1ms^{-1} in April but rise sharply to 0.6ms^{-1} in May (i.e. in a matter of a few weeks), which is the transition period of the monsoon. At this time of the year, the southern branch of the Somali Current is an extension of the EACC that is fed by the North East Madagascar Current (NEMC), a branching off of the westward flowing SEC (Schott et al., 2001). The ROMS simulation shows that the path of the SEC is more irregular due to the effects of the underlying topography (Figure A1) and Rossby waves (Schott and McCreary, 2001). In addition, the ROMS simulation reveals little seasonal variability in the SEC location; however, its magnitude (zonal component) shows strong semi-annual and annual variations (Figure 4.5c).

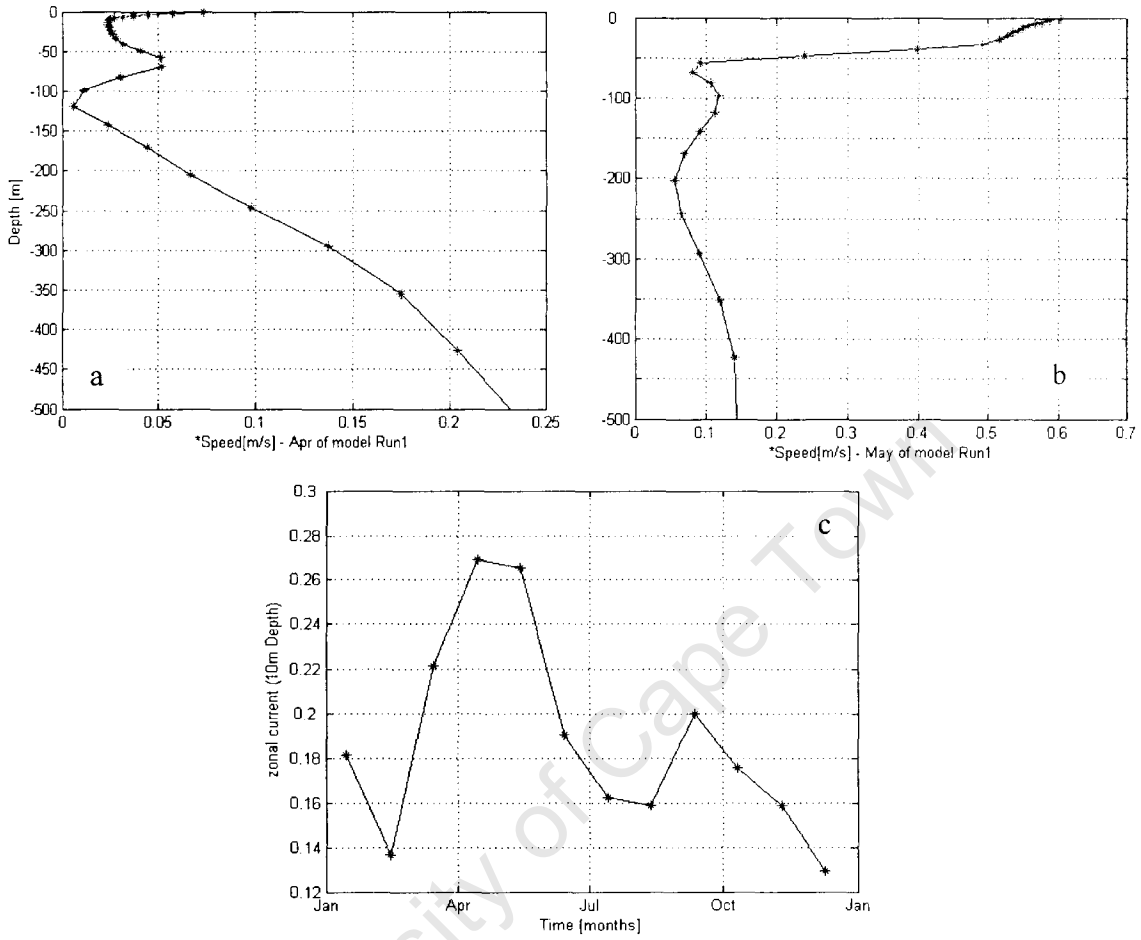

Figure 4.5: The Vertical profile of the Somali Current speeds (ms^{-1}) at 4°N, 47.5°E for the months of: (a) April (b) May. The profiles show that the current is strongest within the first 200m depth of the Ocean, (c) Annual cycle of the zonal component of the SEC.

A special feature in this monsoon transition period (boreal spring) is the Wyrtki jets which have a maximum current speed (~60cms^{-1}) in May, they are clearly visible as eastward flow in the 2°S-2°N equatorial band starting near 54°E (Figure 4.6b). However, the strong parts of the Jet are further offshore in the 70°E to 90°E zone, which is outside the model domain of this study.

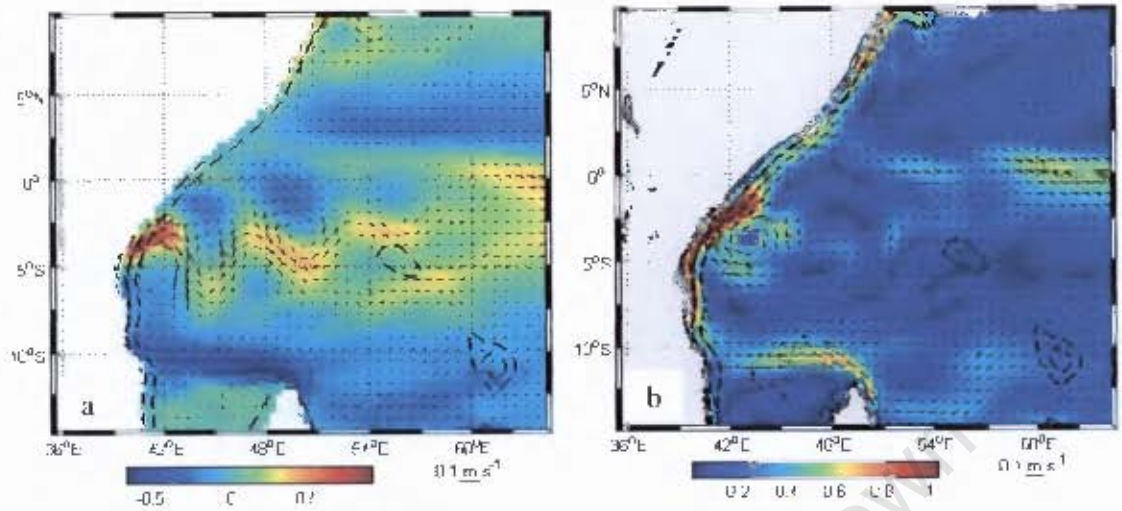

Figure 4.6: Somali basin current speeds (ms^{-1}) for (a) April; (b) May with the Wyrtki jet clearly visible along the 2°N-2°S band, after 60°E.

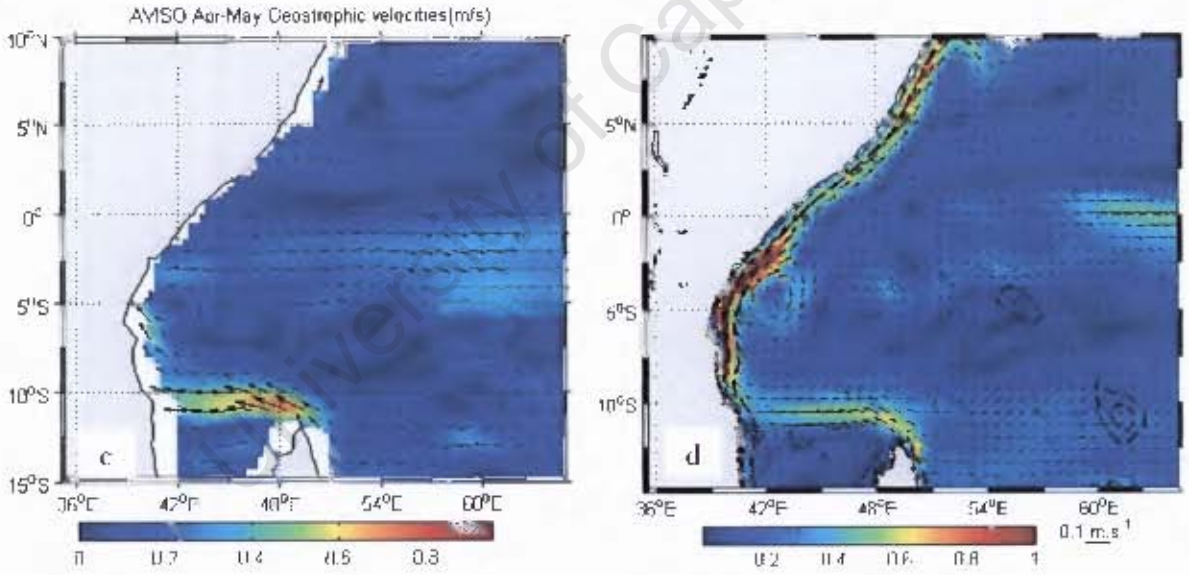

Figure 4.6: (c) AVISO geostrophic velocities (ms^{-1}) for April-May period; and (d) Run1 speed (m/s) with the surface velocities overlaid. The EACC is strong with values of up to 1.2m/s current speed. The boundary current is clearly in early stages of development in Run1; however, the AVISO product has a 50km data gap next to the continent and islands due to land contamination of the satellite radiometer.

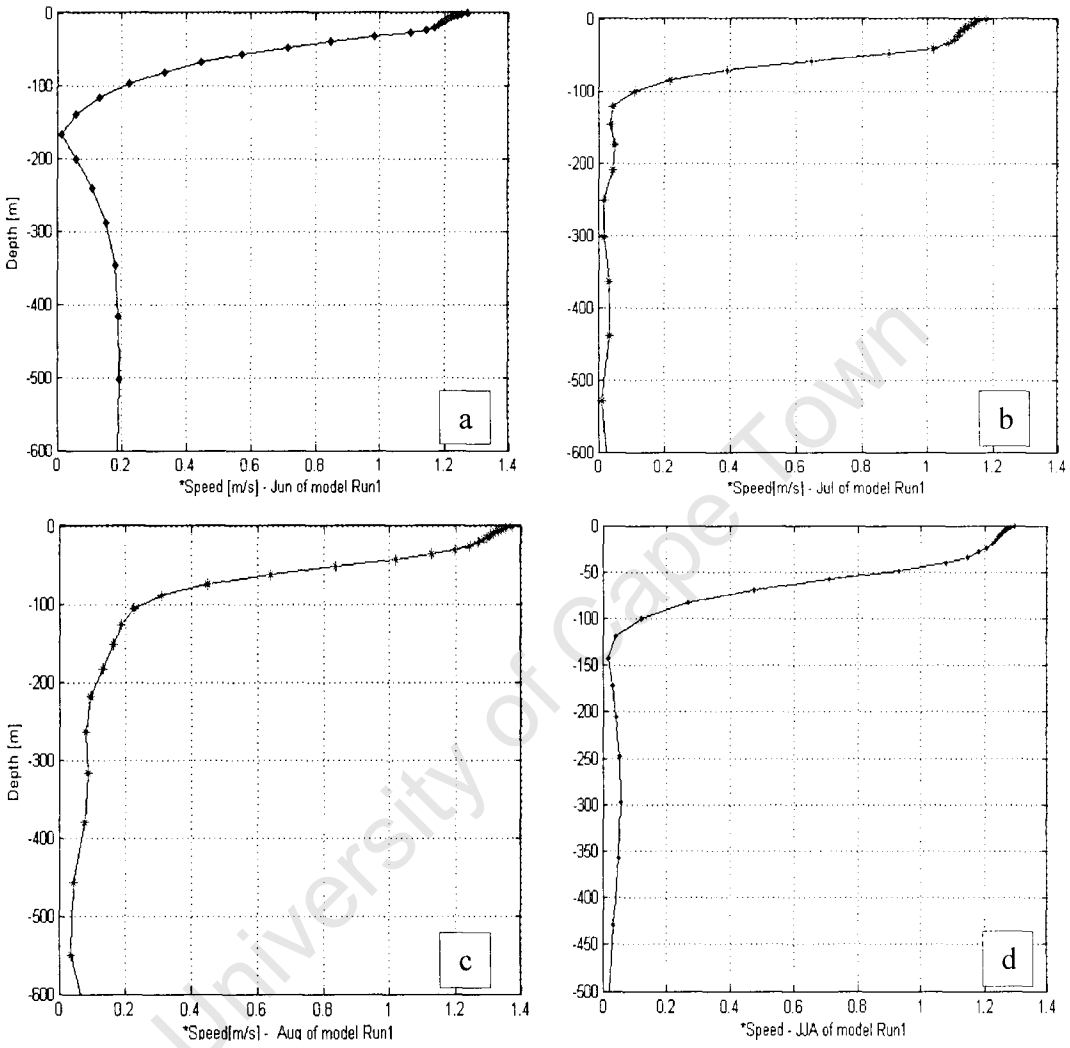

Figure 4.7: Somali Current vertical profiles mean speed (ms^{-1}) for the month of: (a) June at 3°N, 47°E; (b) July at 3°N, 47°E; (c) August at 3°N, 47°E and (d) JJA at 3°N,47°E.

The model simulation indicates that the Somali Current has speeds of well over 1ms^{-1} during the peak Southwest monsoon season of July-Sept. (JAS). This model current is comparable in magnitude to that observed by Schott et al (1997) and compares well with the geostrophic currents derived from the Merged Absolute Dynamic Topography (MADT) AVISO altimetry data (Figure 4.8). However, figures 4.7(a), (b), (c) and (d), indicate that the Somali current is mostly a surface current, occurring in the upper 200m of the ocean, which is in agreement with the findings of Wacogne and Pacanowski (1996). In their study, the GFDL model indicated that the flow below the 150m depth is always northward; the ROMS model indicates a similar northward flow of 0.05ms^{-1} apparent in the depth below 200m.

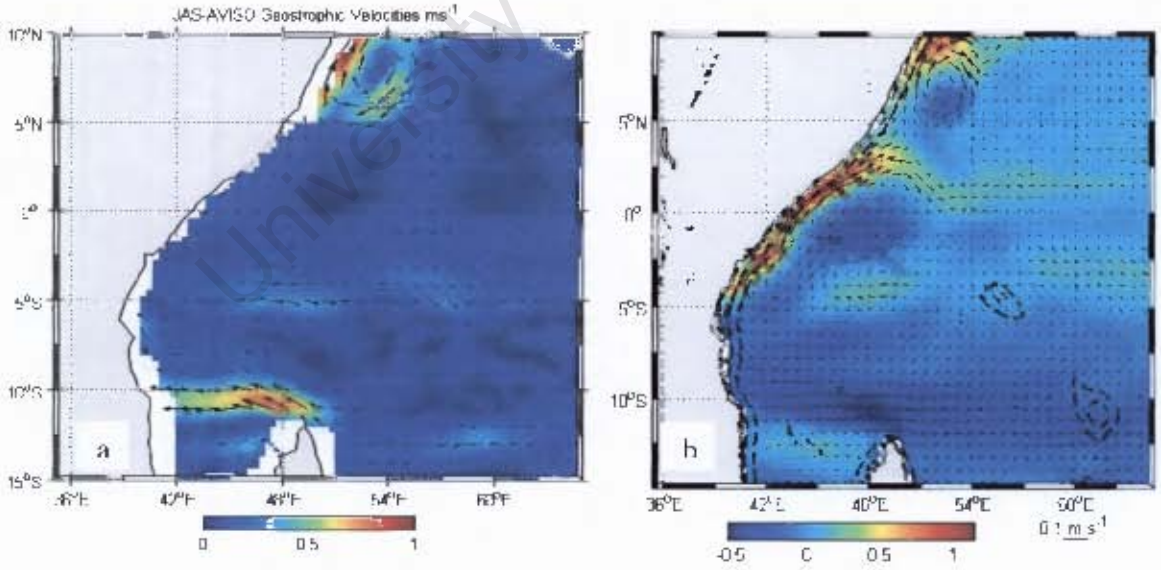

Figure 4.8: (a) Mean AVISO geostrophic velocities (ms^{-1}) for JAS, (b) Mean JAS surface currents (ms^{-1}) from Run1

The baroclinic Somali current and the Great Whirl that occurs between 5°N to 10°N in the boreal summer are well reproduced in the model simulation and compare fairly well with the AVISO Merged Absolute Dynamic Topography (MADT) products (Lagerloef et al., 1999), as seen in figure 4.8(a). After crossing the equator, one part of the Somali Current turns offshore at about 4°N forming a cold upwelling wedge on its left shoulder whereas the other branch recirculates across the equator as the Southern Gyre (Figure 4.8a and b). A second gyre forms near 7°N and is the Great Whirl (GW). Both gyres are well reproduced in the ROMS simulation (Figure4.8b) and compare well with those in Schott et al (2001). As discussed earlier, Levitus (1988) found that during the Southwest summer monsoon, the Ekman flow is directed southward on both sides of the equator, suggesting that there is a southward flow of surface water across the equator in the interior of the ocean.

The Somali Current has been found to be markedly baroclinic; that is, there is a strong variation of velocity with depth associated with horizontal density gradients which comes into being in a matter of a few weeks after the winds over the northern Indian Ocean change to the Southwest Monsoon pattern (Lighthill, 1969). Undercurrents have been observed under the Somali Current during different times of the year (see Figure 4.3a,b , Figure 4.4 and Figure 4.9 a, b). Figure 4.7(c) is a vertical profile of the Somali Current between 2° - 4°N and shows that the Somali current achieves its maximum strength of 1.4m/s in the month of August, with a mean of 1.2m/s in the months of June, July and August.

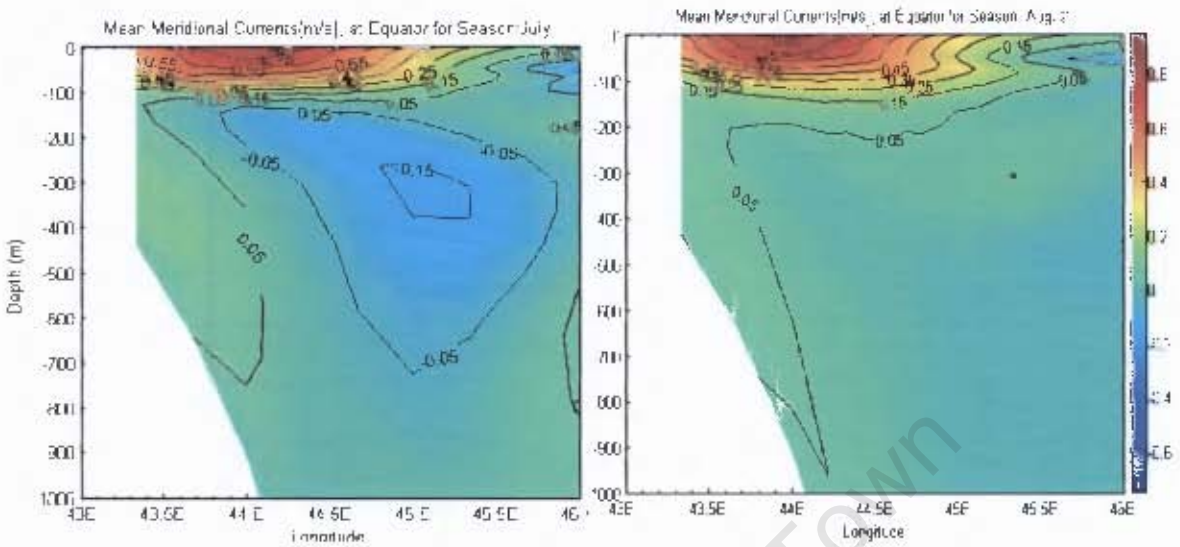

Figure 4.9: (a) Vertical profiles of the Meridional component of the Somali Current (*v*) at 0°N, 43°E-46°E, in July with an undercurrent just below the surface current; and (b) Same as (a) but in August. The contour interval is 0.05 ms^{-1}.

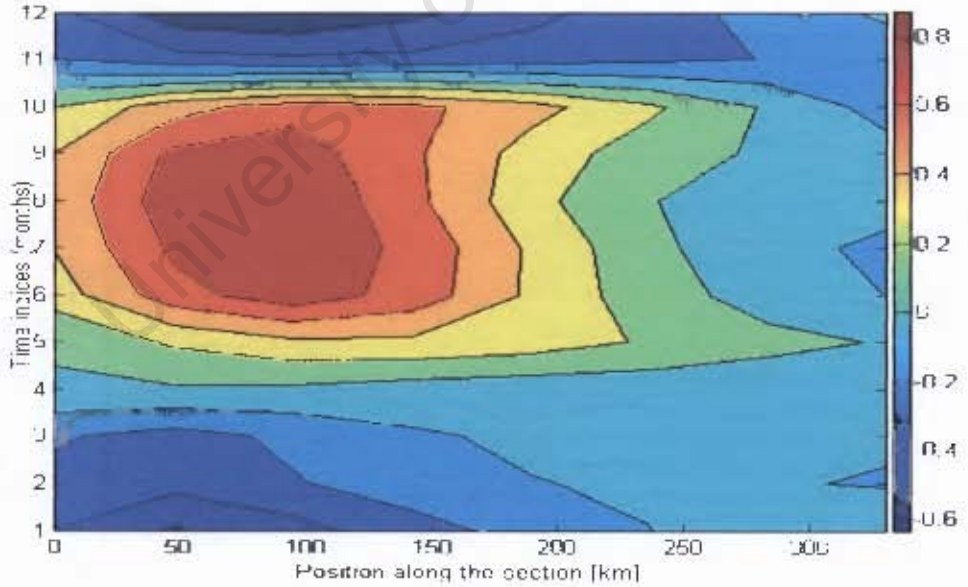

Figure 4.10: Hovmöller section of the meridional component of surface Somali Current crossing the Equator between 43°E - 46°E. The monsoon transition period is in cyan (April/May and October/November), the Somali current (red) during the Southwest monsoon and the Northwest monsoon season (deep blue). Contour interval is 0.2ms^{-1}.

The ROMS model Hovmöller plot (Figure 4.10 and Figure 4.11) compares well with the annual cycle of the monsoon system of the Indian Ocean (Tomczak et al., 1994). It clearly shows a semi-annual variation in the surface to sub-surface flow of the Somali basin. The Somali Current is clearly visible during June-October (the Southwest monsoon period) and is northward flowing. During the northeast monsoon between December to March, the current is southward flowing. During the monsoon transition months of May and November (Figure 4.10), a weakening of the Somali current is apparent.

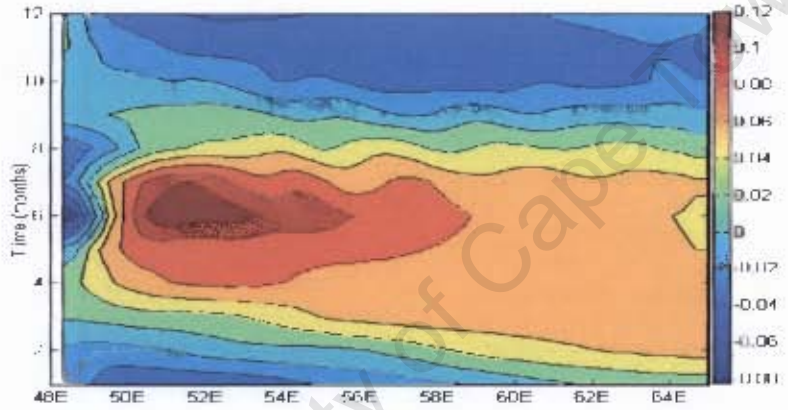

Figure 4.11: Hovmöller of the model sea surface elevation at 5°N. The contour interval is 0.02m.

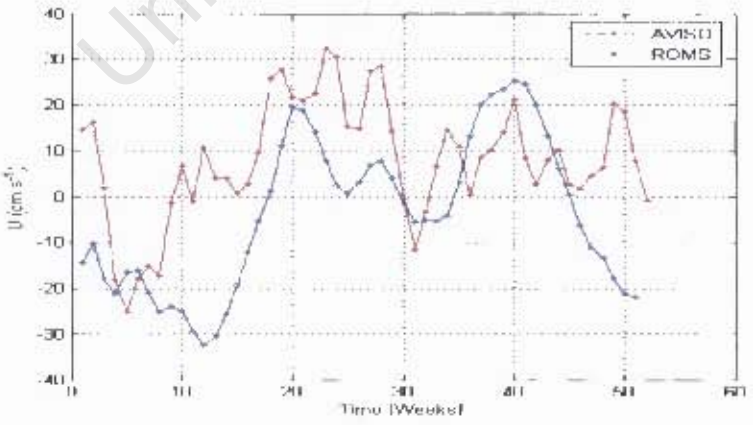

Figure 4.12: Time series of zonal component of surface currents along the equatorial band 1S-1N averaged between 44°E–53.33°E for (Blue) ROMS model and (Red) AVISO geostrophic velocity altimetry data.

The time series of AVISO and ROMS surface currents (Figure 4.12) indicate that though the model and observed variability pattern do not match perfectly, the amplitudes of the zonal current for the two datasets are comparatively similar. The AVISO dataset is the annual mean averaged over an eight-year period between 1996 and 2004 whereas the model data represents a ten-year climatological monthly mean. A wavelet analysis of the two datasets is presented in figure 4.13.

From figure 4.12 and figure 4.13 it is apparent that the zonal current (u) has a semi-annual oscillation with two main peaks, one near the 20th week (May) and one near the 40th Week (October), the transition periods of the monsoon. These peaks reflect the Wyrtki jets. Between the 20th and 30th week, the AVISO dataset shows a short duration eastward (positive) zonal current burst of about 20cms^{-1} that lasts for a few weeks. The model displays a similar single burst around the 20th week. This variability in both datasets is apparent in the frequency-power spectrum of figure 4.13. The wavelet analysis shows a strong intra-seasonal and seasonal signal in both datasets. The ROMS power spectrum (lower panel) shows a weak intra-seasonal signal with a periodicity of 8-weeks and a strong seasonal signal at a periodicity of nearly 26-weeks.

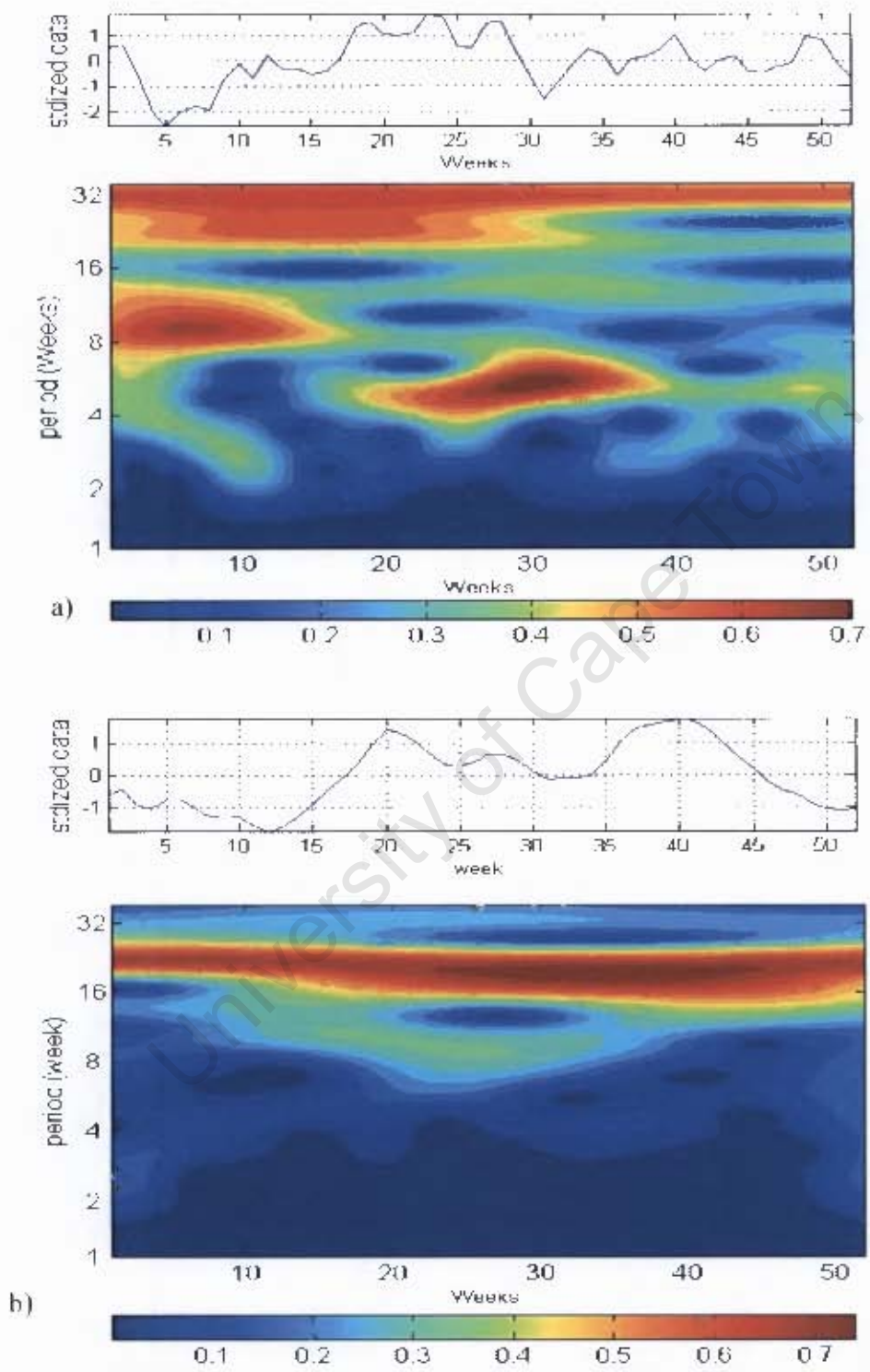

Figure 4.13: Continuous Wavelet analysis for zonal current for figure 4.12 data; (a) Upper panel shows the normalized data for AVISO and (b) The lower panel shows the power spectrum of the ROMS dataset (Melice et al., 2001 and Morlet, 1983).

4.1.1 The South Equatorial Counter Current (SECC)

The SECC is a Somali basin near-surface current that is only apparent during the boreal winter monsoon and not in the boreal summer. This seasonality is in contrast to the SECC in the Pacific and Atlantic that tend to persist throughout the year implying that it is one aspect of the Indian Ocean circulation patterns that come to existence mostly due to the monsoon trade wind reversals. During the boreal winter monsoon, the northward EACC and the reversed (southward) Somali Current cause a confluence between 2°- 3°S at the western boundary (Dueng and Schott, 1978) that merges into an eastward-flowing counter-current, the SECC (Figure 4.14). The SECC has been well defined in the western ocean by hydrographical sections and drifting-buoy currents (Figure 4.15, Lumpkin et al., 2005). The ROMS simulation of the SECC shows that it is constrained to 3°- 6°S and flows eastward across most of the Indian Ocean. Indeed, in the basin interior it is still visible as a continuous band across the Indian Ocean and has been seen to extend up to 95°E in the ship survey of Hacker et al (1998). According to the NOAA/AOML satellite tracked monthly drifter current maps (Figure 4.15); the SECC is best developed in February when it forms a continuous band across the Indian Ocean. However, the model simulation indicates that the current is at a maximum in January. The NOAA/AOML monthly surface current maps are in general agreement with the ROMS simulation of the SECC.

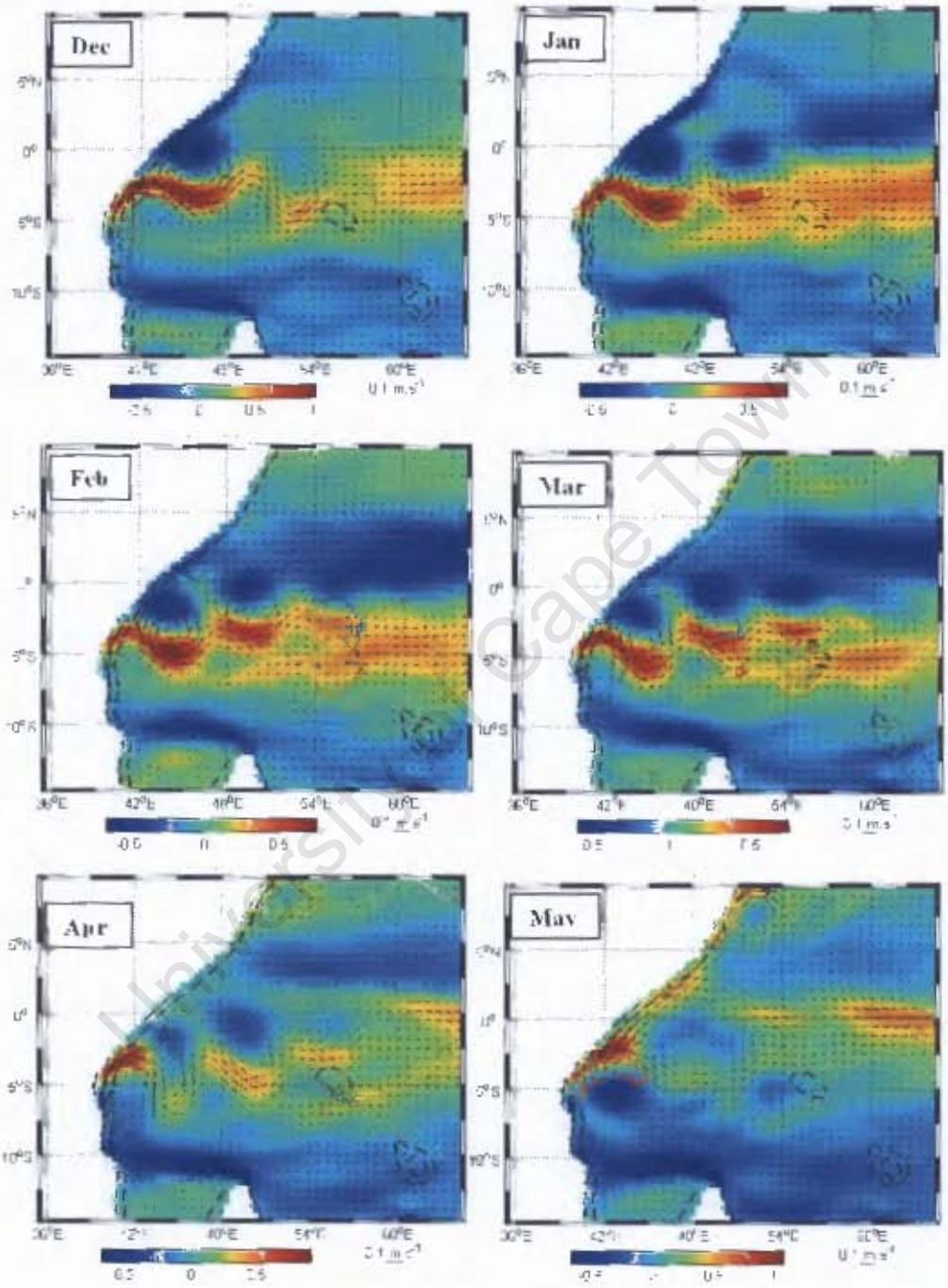

Figure 4.14: (a) SECC speed (ms^{-1}) monthly mean evolution during boreal winter and the transition.

The SECC is visible near 5°S in the NOAA/AOML drifter maps (Figure 4.15) during January to April flowing east with approximate speeds of 50cms^{-1} (0.5ms^{-1}), similar values are apparent in the ROMS simulation. Indeed, from the model evolution maps (Figure 4.14a), the current appears to join the equatorial jet near the equator in May at about 60° - 65°E.

A time series of a section of the SECC (Figure 4.14b) shows the zonal component of the current to display strong semi annual and annual variations whereas the meridional component has a more prominent variation at the higher frequencies and a relatively weak annual cycle. The Morlet wavelet transform (Figure 4.14c) reveals a moderate signal near 32 days during JFM and November-December seasons, and a strong signal is apparent between 64 and 128-day period for SOND. A strong signal with a 256-day period is also apparent in the analysis.

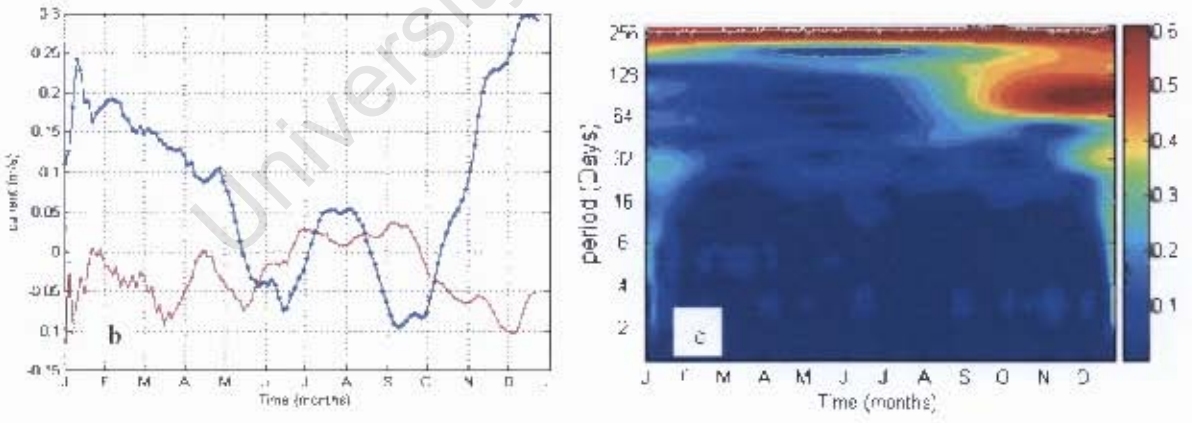

Figure 4.14: (b) Time series of zonal (blue) and meridional (red) components of the SECC in region: 1.85-5.50°S and 44°-53.33°E. and (c) Morlet wavelet transform of the SECC.

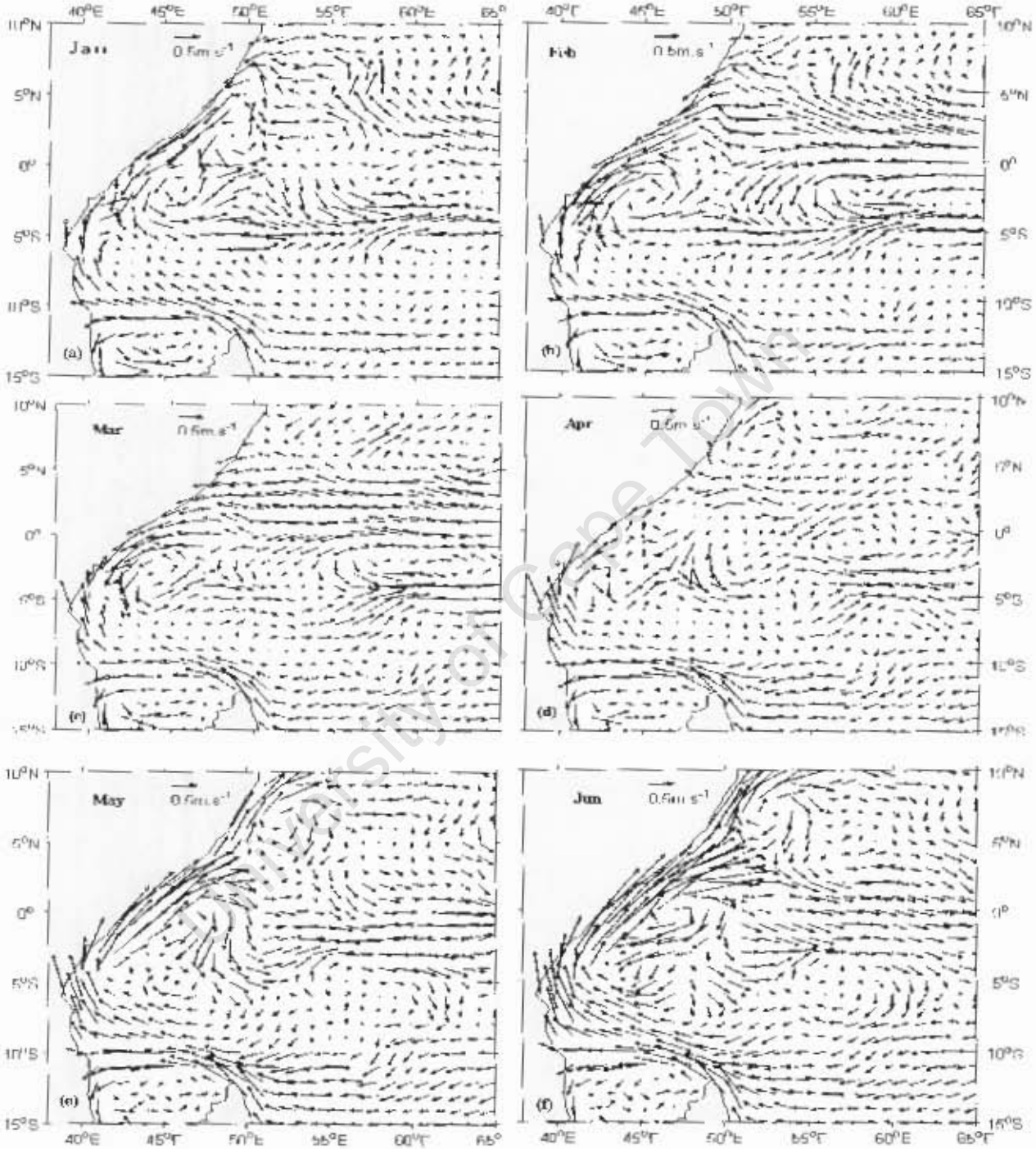

Figures 4.15: (a– f) Monthly mean surface current vectors based on a 1° square grid analysis of NOAA/ AOML satellite tracked surface drifting buoys which corresponds to January to June drifter surface currents. (Redrawn from, Lumpkin et al., 2005)

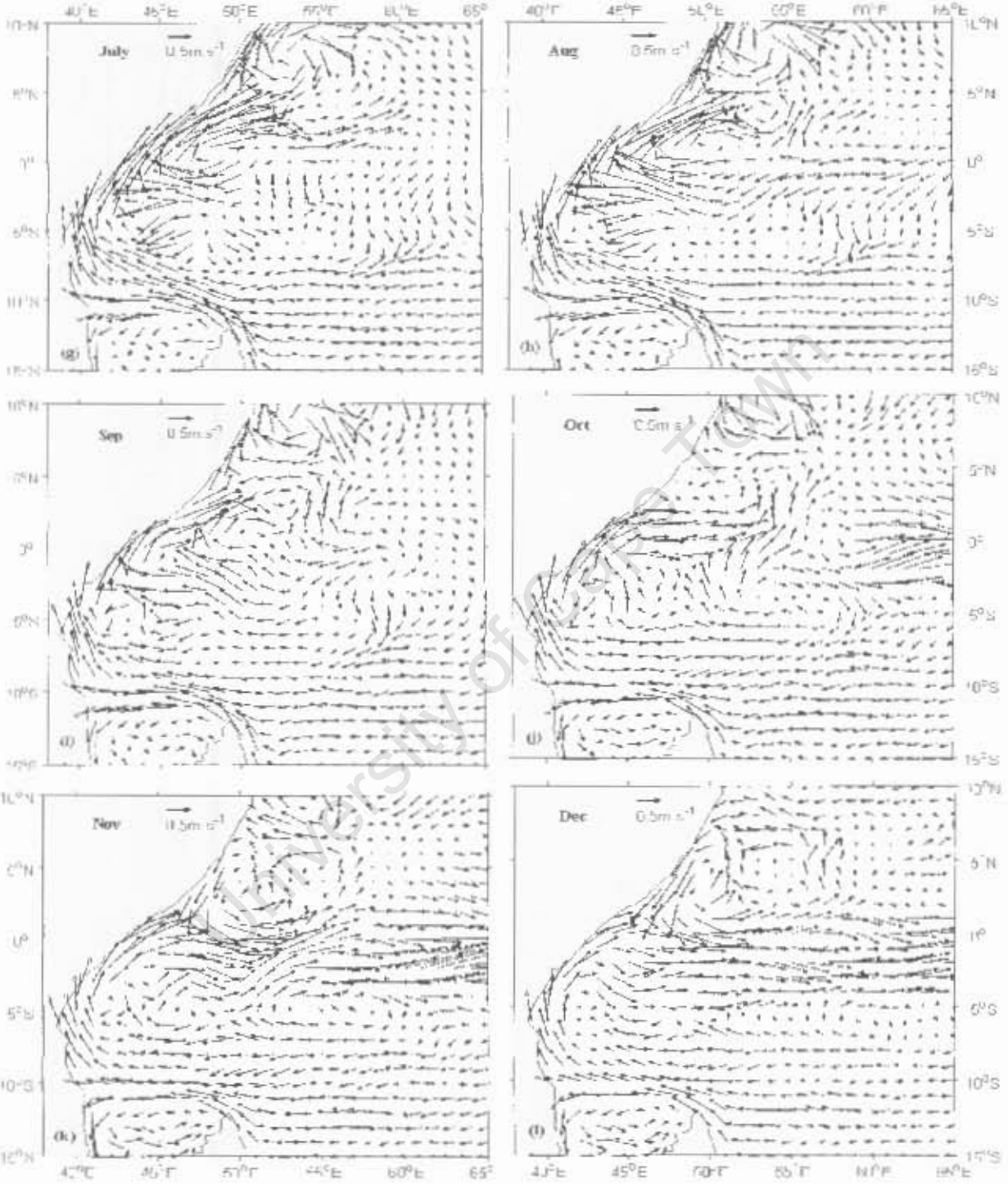

Figures 4.15: (g-l) Monthly mean surface current vectors based on a 1°- square grid analysis of NOAA/AOML satellite tracked surface drifting buoys which correspond to July to December drifter surface currents. (After Lumpkin et al., 2005)

4.1.2 Equatorial Jets

Wyrtki (1973) described an equatorial surface jet in the Indian Ocean which flows eastward during both transition seasons. He demonstrated that in April and May the jet is fed at its western origin at a rate of 13 Sv, in general agreement with the model results of Figure 4.16(a, b) which shows an eastward volume transport of between 5 and 10Sv in May and 15Sv by November. The ROMS model shows (Figure A2: Appendix I) thermocline doming in the 5 -12°S region. The region south of the equator (5°S-10°S) experiences possible open ocean upwelling as a result of Ekman divergence in the southern tropical gyre as well as Rossby wave propagation (Hermes and Reason, 2007). From the time - distance SSH plot (Figure 4.16f), it is apparent that during the transition months of April/May and November/December, the general trend is that of low SSH on the western boundary and a gradual rise of the same as one moves eastwards. This is a reflection of the jets as they transport mass from the western side of the basin towards the east with the subsequent shoaling of the thermocline on the western side and deepening to the east. Wyrtki (1973) observed a vertical lifting of the 20°C isotherm from 120m depth in April to 85m depth in early June.

Equatorial jets of between $0.3ms^{-1}$ and $0.6ms^{-1}$ are apparent from figure 4.16 (c) and (d). The panels indicate that the jets flow eastward with a flow centred on the equatorial axis in May but a slight southern shift by November. A time series plot of the zonal component of surface current at 0°, 62°E, indicates that the monsoon transitions, May and November are the months with maximum zonal flow (Figure 4.16e).

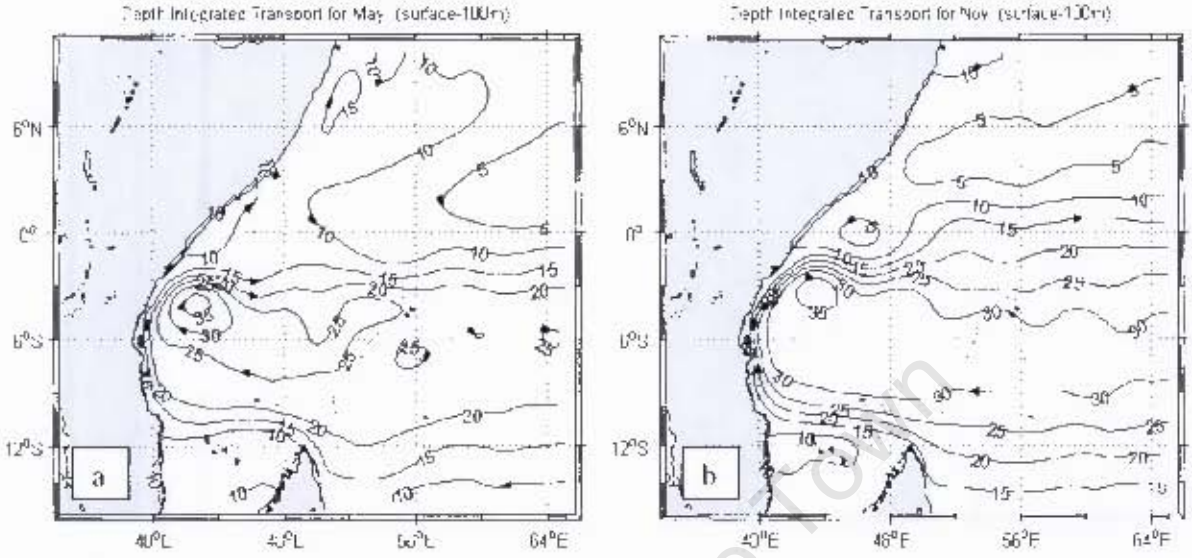

Figures 4.16: ROMS volume transport function ($1Sv=10^6 m^3 s^{-1}$) for the transition months of: (a) May and (b) November. The contour interval is 5Sv.

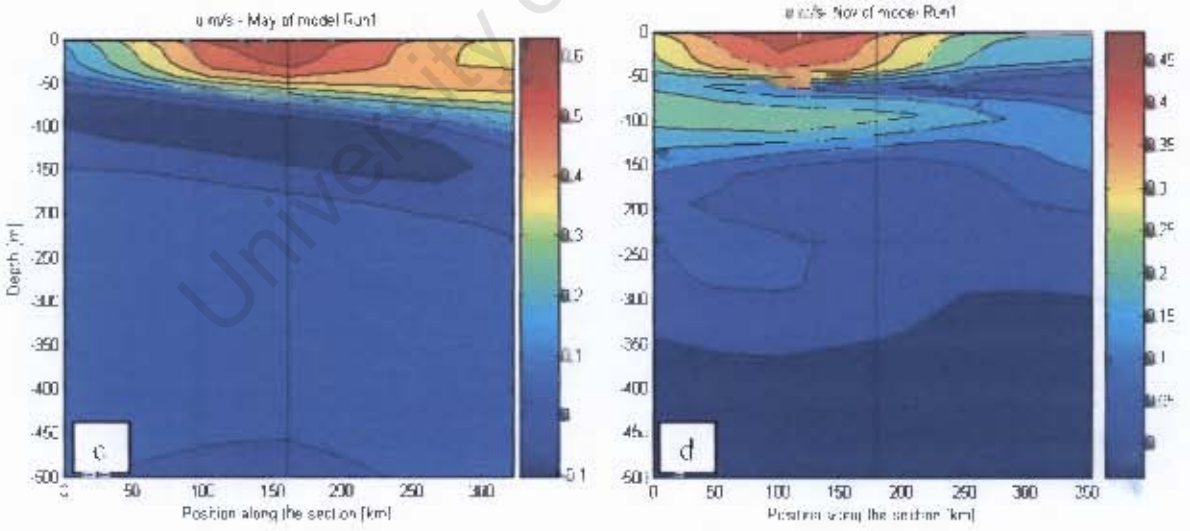

Figure 4.16: (c, d) Depth-Latitude cross sections of the zonal current along the equator at the 62°E longitude. Equatorial jets of $0.6ms^{-1}$ are apparent. Positive values of u (ms^{-1}) are eastward and negative westward. The black line marks the equator (left of black line is South).

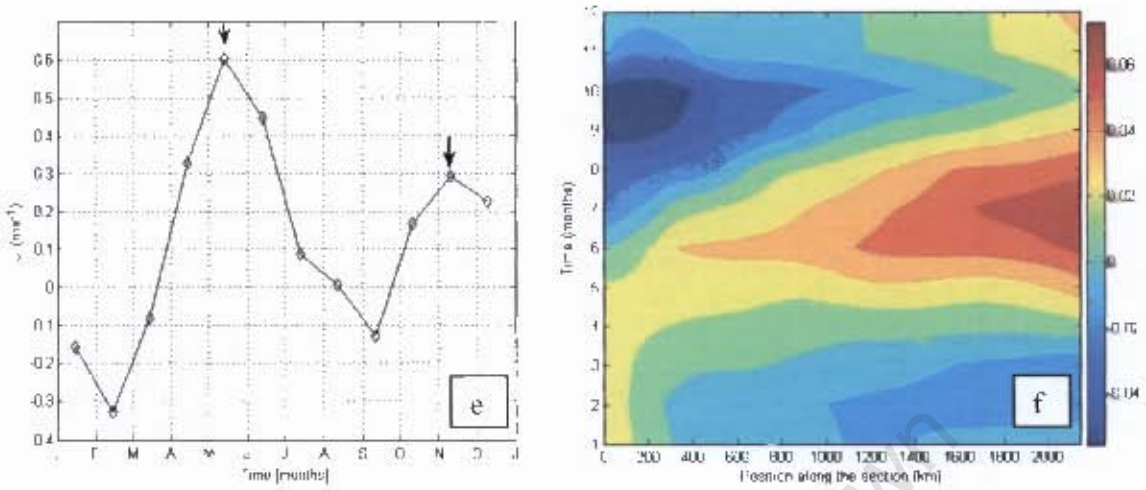

Figure 4.16: (e) Time series of the zonal component of surface current at 0°, 62°E, showing May and November maximums for the *U* (m/s) ; (f) Time-Distance Hovmöller plot of SSH (m) along the Equator (0°, 43-62°E) showing gradual rise in SSH towards the east.

4.2 Volume Transport of the Somali Basin

A ROMS simulation of the Somali basin, driven by COADS climatological monthly mean winds, realistically simulates the major features of the large-scale upper ocean circulation observed in the western Indian Ocean and equatorial regions. During boreal winter (JFM), the main feature in the tropical South Indian Ocean is a basin-wide cyclonic tropical gyre comprised of the South Equatorial Current to the south, the South Equatorial Counter current to the north, and the East African Coastal Current in the west. Rossby waves propagate westward in the shear zone between the South Equatorial Current and the South Equatorial Counter current, and are obstructed and partially reflected by the banks along the Seychelles-Mauritius Ridge (Mascarene Plateau, 60°E, Figure A1; Hermes and Reason, 2007).

In the northern section of the domain, the flow in January (Figure 4.17a) is dominated by a 10Sv transport that is directed equatorward. A closed transport of 5Sv is also apparent in the Northern Hemisphere. In the northeast corner of the domain, a transport of 15Sv is also apparent in both the January and February panels. In

February (Figure 4.17b), the 10Sv boundary flow is fed by an equivalent volume flow that originates from the east and corresponds to the Northeast Monsoon Current (NMC), otherwise known as the North Equatorial Current (NEC). South of the equator there is a 10Sv transport that is eastward and which may be associated with the northern boundary of the SECC, the latter forms part of the basin-wide cyclonic tropical gyre.

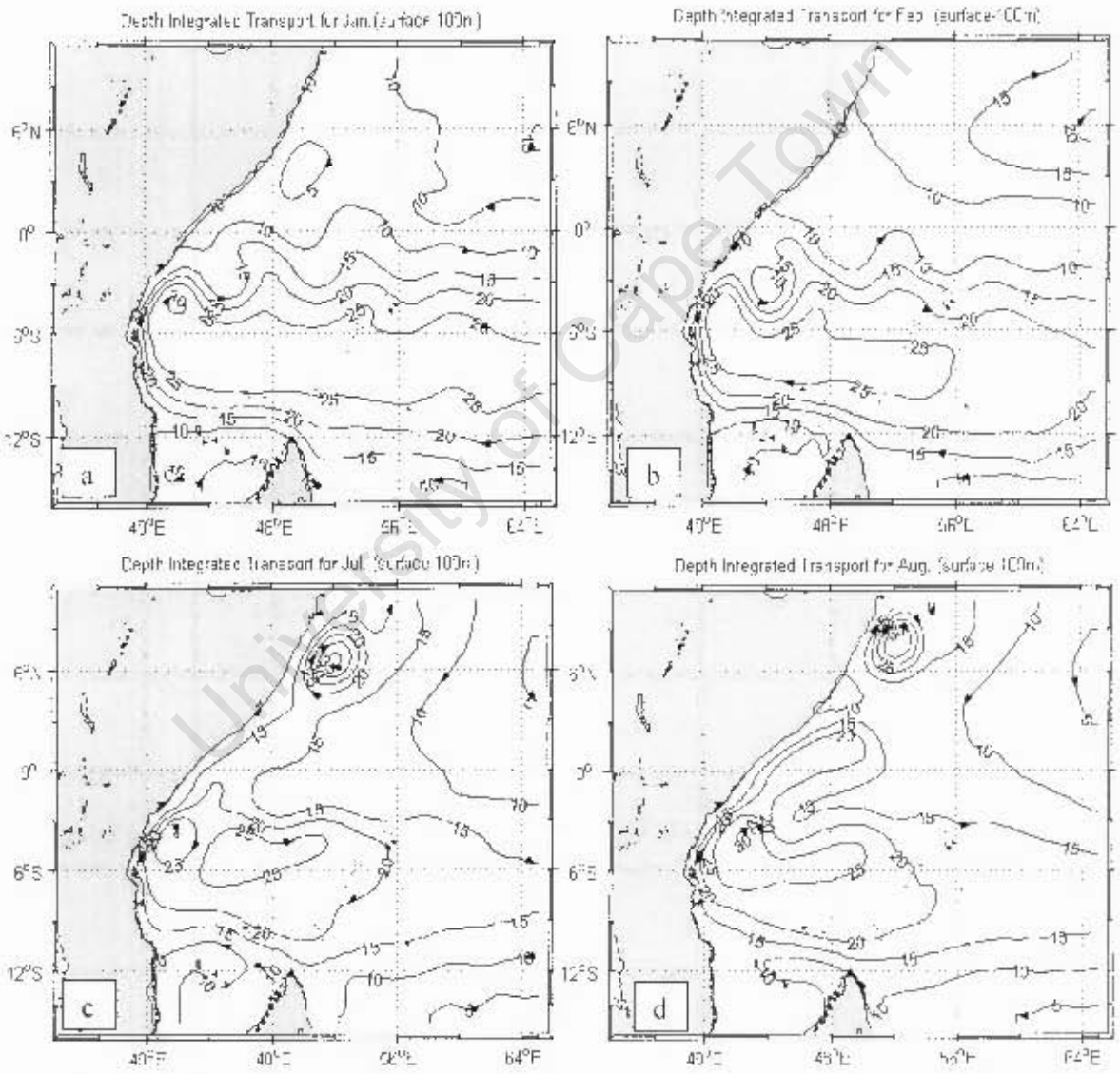

Figure 4.17: ROMS model volume transport function (Sverdrup) for: (a) January, (b) February, (c) July and (d) August. The contour interval is 5Sv.

During February (Figure 4.17b), the model volume transport function indicates that the tropical gyre shifts south and extends further east. The model simulation also compares equally well with the NCEP equivalent Sverdrup transport functions (Figure 2.3). Of particular interest is the reversed surface flow of the Somali current with a southward cross-equatorial transport of 10Sv according to the ROMS simulation. The corresponding NCEP plot (Figure 2.3b) indicates a similar amount of southward cross-equatorial transport. In addition, the SECC has a transport of between 15 – 20Sv during the northeast monsoon.

During the southwest monsoon, the Somali current is fully developed and at its maximum strength. In July (Figure 4.17c), the ROMS simulation indicates a northward cross equatorial transport of 15Sv which strengthens to 20Sv in August. In August (Figure 4.17d), the cross-equatorial current retroflects southwards just after reaching the first upwelling zone at about 4°N and a southward cross equatorial transport is apparent to the interior. A totally closed circulation at 6°N is fully formed by July and shifts northwards of 6°N by mid August; this corresponds to the Great Whirl. In the northeast of the domain, a 10Sv transport is directed southwards, crosses the equator near 60°E and feeds into the SECC. The SEC has an associated transport of 10-15Sv directed westwards whereas the EACC has 25Sv directed north-eastwards.

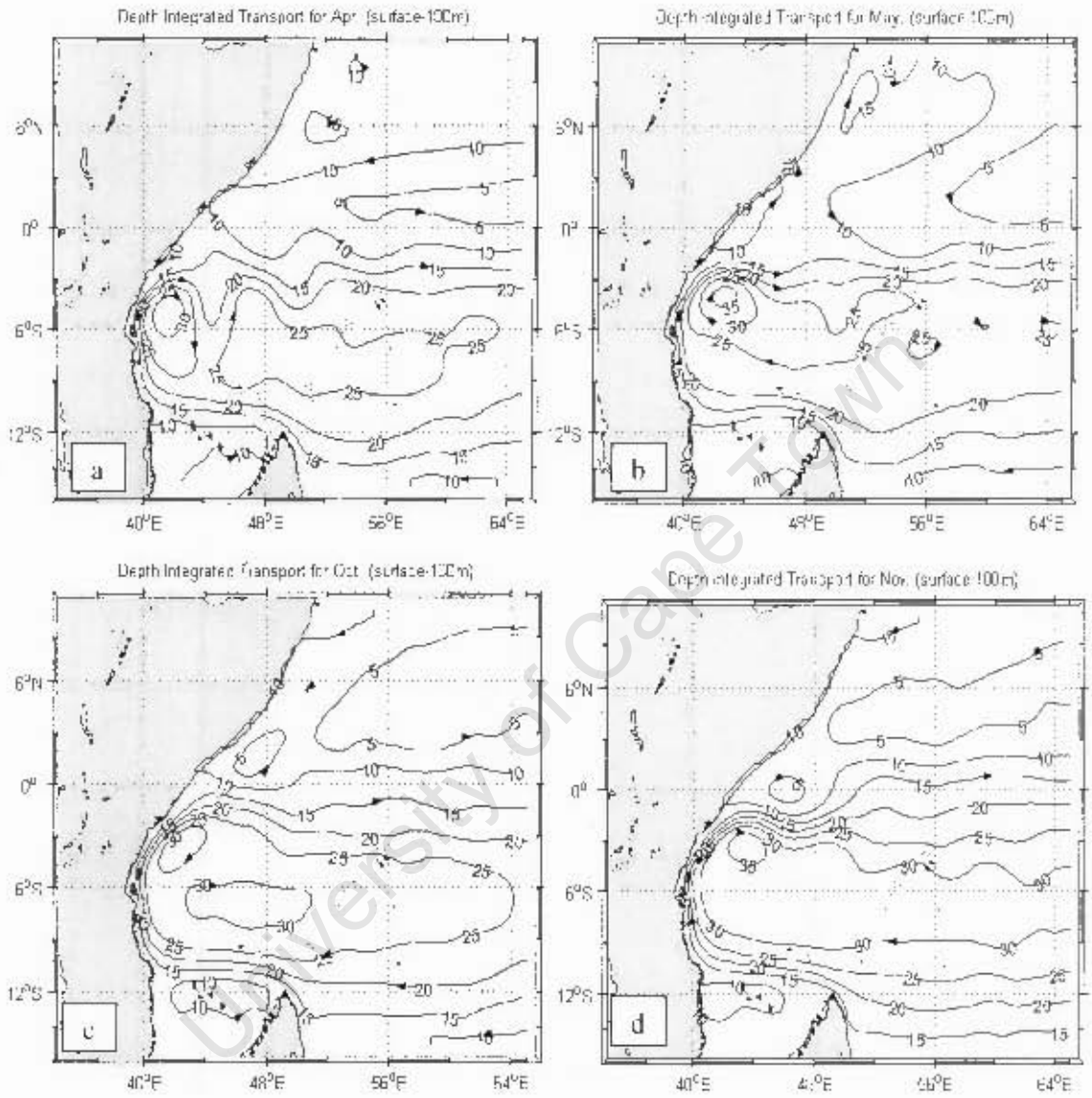

Figure 4.18: ROMS volume transport function (Sverdrup) for the transition periods (a) April, (b) May, (c) October and (d) November. The contour interval is 5Sv.

Figure 4.18 depicts monthly variations in the model transport during the two monsoon transition periods. It is interesting to note that the transport magnitude and flow patterns are fairly similar in both transition months (May, November). Near the southern boundary at Cape Amber, the transport towards the East African coast is about 20Sv, and shows little seasonal variation. This volume is slightly less than that observed by Swallow et al (1988) for the Northeast Madagascar Current (NEMC) who estimated the annual-mean transport of the NEMC from a year-long current meter mooring to be 29.6+8 Sv.

4.3 Kinetic Energy of Somali basin flow field

The kinetic energy (K.E) of the flow field is derived from the U and V component of the surface currents. The spatial distribution of the kinetic energy of the ROMS mean seasonal surface circulation of the Somali basin is as shown in figure 4.19. The JFM panel shows high values of K.E, of approximately $0.4 m^2 s^{-2}$, in the western basin between 0°-10°S. The zone with the highest values is next to the East African coast and corresponds to the EACC. In general, regions with high values of K.E are associated with strong persistent flows. Eddies generated by the shear zone that exists between the SEC and the SECC also have high K.E values of about $0.3\ m^2 s^{-2}$. The SEC flow kinetic energy appears at the northern tip of Madagascar as a westward extending tongue of 0.1 to $0.2\ m^2 s^{-2}$.

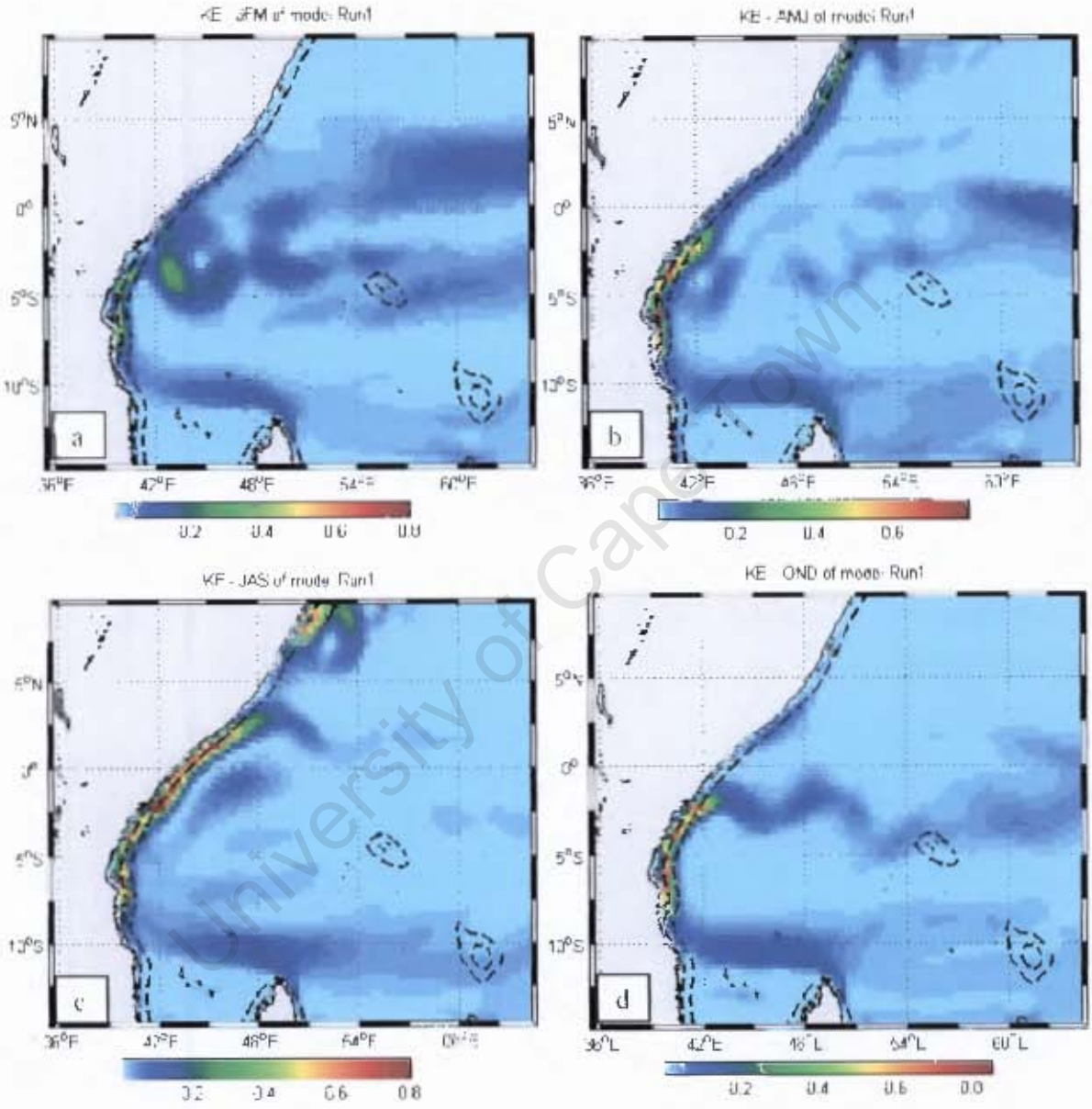

Figure 4.19: Kinetic energy (m^2s^{-2}) of seasonal mean flow field for (a) JFM; (b) AMJ; (c) JAS; (d) OND.

The AMJ panel shows that kinetic energy of the surface flow is still concentrated along the Kenyan and Tanzanian coast even during the monsoon transition period of April/May, with strong K.E values of up to 0.8 m^2s^{-2} associated with a strong persistent EACC. Along the equator, extending from 54°E to 65°E, the stronger kinetic energy values of between 0.1 and 0.2m^2s^{-2} reflect the Wyrtki jets that occur in the inter-monsoon period of April/May and October/November (Figure 4.20).

The JAS panel indicates that the cross equatorial western boundary flow is established with a K.E value of more than 0.8m^2s^{-2} in boreal summer and corresponds to the fully formed northward flowing Somali Current. At approximately 4°N, the higher values of kinetic energy extend offshore with values of under 0.2 m^2s^{-2}. Near 7-10°N at the western boundary, the highest values of K.E (0.6m^2s^{-2}) found in the domain correspond to the Great Whirl.

The OND panel (Figure 4.19d) shows that there is little or no energy north of the equator while south of the equator kinetic energy values of close to 0.8m^2s^{-2} are apparent at the western boundary and correspond to the EACC that flows throughout the year in this region. Kinetic energy values of approximately 0.1m^2s^{-2} with a meandering signature are evident between 1° and 5°S and may be associated with the SECC. In the equatorial band 60°E to 65°E, kinetic energy values of 0.1m^2s^{-2} correspond to equatorial jets (Figure 4.20a, b) during May and November.

A Morlet wavelet analysis of the model domain averaged surface kinetic energy shows prominent features of the seasonally reversing Somali current (Figure 4.20c). The wavelet suggests that maximum energy is apparent at the annual period. Minimum energy occurs in years 3-4 and 6-7. While the semi-annual signal is not well defined, signals with a period of 8 -10 months are apparent in the wavelet plot.

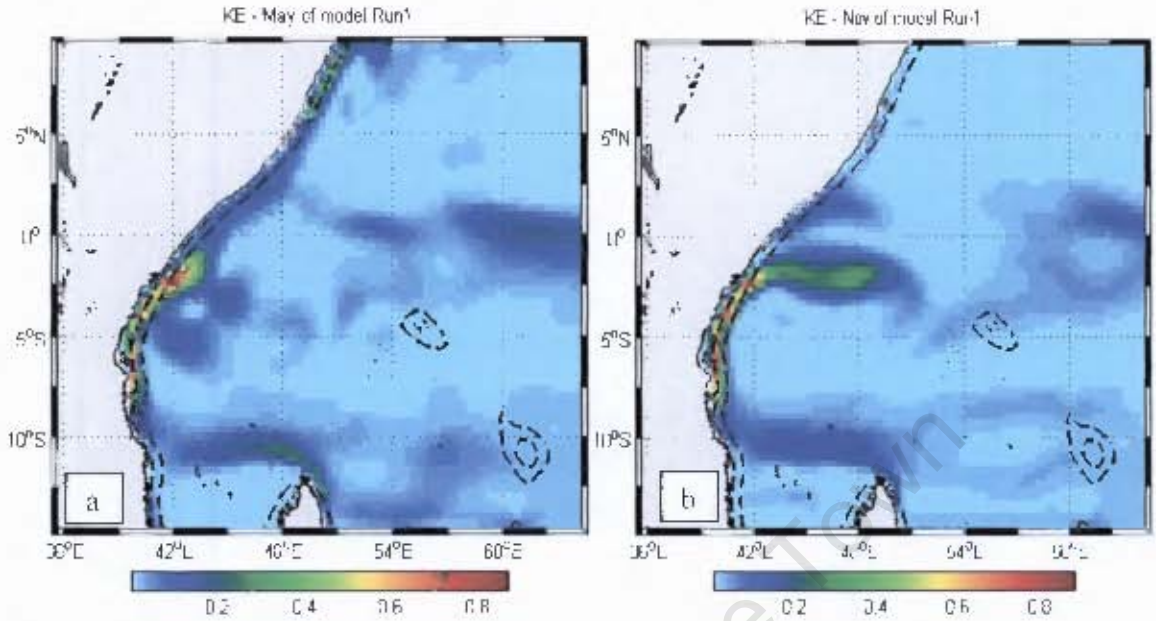

Figure 4.20: Kinetic energy (m^2s^{-2}) of monthly mean flow field during the transition months of (a) May and (b) November.

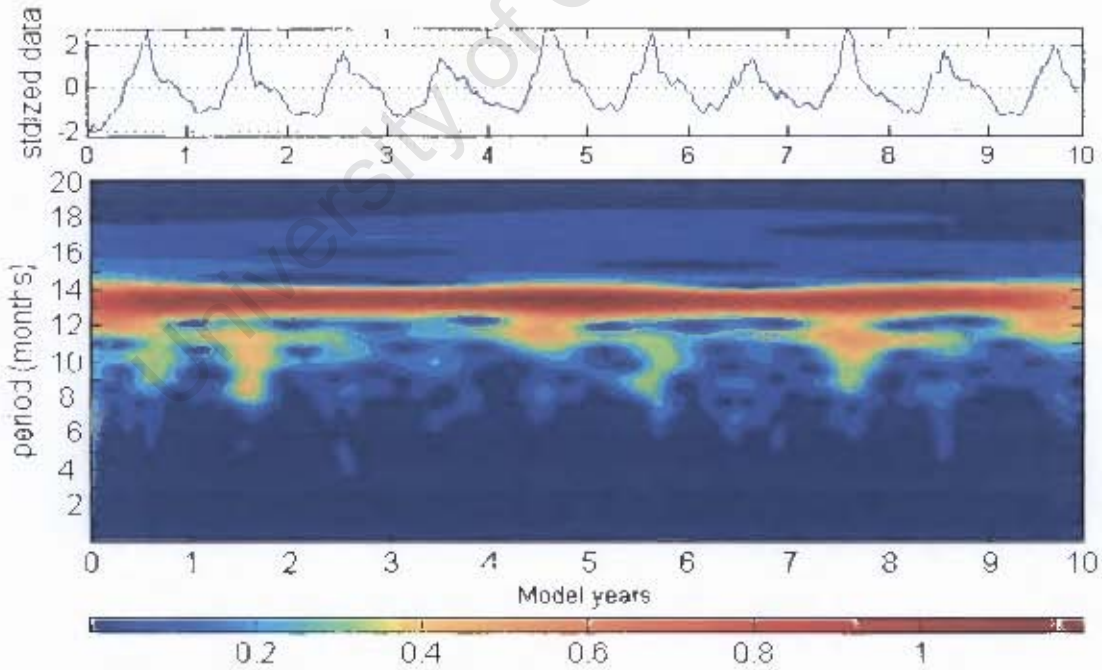

Figure 4.20: (c) Wavelet analysis of the surface kinetic energy (m^2s^{-2}) for a 10-year model integration cycle for the Somali basin. Upper panel is the standardized and de-trended dataset and lower panel is the corresponding Morlet wavelet transform.

4.4 SST of the Somali Basin

The spatial plot of Figure 4.21 contrasts the model sea surface temperature (left panels) with the TMI Satellite derived SST monthly means (right panels) averaged for the period 2002 to 2004. In both model and satellite derived fields, a zone of cool SST (26°-27°C) is apparent adjacent to the western boundary in the region between 4°S and 10°N during the month of January. The warmer temperatures (≈30°C) for this month generally occur in the region between 5°S and 15°S. This period is characterized by a distinct spatial distribution of SST with the southwestern section having warmer waters and the northwestern section cooler waters. Between the two pools is a zone of strong temperature gradient apparent in both datasets. In some places, the temperature difference is in the range of 2°C. Large temperature gradients are generally associated with horizontal circulations and contribute to heat advection towards the cooler zones. The zone of cool waters is marked by strong northeasterly winds (Figure 4.22a). The model SST agrees reasonably well with the TMI satellite SST data. In the northern domain, the net surface heat flux is negative ($-40 Wm^{-2}$) during January (Figure 4.23a) which points to heat loss in the upper ocean due to the strong northeasterly winds prevailing in that region during this period (Figure 4.22a). The southern domain which has weak southeasterly wind (Figure 4.22a) has surface net heat gain of between 40 and $80 Wm^{-2}$ and a corresponding rise in SST is evident in both datasets (Figure 4.21a, b).

During April, the model SST data is consistent with that derived from TMI satellite SST data (Figure 4.21.c, d). During this period, the warmest SST (≈30°C) lie in the domain north of 10°S while east of Madagascar, slightly cooler SST are apparent. The SST to the south reflects the SEC and NEMC at a cooler 27-28°C. During the month of April, the winds have a strong southeasterly component in the southern domain bounded by 6°S and 15°S (Figure 4.22b) with a corresponding mild (near-zero) net heat loss (Figure 4.23b) and consequently milder SST (Figure 4.21c, d) in this region. On the other hand, most of the domain north of 6°S is dominated by weak wind stresses and

net surface heat gain (≈100Wm^{-2}) and hence elevated SST occurs in both datasets in this region (Figure 4.21c, d).

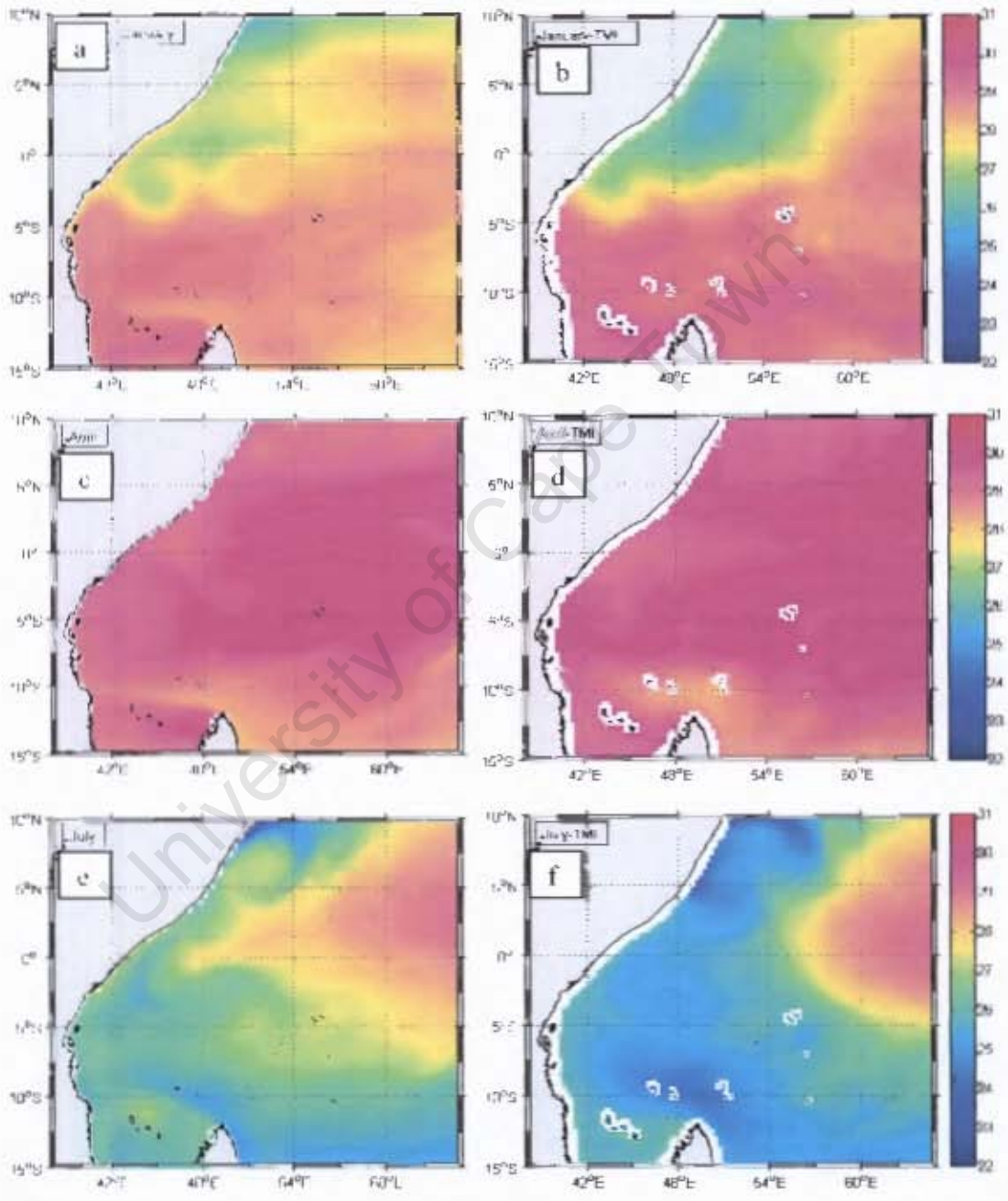

Figure 4.21: Contrast between model temperatures (°C) at the surface (10m depth) with the TMI-SSTs for (a- b) January; (c-d) for April, and (e-f) July.

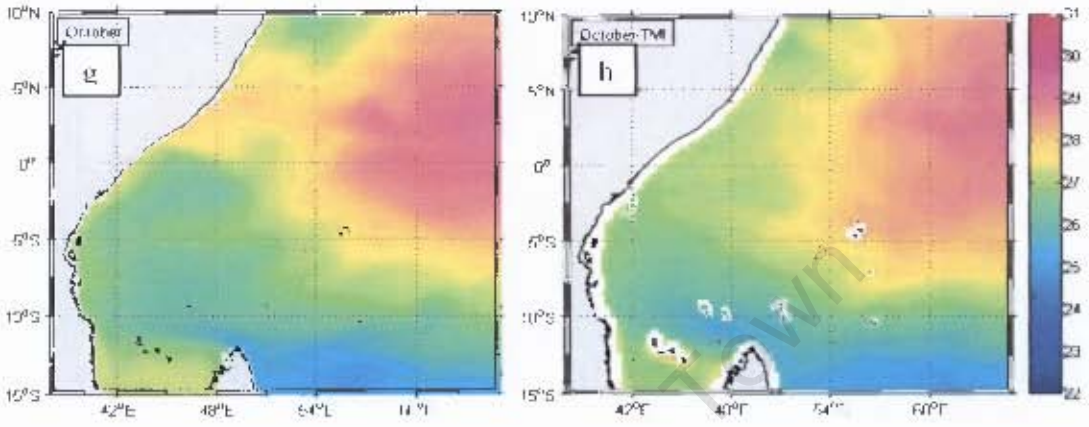

Figure 4.21: (g, h) Contrast between model temperature at the surface (10m depth) with the TMI-SSTs of October. Note the data gap along the coastal zone in the TMI-SST due to contamination of Satellite radiometer by continental or Island landmasses.

By July, the strong southwesterly monsoon winds have cooled the tropical northwestern Indian Ocean and this cooling is evident in both datasets (Figure 4.21e, f). Strong alongshore winds lead to increased offshore Ekman transport and this has the effect of entraining cool thermocline waters to the ocean surface, hence upwelling off Somalia. The net result is a cooler ocean surface than the surrounding air with a resultant net heat gain (50 to 100Wm^{-2}) by the Somali coastal ocean in this area (Figure 4.23c). This period reveals the coolest SST (22°C) in the coastal upwelling zones near 4-5°N and 7-10°N. Further to the northeast of model domain, warmer temperatures (28° - 30°C) are apparent. This warming could be due to the weak wind stress (Figure 4.22c) in this area due to the reversal of wind direction as they cross the equator. The surface net heat flux panel for July (Figure 4.23c) suggests weak net surface heat gain to the ocean in this area of warm SST. South of 10°S, a cool tongue (25°C) protrudes from Cape Amber towards the western boundary. Enhanced

southeast trades that are apparent in the wind stress pattern (Figure 4.22c) result in evaporation and subsequently upper-ocean mixing that leads to the cool tongue of water. Strong heat loss (50-100Wm^{-2}) from the ocean is also evident in this region (Figure 4.23c).

During the month of October, the Southwest monsoon winds off Somalia are less intense and the Northeast monsoon winds are in early development stage, thus the climatological southeasterly trade winds to the southeast of the model domain are dominant as apparent in figure 4.22d. The southeast trades tend to cool the tropical South Indian Ocean (Figure 4.21g, h) and this cooling (25 -26°C) is evident in both datasets in October. The upper ocean surface cooling in the southeast domain is accompanied by relatively weak net heat gain (20 - 40Wm^{-2}) by the ocean (Figure 4.23d). A region of net heat gain into the ocean (80 to 120Wm^{-2}) is apparent along the western boundary and seems to correspond to relatively cooler SST that exists in the surrounding area.

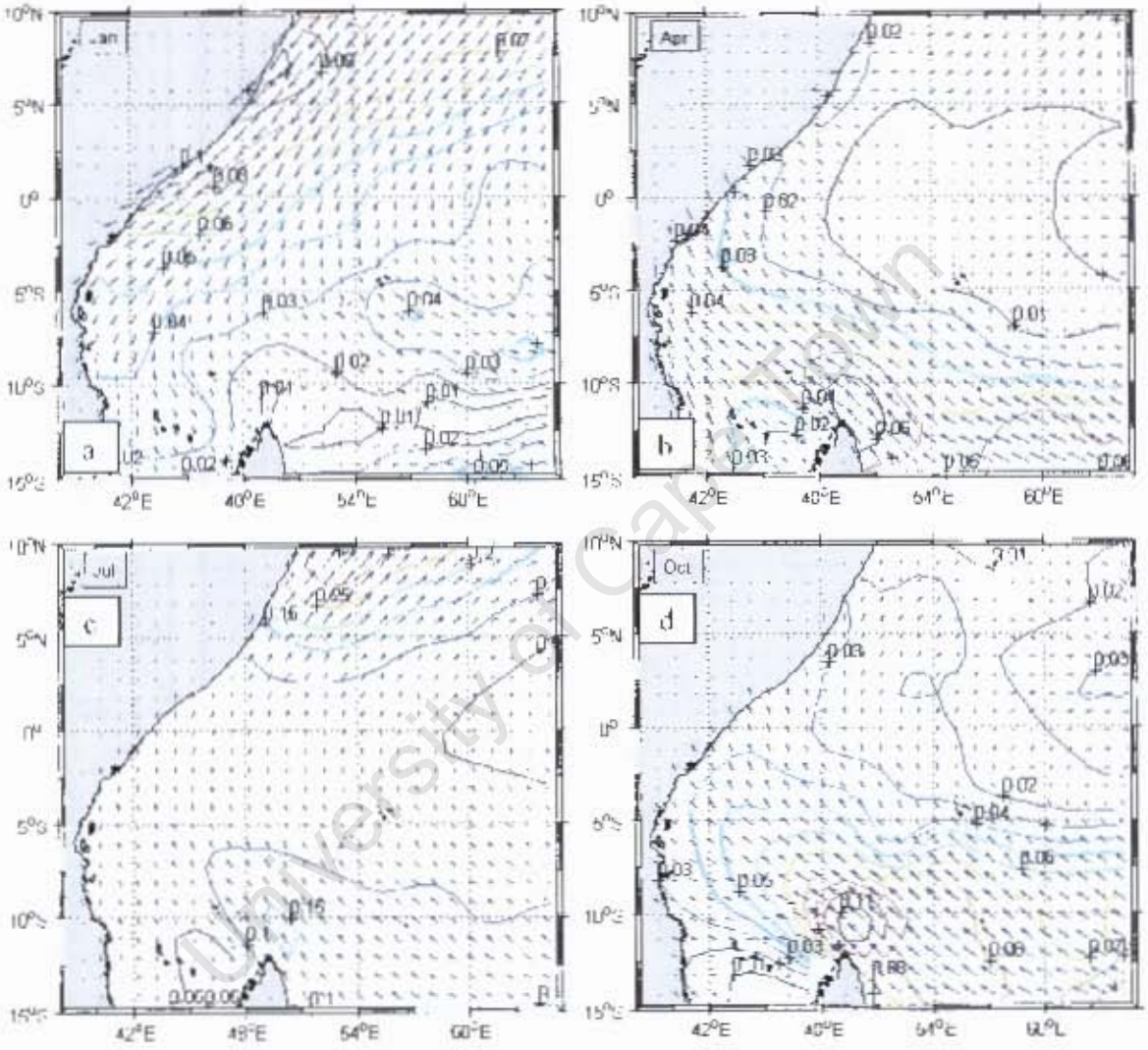

Figure 4.22: COADS wind stress field over the Somali basin for; (a) January, (b) April, (c) July and, (d) October. The contours indicate the magnitude of the wind stress (Nm^{-2}). The contour interval is 0.01 Nm^{-2}.

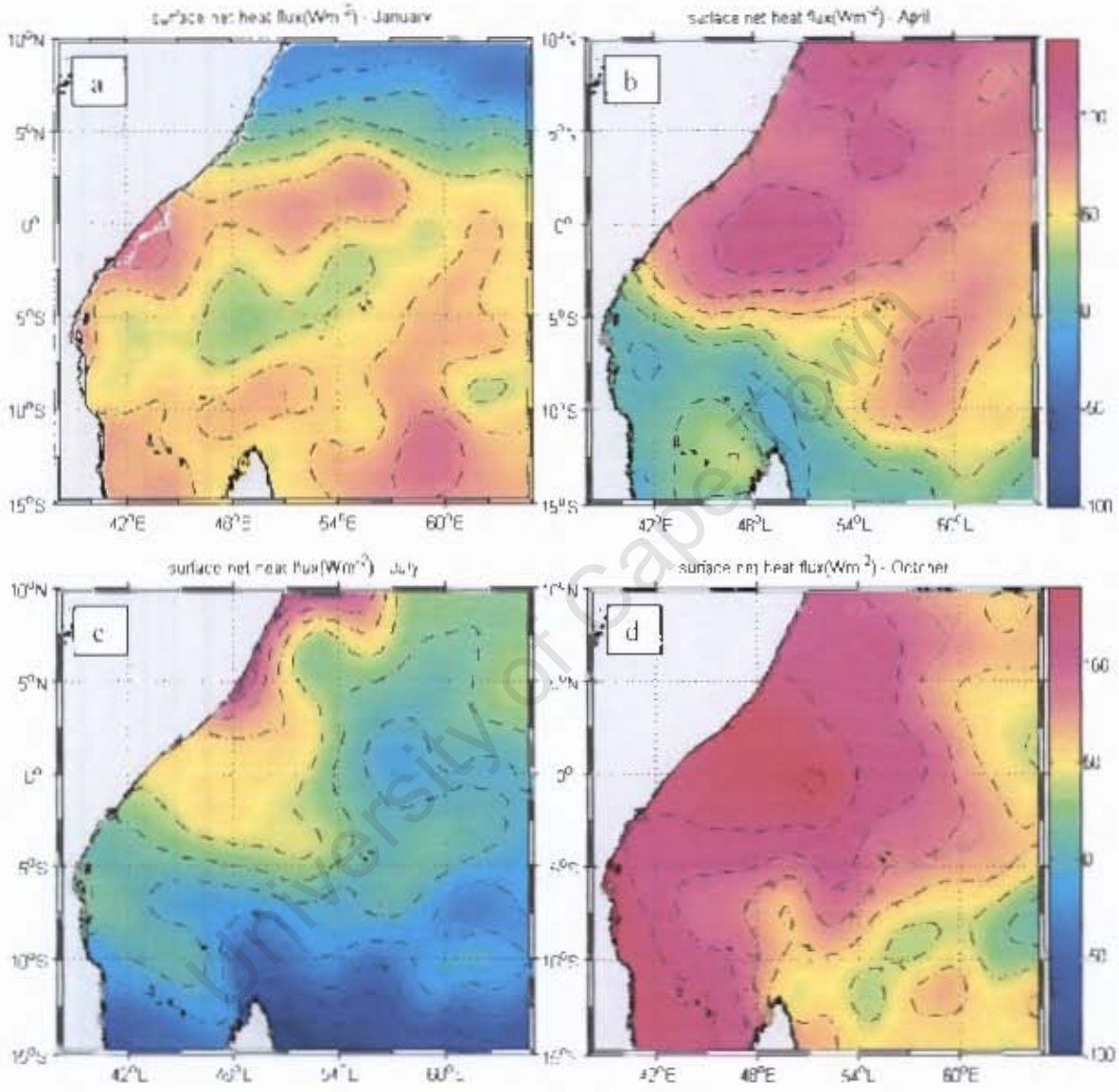

Figure 4.23: Annual cycle of the model surface net heat flux (W/m^2) in the Somali basin for: January, (b) April, (c) July, and (d) October.

4.5 Summary

In this chapter, the Regional Ocean Modelling system (ROMS) has been applied to investigate the surface circulation of the Somali basin. ROMS has been forced with COADS surface marine observations (ship-drift) monthly climatology winds and fluxes. The boundary conditions of salinity and temperature are from the World Ocean Atlas marine climatology datasets. This chapter has several sections, namely; the first section discussed the various aspects of the model climatological simulation of the Somali basin circulation, the second one considered the volume transport in the Somali basin as reproduced by the model, and the third section focused on the spatial temperature distribution in the Somali basin and the resulting heat flux. All of the above-mentioned aspects were studied on intra-seasonal to annual time scales and with the monsoon reversal being the main point of interest.

The first section showed that the model does simulate the general current flow pattern of the Somali basin reasonably well. The seasonal reversal of the Somali current is consistent with observations, achieving a maximum flow speed of close to $1.4ms^{-1}$ in August. The reversal of the Somali current during the northeast monsoon is also apparent in the simulation. Other major circulation features such as the Great Whirl, which occurs during the Southwest monsoon and the Southern gyre are also apparent in the simulation. The position and size of the gyre system are in agreement with observations (Schott and Quadfasel., 1982; Schott et al., 2001). The EACC and the SECC are also major features of the Somali basin circulation that are equally apparent from the model simulation.

The second section dealt with the volume transports in the Somali basin. The model simulations of volume transport are in general agreement with observations (Schott and McCreary, 2001). During the northeast monsoon, a 10Sv southward transport is apparent near the Somali coast. The northward flowing EACC with transport of about 25Sv merges with the Somali current to form shear zone with strong eddies with

associated transport of about 30Sv. A cyclonic tropical gyre south of the equator is apparent during this period.

During the southwest monsoon, the western boundary Somali Current is fully formed by July with a northward transport of 15Sv. A strong anti-cyclonic eddy forms near 6°N in July, then gradually shifts northward along the western boundary in August. The seasonal variation of the transport is also investigated during the monsoon transition periods. Distinct volume transport patterns are apparent and they include the cyclonic tropical gyre to the south. In April, the tropical gyre has two separate closed circulations, which apparently coalesce into one system by May. This pattern is repeated in October and November. The SEC displays little variations in its mean position but a marked variation in the magnitude of its zonal component is apparent.

The third section dealt with the seasonal variation in SST. The interaction between SSTs, surface net heat flux and wind stress over the Somali basin is also investigated based on the model output. During the austral summer (January), the southern domain generally has elevated SST associated with weak southeast trade winds and a corresponding heat gain. During the monsoon transition months of April and October, cool SST in the south of the domain are evident in both datasets and are associated with the strong southeasterly trades. A prominent feature is evident during the JAS period when the strong southwesterly monsoon winds enhanced by the Somali jet generate an upwelling zone along the Somali coast with cool tongues forming around 4°N and 9-10°N respectively.

CHAPTER 5

5.0 CONCLUSIONS AND RECOMMENDATIONS

This chapter presents conclusions emerging from the model study of the monsoon reversal and surface circulation in the East African coastal ocean (Somali basin). To investigate variability in the Somali basin during all the four seasons and during the monsoon transition, a regional ocean model (ROMS) was used in this study. The model forced with the COADS surface marine monthly climatological datasets for the period 1945 -1989, was used to investigate the circulation of the Somali basin, the volume transport and the SST seasonal variation.

An understanding of ocean circulation, dynamics, thermodynamics and mixed layer processes is crucial for understanding climate variability and prediction of regions adjacent to the ocean (e.g. Reason et al., 2000 and 2002). Indeed, Anderson and Moore (1979) have shown that changes in the Southern Hemisphere trade winds with the monsoons can affect the Somali Current north of the equator. Knowledge of the South Indian Ocean is also necessary for understanding larger scale phenomena. Madden and Julian (1972) postulated an Indian Ocean source for observed 40- to 50-day atmospheric oscillations. Much of East Africa receives most of its ITCZ based rainfall during the monsoon transition period of April/May (boreal spring) and October/November (boreal autumn). The complex processes involved in ocean-atmosphere coupling in the East African region and in other parts of the tropical regions are still not well understood.

Model studies using climatological forcing fields (as in this study) and having high vertical near-surface resolution are beneficial to ocean circulations studies due to the fact that it becomes possible to visualize the ocean in multi-dimensional scale of for

instance, time, SSH, ocean depth and spatial scales all at once. This has the added benefit of exposing hitherto complex upper ocean interactive processes and thus presents a more comprehensive (3 or 4-dimensional) picture of the ocean. In addition, models have proven useful in studying the response of the upper ocean to changing winds and help to integrate and interpret a plethora of widely varied datasets that range from the state-of-the-art satellite derived altimetry data to ship drift observations. With this in perspective, the upper ocean flow pattern of the Somali basin is diagnosed using ROMS.

The Indian Ocean differs from the other two world oceans in not possessing an eastern equatorial upwelling regime (Schott, 2004). In the Southern Hemisphere, the annual mean upwelling at the northern rim of the southeast trades causes a zonally extended open-ocean upwelling regime that is apparent in thermocline doming in the 3° - 12°S region. A further peculiarity of the Indian Ocean is given by the fact that right at the equator the winds are northward, mostly in the Somali basin and enhanced by the Somali jet of the summer monsoon. As a result, northward surface currents occur on the equator, against the southward Ekman transport in both hemispheres. The consequence is a shallow equatorial roll, confined to the upper ocean, with the Ekman flow passing southward underneath the northward surface flow (Miyama et al., 2003). Model studies (ROMS) forced with climatological wind fields and with high vertical near-surface resolution (more than 15 sigma-levels in the 0 – 500m depth) indicate that there exists a vertical meridional overturning circulation within a narrow band around the equator, with northward (southward) surface currents crossing the equator during the boreal summer (winter) monsoon with sub-surface counter flow underneath. The counter flow is thought to connect the southward (northward) Ekman transports from one side of the equator to the other during boreal summer (winter) monsoon. This meridional overturning cell carry warm surface water pole-ward and southward and colder thermocline water northward which upwells at around 4 - 6°N (e.g. Lee and Marotzke, 1997).

The surface flow pattern of the Somali basin is characterized by the seasonally reversing Somali current along the Somali coast, which ROMS realistically simulates and which is in agreement with observations (e.g. Wyrtki, 1971 and 1973; Woodberry et al., 1989; Schott, 1983; Swallow et al., 1983; Schott et al. 1988; and Swallow et al., 1988). During the JFM period (northeast monsoon), the climatological winds in the Northern Hemisphere have a dominantly northeasterly component that tends to force the surface flow southwards along the Somali coast and hence drives a southward flowing Somali Current. However, from the model diagnosis, a northward flowing undercurrent exists in the sub-surface depths of between 150 – 200m in general agreement with observations (Schott et al., 2001; Wyrtki, 1971 and 1973).

Another dominant feature simulated by the model during JFM is the tropical Southern Hemisphere circulation of the cyclonic tropical gyre with the westward flowing South Equatorial Current (SEC) at 12°S as its southern boundary. The SEC splits at the coast of Madagascar into northward and southward branches. The northward branch is the NEMC that joins the EACC to form the western boundary of the gyre. The SECC, fed by the merging of the EACC and the southward flowing Somali Current, forms the northern boundary of the Southern Hemisphere tropical gyre. The western part of the gyre is a region of high eddy activity, associated with the shear zone that exists between the westward flowing SEC and the eastward flowing SECC in agreement with observations (Lumpkin et al., 2005). The gyre is characterised by low SSH and thermocline doming to the northeast of Madagascar. In addition, the Southern Hemisphere tropical gyre seems to persist throughout the year apart from in August when the SECC is weakest. The annual persistence of the Southern Hemisphere tropical gyre is partly attributed to the southeast trades that also seem to persist for the annual cycle.

During the JAS period (southwest monsoon), the situation in the Northern Hemisphere is reversed, with the southeast trades joining with the Southwest monsoon winds, enhanced by the strong Somali jet, causing the surface flow along the Somali coast to be generally northward. Again, as in the case of the northeast monsoon, an

undercurrent with an opposing flow to the surface current is evident in the simulation consistent with observations (Leetma, 1972, Luther et al., 1985, Schott, 2001). The anti-cyclonic Great Whirl forms between 7° and 10°N, while the Southern Gyre is observed between 4°- 5°N. The formation of the Southern Gyre may be caused by alongshore winds near the equator as shown by McCreary and Kundu (1988), but Anderson and Moore (1979) pointed out that the curl of the wind near the equator can be important in determining the latitude at which the current turns offshore.

The monsoon transition periods of April/May and October/November are marked by westerly bursts of winds along the equatorial zone with the resulting equatorial jets between 60°E to 90°E. The model showed that the appearance of the jets is accompanied by low SSH along the East African coast (western boundary) and a rise of the SSH on the eastern end of the domain. The net result is mass transport from the western end of the basin towards the east.

In general, the ROMS model realistically simulates all the known upper ocean circulation patterns of the Somali basin including the EACC, Somali Current reversals and related undercurrents and the tropical South Indian Ocean tropical gyre system among others.

The seasonal to annual variation of the SST was also investigated using ROMS. The model output seems to suggest that the model is slightly warmer than the satellite derived TMI-SST especially in the months of January, July and October in most of the model domain. An analysis of SST, heat flux and winds stresses suggest a general trend of strong winds being associated with general cooling of SST and net heat gain to the upper ocean. Anomalies to this general trend are also apparent and it is proposed that these are either a result of the wind reversals during the monsoon transitions or possibly are caused by non-local forcing such as planetary waves, which have been known to propagate in this region especially during the southwest monsoon (e.g. Perigaud and Delecluse, 1992, Schott et al., 2001, Hermes and Reason, 2007).

Recommendations are towards a further investigation of the ocean-atmosphere couplings especially with respect to wind stress, SST and heat flux co-variability. Further model studies are proposed especially to try and establish whether the Somali basin SST mainly vary due to Ekman transport (the dynamical offset of winds) rather than thermodynamic effects of the winds, that is, SST are influenced by surface heat flux/evaporation. A comprehensive understanding of East African coastal ocean circulation, dynamics, thermodynamics and mixed layer processes is crucial for understanding climate variability and prediction of regions adjacent to the ocean. It is hoped that future studies will involve ocean-atmosphere coupled models.

REFERENCE:

Anderson, D.L.T., 1976: The low-level jet as a western boundary current. *Monthly Weather Review,* **104**, 907-921.

_____, and D.W. Moore, 1979: Cross-equatorial inertial jets with special relevance to very remote forcing of the Somali Current. *Deep Sea Research*, **26**, 1-22.

Arakawa, A., and V.R. Lamb, 1977: Methods of computational physics. *Academic Press*, **17**, 174-265.

Asnani, G.C., 1993: Tropical Meteorology I & II, Published by G. C. Asnani, c/o Indian Institute of Tropical Meteorology, Pashan, Pune-411008, India, pp. 1202.

Bannon, P.R., 1979: On the dynamics of the East African Jet: I. Simulation of the mean conditions for July. *Journal of Atmospheric Science,* **36**, 2139-2168.

_____, 1979: On the dynamics of the East African Jet, II, Jet transients. *Journal of Atmospheric Science*, **36**, 2153 – 2168.

Boyd, A.J. and F.A. Shillington, 1994: Physical forcing and circulation patterns on the Agulhas Bank. *South African Journal of Science,* **90**, 114 – 122.

Canuto, V.M., A. Howard, Y. Cheng, M.S. Dubovikov, 2001: Ocean turbulence I: one-point closure model. Momentum and heat vertical diffusivities. *Journal of Physical Oceanography,* **31**, 1413-1426.

Chereskin, T.K., W.D. Wilson, H.L. Bryden, A. Field and J. Morrison, 1997: Observations of the Ekman balance at 8°30'N in the Arabian Sea during the 1995 southwest monsoon. *Geophysical Research Letters*, ***24***, 2541–2544.

Colberg, F. and C.J.C. Reason, 2006: A model study of the Angola Benguela Frontal Zone: Sensitivity to atmospheric forcing. *Geophysical Research Letters*, **33**(19), L19608, [doi: 10.1029/2006GL027463].

Conkright, M.E., R.A. Locarnini, H.E. Garcia, T.D. O'Brien, T.P. Boyer, C. Stephens, J. I. Antonov, 2002: World Ocean Atlas 2001: Objective analyses, data statistics, and figures, CD-ROM documentation. *Technical Report of National Oceanographic Data Centre*, Silver Spring, MD.

Cox, M.D. 1979: A numerical study of Somali Current eddies. *Journal of Physical Oceanography*, **9**, 311–326.

Da Silva, A.M., C.C. Young-Molling, S. Levitus, 1994: Atlas of surface marine data 1994, vol.1, algorithms and procedures. NOAA Atlas NESDIS 6. *Technical Report of U.S. Department of Commerce, NOAA*, pp.83.

Di Lorenzo, E., Miller, A.J., Neilson, D.J., Cornuelle, B.D., Moisan, J.R., 2003: Modeling observed California Current mesoscale eddies and the ecosystem response. *International Journal of Remote Sensing*, **25** (7-8), 1307-1312.

Dueng, W., and F. Schott, 1978: Measurements in the source region of the Somali Current during the monsoon reversal. *Journal of Physical Oceanography*, **8**, 278–289.

Fairall, C.W., E.F. Bradley, D.P. Rogers, J.B. Edson and G.S. Young, 1996: Bulk parameterization of air-sea fluxes for tropical ocean-global atmosphere Coupled-Ocean Atmosphere Response Experiment. *Journal of Geophysical Research*, **101**, 3747-3764.

Findlater, I., 1969: A major low-level air current near the Indian Ocean during the northern summer. *Quarterly Journal of the Royal Meteorological Society*, **95**, 362-380.

_____, 1969: Inter-Hemispheric transport of air in the lower troposphere over the Western Indian Ocean. *Quarterly Journal of the Royal Meteorological Society*, **95**, 400 - 404.

Fischer, J., F. Schott, and L. Stramma, 1996: Currents and Transports of the Great Whirl-Socotra Gyre System during the Summer Monsoon August 1993. *Journal of Geophysical Research*, **101**, 3573–3587.

Galperin, B., L.H. Kantha, S. Hassid, and A. Rosati, 1988: A quasi-equilibrium turbulent energy model for geophysical flows. *Journal of Atmospheric Science*, **45**, 55-62.

Garrat, J.R., 1977: Review of drag coefficients over oceans and continents. *Monthly Weather Review,* **105**, 915-929.

Hacker, P., E. Firing, J. Hummon, A. Gordon, and J.C. Kindle, 1998: Bay of Bengal currents along the northeast monsoon. *Geophysical Research Letters*, ***25***, 2769–2772.

Haidvogel, D.B., H.G. Arango, K. Hedstrom, A. Beckmann, P. Malanotte-Rizzoli, and A.F. Shchepetkin, 2000: Model evaluation experiments in the North Atlantic Basin: Simulations in nonlinear terrain-following coordinates. *Dynamics of Atmospheres and Oceans*, **32**, 239-281.

_____, and A. Beckmann, 1999: Numerical Ocean Circulation Modelling. Series on Environmental Science and Management, Vol. **2**, Imperial College Press, pp. 319.

Halpern, D., Freilich, M.H., and Weller, R.A., 1998: Arabian sea surface winds and ocean transports determined from ERS-1 scatterometer. *Journal of Geophysical Research*, **103** (C4), 7799–7805.

Han, W., J.P. McCreary Jnr., D.L.T. Anderson, and A.J. Mariano, 1999: On the dynamics of the eastward surface jets in the equatorial Indian Ocean. *Journal of Physical Oceanography*, **29**, 2191–2209.

Hastenrath, S., and L. Greischar, 1991: The monsoonal current regimes of the tropical Indian Ocean: observed surface flow fields and their geostrophic and wind-driven components. *Journal of Geophysical Research*, **96**, 12619–12633.

Hellerman, S., and M. Rosenstein, 1983: Normal monthly wind stress over the world ocean with error estimates. *Journal of Physical Oceanography*, **13**, 1093–1105.

Hermes J.C., and Reason C.J.C., 2008: Annual cycle of the South Indian Ocean (Seychelles-Chagos) thermocline ridge in a regional ocean model. *Journal of Geophysical Research*, [doi: 10.1029/2007JC004363].

_____, and C.J.C. Reason and J.R.E. Lutjeharms, 2007: Modelling the Variability of the Greater Agulhas Current System. *Journal of Climatology,* **20**, 3131- 3144

_____, and C.J.C. Reason, 2005: Ocean Model Diagnosis of Inter-annual Coevolving SST Variability in the South Indian and South Atlantic Ocean. *Journal of Climate*, **18**, 1-19.

Indeje, M., F.H.M. Semazzi, 2000: Relationships between QBO in the lower equatorial stratospheric zonal winds and East Africa seasonal rainfall. *Meteorology and Atmospheric Physics,* **73,** 227-244.

Ininda, J.M, 1998: Simulation of the impact of sea surface temperature anomalies on the short rains over East Africa. *Journal of African Meteorological Society,* **3**, 127-138.

Jensen, T.G., 1991: Modelling of the Seasonal Undercurrents in the Somali Current System. *Journal of Geophysical Research*, **96**, 22,151-22,167.

Kalnay, E., 1996: The NCEP-NCAR 40-year reanalysis project. *Bulletin of the American Meteorological Society*, **77,** 437 – 471.

Kantha, L.H., C.A. Clayson, 1994: Numerical Models of Oceans and Oceanic Processes. *International Geophysics Series*, Academic Press San Diego, **66**, pp.940.

Kijazi, A.L., and C.J.C. Reason, 2005: Relationship between intra-seasonal rainfall variability of coastal Tanzania and ENSO. *Theoretical Applied Climatology*, **82**, 153-176.

Knox, R., 1987: The Indian Ocean Interaction with the monsoon, in Monsoons. Edited by J. S. Fein and P. L. Stephens, John Wiley, New York, pp. 365-398.

Krishnamurti, T.N., 1971: Observational study of the tropical upper tropospheric motion field during the northern hemisphere summer. *Journal of Applied Meteorology*, **10**, 1066-1096.

_____, 1971: Tropical east-west circulation during the northern summer. *Journal of Atmospheric Science*, **28**, 1342-1347.

_____, and T. Bhalme, 1976: Oscillations of a monsoon system, Observational aspects. *Journal of Atmospheric Science*, **33**, 1937-1934.

_____, and V. Wong, 1979: A planetary scale boundary-layer model for the Somali jet. *Journal of Atmospheric Science,* **36**, 1895-1907.

_____, P. Ardanuy, Y. Ramanathan, and R. Pasch, 1990: On the onset vortex of the summer monsoon. *Monthly Weather Review*, **109**, 344-363.

Lagerloef, G.S.E, G.T. Mitchum, R.B. Lukas, P.P. Niller, 1999: Tropical Pacific near surface currents estimated from altimeter, wind and drifter data. *Journal of Geophysical Research*, **104**, 313-326.

Large, W.G., J.C. McWilliams, and S.C. Doney, 1994: Oceanic vertical mixing: a review and a model with a non-local boundary layer parameterization. *Reviews of Geophysics*, **32**, 363-403.

_____, and S. Pond, 1982: Open Ocean Momentum Flux Measurements in Moderate to Strong Winds. *Journal of Physical Oceanography*, **11**, 324-336.

Lee, T., and J. Marotzke, 1997: Inferring meridional mass and heat transports of the Indian Ocean by fitting a GCM to climatological data. *Journal of Geophysical Research,* **102**, 10585-10602.

Leetmaa, A., 1972: The response of the Somali Current to the southwest monsoon of 1970. *Deep-Sea Research*, **19**, 397–400.

Levitus, S., 1988: Ekman volume fluxes for the world ocean and individual ocean basins. *Journal of Physical Oceanography*, **18**, 271–279.

_____, S. and T. Boyer, World Ocean Atlas, Vol. 4, 1994: Temperature, NOAA Atlas NESDIS 4, NOAA, Washington, DC, pp. 117.

Lighthill, M.J. 1969: Dynamic response of the Indian Ocean to the onset of the southwest monsoon. *Philosophical Transactions of the Royal Meteorological Society,* A**265**, 45–92.

Lumpkin, R. and Z. Garraffo, 2005: Evaluating the Decomposition of Tropical Atlantic Drifter Observations. *Journal of Atmospheric and Oceanic Technology,* **22**(9), 1403-1415.

Luther, M.E., and J.J. O'Brien, 1985: A model of the seasonal circulation in the Arabian Sea forced by observed winds. *Progress in Oceanography*, **14**, 353–385.

Luyten, J.R., and J.C. Swallow, 1976: Equatorial undercurrents. *Deep-Sea Research*, ***23***, 999 –1001.

_____, J.R, M. Fieux, and J. Gonella, 1980: Equatorial Currents in the Western Indian Ocean. *Science,* **209**, 600-603.

Madden, R.A., and P.R. Julian, 1972: Description of global-scale circulation cells in the tropics with a 40–50 day period. *Journal of Atmospheric Science*, ***29***, 1109–1123.

Marchesiello, P., J.C. McWilliams, and A. Shchepetkin, 2003: Equilibrium structure and dynamics of the California Current System. *Journal of Physical Oceanography*, **33**, 753-783.

McCreary Jnr, J.P., P.K. Kundu and R.L. Molinari, 1993: A numerical investigation of the dynamics, thermodynamics and mixed-layer processes in the Indian Ocean. *Progress in Oceanography*, **31**,181-244.

_____, and P.K. Kundu, 1988: A numerical investigation of the Somali Current during the Southwest Monsoon. *Journal of Marine Research*, ***46***, 25-58.

McPhaden, M., 1982: Variability in the central Indian Ocean. Part I: Ocean dynamics. *Journal of Marine Research*, **40**, 157–176.

Melice, J.L., A. Coron, and A. Berger, 2001: Amplitude and Frequency Modulations of the Earth's Obliquity for the Last Million Years. *Journal of Climate*, **14**, 1043-1053.

Mellor, G.L. and T. Yamada, 1982: Development of a turbulence closure model for geophysical fluid problems. *Reviews of Geophysics and Space Physics*, **20**, 851-875.

Miyama, T., J.P. McCreary Jr, T.G. Jensen, J. Loschnigg, S. Godfrey, and A. Ishida, 2003: Structure and dynamics of the Indian Ocean cross-equatorial cell. *Deep-Sea Research, Part II,* **50**, 2023-2047.

Monterey, G. and S. Levitus, 1997: Seasonal Variability of Mixed Layer Depth for the World Ocean. NOAA Atlas NESDIS 14, U.S. Gov. Printing Office, Wash., D.C., pp. 96.

Morlet, J., 1983: Sampling theory and wave propagation. *Issues in Acoustic Signal/Image Processing and Recognition,* NATO ASI Series, **1**, Springer, 233–261.

Mukabana, J.R. and R.A. Pielke, 1996: Investigating the influence of synoptic-scale monsoonal winds and meso-scale circulation on diurnal weather patterns over Kenya using a meso-scale numerical model. *Monthly Weather Review,* **124**, 224–243.

Mutai C.C., and M.N. Ward, 2000: East African rainfall and the tropical circulation/convection on intra-seasonal to inter-annual timescales. *Journal of Climate,* **13**, 3915-3939.

O'Brien, J.J., and H.E. Hurlburt, 1974: An equatorial jet in the Indian Ocean theory. *Science*, ***184***, 1075-1077.

Ogallo L.J, 1988: Relationship between seasonal rainfall in East Africa and Southern Oscillation. *Journal of Climatology,* **8**, 34–43.

Patterson, S.L. 1985: Surface circulation and kinetic energy distributions in the Southern Hemisphere Oceans from FGGE drifting buoys. *Journal of Physical Oceanography,* **15***,* 865–884.

Peliz, A., J. Dubert, D.B. Haidvogel, and B. Le Cann, 2003: Generation and unstable evolution of a density-driven Eastern Poleward Current: The Iberian Poleward Current. *Journal of Geophysical Research*, **108**(C8), 3268, [doi: 10.1029/2002JC001443].

Penven, P., P. Marchesiello, L. Debreu and J. Lefevre, 2008: Software tools for pre- and post-processing of oceanic regional simulations, *Environmental Modelling Software*, **23**, 660-662.

_____, L. Debreu, P. Marchesiello, J.C. McWilliams, 2006. Application of the ROMS embedding procedure for the Central California Upwelling System. *Ocean Modelling,* **12**, 157-187.

_____, P., V. Echevin, J. Pasapera, F. Colas, J. Tam, 2005: Average circulation, seasonal cycle and mesoscale dynamics of the Peru Current System: A modelling approach. *Journal of Geophysical Research*, **110**, C10021, [doi: 10.1029/2005JC00 2945].

_____, P., C. Roy, J.R.E. Lutjeharms, A. Colin de Verdiere, A. Johnson, F. Shillington, P. Freon, G. Brundrit, 2001: A regional hydrodynamic model of the Southern Benguela. *South African Journal of Science,* **97**, 472-476.

Perigaud, C., and P. Delecluse, 1992: Annual sea level variations in the southern tropical Indian Ocean from Geosat and shallow water simulations. *Journal of Geophysical Research*, ***97,*** 20169–20178.

Picaut, J. 1989: Use of the geostrophic approximation to estimate time-varying zonal currents at the Equator. *Journal of Geophysical Research,* **94**, 3228-3236.

Umlauf, L., H. Burchard, 2003: A generic length-scale equation for geophysical turbulence models. *Journal of Marine Research*, **61**, 235-265.

Ramage, C., 1971: Monsoon Meteorology. *International Geophysics Series*, Academic Press, San Diego, California, ***15***, pp. 296.

Rao, R.R., R.L. Molinari, and J.F. Festa, 1989: Evolution of the climatological near-surface thermal structure of the tropical Indian Ocean: 1. Description of mean monthly mixed layer depth, and sea surface temperature, surface current, and surface meteorological fields. *Journal of Geophysical Research*, **94**, 10801–10815.

Reason, C.J.C., R.J. Allan, J.A. Lindsey, and T.J. Ansell, 2000: ENSO and climatic signals across the Indian Ocean basin in the global context: Part I, inter-annual composite patterns. *International Journal of Climatology*, **20**, 1285-1327.

_____, M. Rouault, J.L. Melice, and D. Jagadheesha, 2002: Winter rainfall variability in SW South Africa and large-scale ocean-atmosphere interactions. *Meteorology and Atmospheric Physics*, **80**, 19-29.

Schoenefeldt, R., and F.A. Schott, 2006: Decadal variability of the Indian Ocean cross-equatorial exchange in SODA. *Geophysical Research Letters,* ***33***, L08602, [doi:10.1029/2006GL 025891].

Schott, F., and D. Quadfasel, 1982: Variability of the Somali Current and associated upwelling. *Progress in Oceanography*, ***12***, 357–381.

_____, 1983: Monsoon response of the Somali Current and associated upwelling. *Progress in Oceanography,* **12,** 351–382.

_____, M. Fieux, J. Kindle, J. Swallow, and R. Zantopp, 1988: The boundary currents east and north of Madagascar, 2, Direct measurements and model comparisons. *Journal of Geophysical Research*, **93**, 4963-4914.

_____, Swallow, J.C., and M. Fieux, 1990: The Somali Current at the equator: annual cycle of currents and transports in the upper 1000 m and connection to neighboring latitudes. *Deep-Sea Research*, **37**, 1825–1848.

_____, Fischer, J., U. Garternicht, and D. Quadfasel, 1997. Summer monsoon response of the Northern Somali Current. *Geophysical Research Letters*, **24**, 2565–2568.

_____, and J.P. McCreary, 2001: The monsoon circulation of the Indian Ocean. *Progress in Oceanography,* **51**, 1–123.

_____, 2004: Shallow overturning circulation of the Western Indian Ocean. *Philosophical Transactions of the Royal Society,* A**363**, 143–149.

Shchepetkin, A., and J.C. McWilliams, 1998: Quasi-monotone advection schemes based on explicit locally adaptive dissipation. *Monthly Weather Review,* **126**, 1541-1580.

_____, 2003: A method for computing horizontal pressure-gradient force in an ocean model with a non-aligned vertical coordinate. *Journal of Geophysical Research*, **108**(C3), 3090, [doi: 10.1029/2001JC001047].

_____, 2005: The Regional Oceanic Modelling system (ROMS): A split-explicit, free-surface, topography following coordinate oceanic model. *Ocean Modelling,***9**, 347–404.

Shillington, F.A., 1998: The Benguela upwelling system off southwestern Africa. *The Global Coastal Ocean,* John Wiley and Sons, New York, pp. 587.

Shukla, J., and M.J. Fennessy, 1994: Simulation and predictability of monsoons, in Proceedings of the International Conference on Monsoon Variability and Prediction. *Technical Report WCRP- World Climate Research Programme, Geneva, Switzerland*, **84**, 567–575,

Smith S.D., 1988: Coefficients for sea surface wind stress, heat flux, and wind profiles as a function of wind speed and temperature. *Journal of Geophysical Research*, **93**, 15467–15472.

Song, Y. and D.B. Haidvogel, 1994: A semi-implicit ocean circulation model using a generalized topography-following coordinate system. *Journal of Computational Physics*, **115**(1), 228-244.

Styles, R. and S.M. Glenn, 2000: Modelling stratified wave and current bottom boundary layers in the continental shelf. *Journal of Geophysical Research,* **105**, 24119–24139.

Swallow, J.C., R.L. Molinari, J.G. Bruce, O.B. Brown and R.H. Evans, 1983: Development of near-surface flow patterns and water mass distribution in the Somali Basin in response to the southwest monsoon of 1979. *Journal of Physical Oceanography,* **13**, 1398–1415.

_____, M. Fieux, and F. Schott, 1988: The boundary currents east and north of Madagascar, 1, geostrophic currents and transports. *Journal of Geophysical Research*, **93**, 4951–4962.

Tomczak, M and S.J. Godfrey, 1994: Regional Oceanography: an Introduction. *Pergamon Press*, New York, pp. 422.

Torrence, C. and G.T. Compo, 1998: A Practical Guide to Wavelet Analysis. *Bulletin of the American Meteorological Society,* **79** (1), 61–78.

Trenberth, K.E., K. Miller, L. Mearns, and S. Rhodes, 2000: Effects of Changing Climate on Weather and Human Activities. Understanding Global Change. *Earth Science and Human Impacts Series, Global Change Instruction Program*, UCAR. University Science Books, pp. 46.

Wacongne, S., and R. Pacanowski, 1996: Seasonal heat transport in a primitive equations model of the tropical Indian Ocean. *Journal of Physical Oceanography*, **26**, 2666–2699.

Warner, J.C, C.R. Sherwood, H.G. Arango, and R.P. Signell, 2005: Performance of four Turbulence Closure Methods Implemented using a Generic Length Scale Method. *Ocean Modelling*, **8**, 81-113.

Washington, W.M., and S.M. Dagupatty, 1975: Numerical simulation with the NCAR global circulation model of the mean conditions during the Asian-African summer monsoon. *Monthly Weather Review*, **103,** 105-114.

Webster, P.J., V.O. Magana, T.N. Palmer, J. Shukla, R.A. Tomas, M. Yanai, and T. Yasunari , 1998: Monsoons: Processes, predictability, and the prospects for prediction. *Journal of Geophysical Research,* **103**, 14,451-14,510.

_____, 1999: Coupled ocean-atmosphere dynamics in the Indian Ocean during 1997-98. *Nature*, **401**, 356-360.

Wilkin, J.L., H.G. Arango, D.B. Haidvogel, C.S. Lichtenwalner, S.M. Durski, and K.S. Hedstrom, 2005: A regional Ocean Modeling System for the Long-term Ecosystem Observatory. *Journal of Geophysical Research*, **110**, C06S91, [doi: 10.1029/2003JC00 2218].

Woodberry, K.E., E.M. Luther, and J.J. O'Brien, 1989: The Wind-Driven Seasonal Circulation in the Southern Tropical Indian Ocean. *Journal of Geophysical Research*, **94**, 17,985-18,002.

Wyrtki, K., 1971: Oceanographic atlas of the International Indian Ocean Expedition. *National Science Foundation*, Washington, D.C., pp. 531.

_____, 1973: An equatorial jet in the Indian Ocean. *Science*, **181,** 262 - 264.

APPENDIX I:

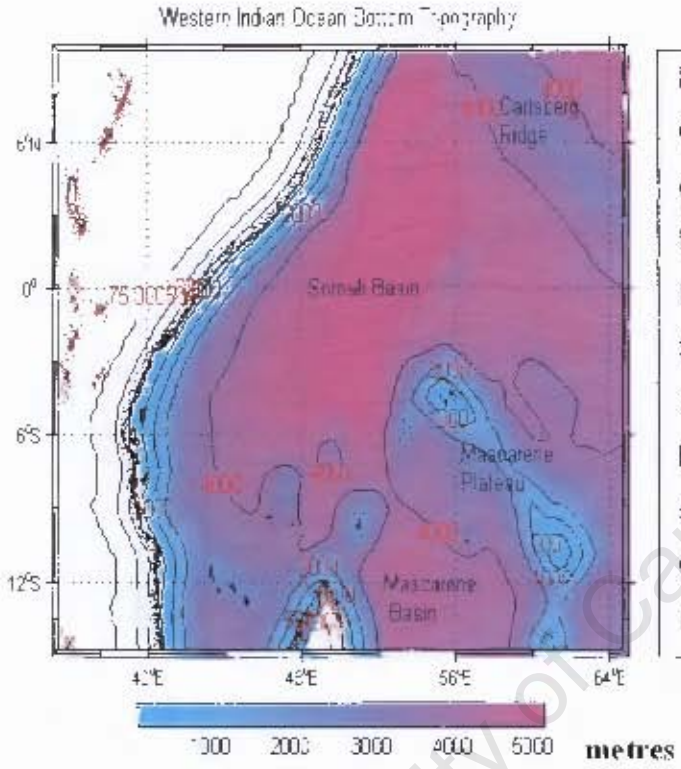

Figure A-1: Western Indian Ocean Bottom Topography (metres) showing Somali basin, Part of Mascarene basin, the Mascarene Plateau flanked by the Seychelles bank to the north and *Saya de Malha* banks, Nazareth banks and Cargados carajos shoals to the south. The Carlsberg ridge is visible to the northeast corner of map.

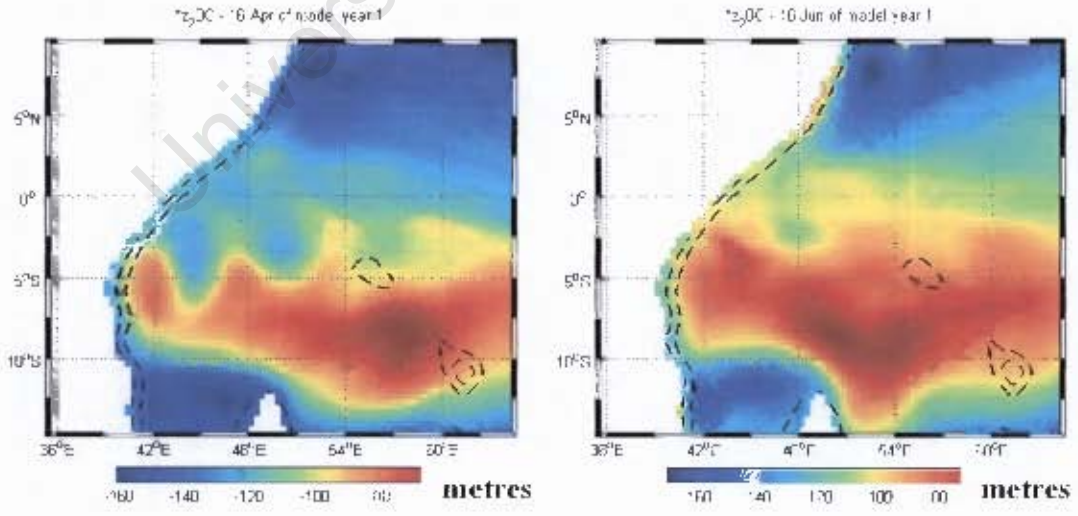

Figure A-2: Thermocline lifting (Doming in metres from ocean surface) during the monsoon transition April and June months. There is evidence of thermocline lifting in the south of the domain.